UNIONE EUROPEA
Fondo Sociale Europeo

Ministero dell'Istruzione, dell'Università e della Ricerca

PON RICERCA E INNOVAZIONE 2014 - 2020

Università degli Studi della Campania *Luigi Vanvitelli*

Scuola di Medicina e Chirurgia
Dipartimento di Salute Mentale e Fisica e Medicina Preventiva

PHD SCHOOL IN LIFE SCIENCES

PHD PROGRAM IN

CLINICAL AND EXPERIMENTAL MEDICAL SCIENCES

XXXIV Cycle

Scientific disciplinary sector: MED/14

Thesis title:

A new *in vivo* multiphoton microscopy based approach to study the peritoneal membrane changes induced by peritoneal dialysis

TUTOR
Prof. Francesco Trepiccione

CANDIDATE
Dr. Luciano D'Apolito

Coordinator of PhD course
Prof. Armida Mucci

Academic year 2020-2021

UNIONE EUROPEA
Fondo Sociale Europeo

Ministero dell'Istruzione, dell'Università e della Ricerca

PON RICERCA E INNOVAZIONE 2014 - 2020

Università degli Studi della Campania *Luigi Vanvitelli*

Scuola di Medicina e Chirurgia
Dipartimento di Salute Mentale e Fisica e Medicina Preventiva

PHD SCHOOL IN LIFE SCIENCES

PHD PROGRAM IN
CLINICAL AND EXPERIMENTAL MEDICAL SCIENCES
XXXIV Cycle

Scientific disciplinary sector: MED/14

Thesis title:
A new *in vivo* multiphoton microscopy based approach to study the peritoneal membrane changes induced by peritoneal dialysis

TUTOR

Prof. Francesco Trepiccione

CANDIDATE

Dr. Luciano D'Apolito

Coordinator of PhD course
Prof. Armida Mucci

Academic year 2020-2021

SUMMARY

Abstract

Peritoneal dialysis (PD) is a renal replacement therapy that allows the elimination of metabolic waste products and excess body fluid through the peritoneal membrane.
Glucose is the most used osmotic agent into the dialysate and by reclaiming water into the peritoneum favor by convection the excretion of toxins. Direct chemical diffusion is an additional clearance mechanism that occurs between the blood stream and the dialysate. However, high glucose concentration in the dialysate is considered crucial for the pathogenesis of peritoneal fibrosis, angiogenesis, epithelial to mesenchymal transition (EMT). These are the event that mostly contributes to the peritoneal membrane aging and fibrosis resulting in ultrafiltration and clearance failure.
The pre-clinical research in this field suffers for the absence of valid and reproducible *in vivo* systems and so for it is limited to *in vitro* system of mesenchymal or endothelial cells lines.
So, this PhD project aims to achieve these purposes:

1. setting of a method to investigate *in vivo* all the components of the peritoneal membrane by mean of two photon microscopy;
2. testing the role of oleuropein (Ole) as agent preventing the senescence of the peritoneal membrane;
3. testing the role of glucose sparing dialysate on the senescence of the peritoneal membrane;
4. setting of a method for *in vivo* measurements of blood flow velocity inside peritoneal vessels.

Multiphoton microscopy allows *in vivo* evaluation of the framework of mesothelial cells and their underlying layer of collagen fibers that contributes to the sub-mesothelial space.
We have implemented the surgical procedure in order to optimize the stability of a flap of parietal peritoneum to directly observe at the scope.

In order to test the sensibility of our approach to the evaluation of the senescence of peritoneal membrane, we tested the effect of Ole in preventing the damage induced by

standard dialysate with high glucose concentration. Ole reduced both the thickness and the organization of the collagen fibers and the vascular network, including the number of branch points.

Another treatment carried out using a glucose sparing solution had shown beneficial effects against the triggering of fibrotic and angiogenetic phenomena induced by conventional dialysate. This novel formulation could represent a valid substitute for conventional solutions due to the better bio-compatibility.

In vivo multi-photon microscopy allows the continuous acquisition of the movement of erythrocytes inside the vessels and has high accuracy in the measurement of blood flow.

The measurements on the flow of vessels of microcirculation (arterioles, capillaries, post-capillary venules) determined that exposure to hypotonic solutions increased significantly the flow in large-diameter vessels due to better permeability and hemodilution.

The developed method has potential for a dynamic and reliable *in vivo* approach. Studies are ongoing to validate the effects of drugs and dialysates with different osmotic and electrolytic compositions on the dialysis capacities of the peritoneal membrane and on the blood flow in peritoneal capillaries.

This method offers great potential for testing new pharmacological approaches aimed at preserving the structural and functional integrity of the peritoneum and for the validation of substances, such as natural extracts with beneficial effects against the damage induced in the long term by conventional dialysis solutions.

Introduction

1. Peritoneal Dialysis

Peritoneal dialysis (PD) is a renal replacement therapy for patients with end stage kidney disease (ESKD). PD uses the peritoneum as an exchange membrane and consists of the cyclical introduction of solution (dialysate) inside the abdomen through the permanent implantation of a peritoneal catheter connected, via a connection device, to the dialysate bags (Figure 1). Exchange of solutes and removal of fluid from the blood in the peritoneal capillaries takes places through the infusion of 2 liters of a PD solution into the peritoneal cavity [1].

This therapy can be done manually, in the case of continuous ambulatory peritoneal dialysis (CAPD) or through the use of a machine (named cycler because allow cycle of infusion and drainage of dialysate) in the automated mode (APD).

The effluent is then drained after a dwell time (usually 4 hours) before fresh dialysate is re-infused manually (CAPD). This exchange can be repeated up to 4 -5 times per day. With APD the cycler infuses fresh dialysate every hour or fraction of hours along the entire night (8 hours).

Shorter dwell time allows patients to maximize small solute clearance while retaining enough dialyzed glucose to allow for adequate ultrafiltration [2-4]. However, it should be noted that while the clearance of small solutes is improved with shorter cycles, the clearance of medium molecules may be worsened, as these molecules diffuse poorly across the peritoneal membrane and take longer to equilibrate [5]. These recommendations for fast transporters have been endorsed by the International Society for Peritoneal Dialysis (ISPD) [4], the UK Renal Association (UKRA) [6] and the European Best Practice Guidelines (EBPG) [6, 7].

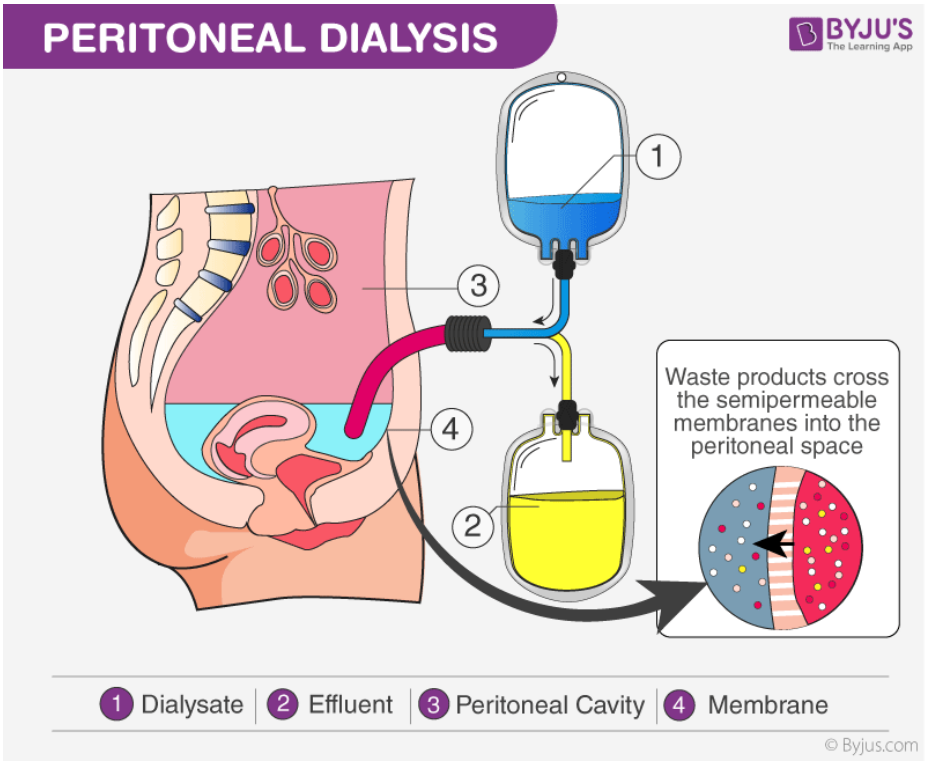

***Figure 1**- Peritoneal dialysis treatment. byjus.com/biology/peritoneal-dialysis/*

PD solutions are composed by physiological concentrations of chloride, calcium, sodium, magnesium, a pH buffer (lactate and/or bicarbonate) and an osmotic agent to remove excess fluid from the patient via both the water-exclusive aquaporin and the small-pore, solute-coupled fluid pathways [8]. The main osmotic agent used in standard PD solution is glucose, due to its efficiency, low cost and acceptable safety profile.

As kidney function fails, waste products, such as urea and creatinine, accumulate in the blood. To remove this waste, peritoneal dialysis is used to filter the blood inside the body.

The peritoneal membrane allows waste products and excess body fluid to pass from the blood to the dialysis solution. This waste is then excreted when the solution used is drained from the abdomen [9]. The amount of waste and excess fluids that are removed from the blood stream is affected by a variety of factors, including the underlying disease causing the ESKD and intrinsic features of the peritoneal membrane as permeability to water or solutes and blood supply among the most important. One of the unmet questions in the field is that the quality of the peritoneal

membrane cannot be predicted before starting this therapy, basically after catheter implantation and starting the exchange.

2. Peritoneal Dialysis burden in ESKD

Chronic kidney disease (CKD) is a progressive, permanent and irreversible reduction in kidney function. This condition is the last stage of long-term (chronic) kidney disease and involves a gradual loss of kidney function.

In this condition when the kidneys function for less than 10% of their potential, the patient reaches a stage of renal function so reduced that it can no longer guarantee a state of well-being or even survival and such as to require replacement therapy of the kidney function that can range from peritoneal dialysis, together with kidney transplantation from a living or deceased donor (not always possible) to extra-corporeal dialysis or hemodialysis (HD).

10% of the world population is affected by chronic kidney disease. Estimates to 2030 speak of 5.4 million in Italy [10].

Currently over 60% of patients who start dialysis every year are over 72 years old. The number of patients requiring the above mentioned dialysis treatments is estimated to be 1.4 million globally and is growing annually with an 8% share [11].

CAPD is the main peritoneal dialysis approach used in developing countries, less so in more developed countries [12].

In Italy, the data of the Italian Dialysis and Transplant Registry report about 4,500 patients undergoing treatment with peritoneal dialysis, about 42,000 undergoing hemodialysis and over 27,000 with kidney transplantation.

Looking at dialysis alone, 11% of the world population on dialysis is subjected to PD [10].

Despite the numbers, PD compared to hemodialysis is physiologically less stressful, does not require invasive vascular access, allows to patients greater flexibility, since it

can also be performed at home, is well tolerated by the patient, guaranteeing a better quality of life, but above all, it is cheaper [13]. Furthermore, PD is more green and eco-friendly than hemodialysis due to the lower use and waste of water [14].

However, PD is a method that seems limited due to the modest transport capacity of the peritoneal membrane. Its real effectiveness and the rational use of PD continues to be closely linked to the use of adequate mathematical models, such as that of the three-pore model (TPM).

Like all therapies, PD needs new developments and outcomes from world of research. For greater reliability of the therapy it will be necessary to focus on:

- Development of new methodologies to predict, identify or monitor the physiology of peritoneum or injury;
- Evaluation of peritoneal membrane function testing new strategies;
- Therapeutic interventions to protect the peritoneum;
- Alternative solutions or device development to optimize clinical management of therapy.

3. Peritoneal Membrane

The peritoneal membrane is a thin layer that lines the abdomen. It is a semi-permeable structure that reduces friction between the abdominal organs by producing lubricants and surfactants [8]. It covers the peritoneal cavity, covering a surface that is close to that of the skin [15] (about 1.73 m^2 for a person of 70 kg). Peritoneal membrane is the largest and the most serosal membrane of the human body important for maintaining an intra-abdominal homeostatic equilibrium and characterized by a particular structure and function. It plays an important role in maintaining homeostasis in the abdomen and pelvis. It facilitate the movement of the intra-abdominal organs, it contributes to the fluid exchange mechanism and play a role in the immune response [16].

Given its extension, it is not possible to measure the total blood flow directly, but an estimate can be obtained by means of gas (H2) clearance techniques [9]: 100-150 ml / min in adults.

It consists of a parietal layer (which represents 10% of the entire peritoneal membrane), the outermost layer which covers the internal surface of the abdominal-

pelvic cavity wall and of a visceral layer (90%), the innermost which covers most of the viscera contained within the abdominal cavity.

Between these two layers there is the peritoneal cavity which is completely closed and filled only by a small amount of serous fluid (about 50 mL) which acts as a lubricants allowing the two layers to flow between them without excessive friction and favoring the movement that the organs perform during their functions. The visceral and parietal peritoneum have a similar structural composition consisting of three distinctive layers: the mesothelium, a basal lamina and the sub-mesothelial stroma [17] (Figure 2). Mesothelial cells are from mesodermal origin, but possess both epithelial and mesenchymal features [17]. Three types of mesothelial cells have been described: flattened mesothelial in intestinal, omental and parietal mesothelial, a cuboidal cell type in visceral peritoneum, an intermediate mesothelial cell type in the diaphragm and gastric peritoneum. This morphologic heterogeneity suggests the different function of the mesothelial cells at different anatomical locations.

Mesothelial cells contain microtubules and microfilaments, glycogen, vesicles and vacuoles, few mitochondria, a poorly developed Golgi apparatus and little rough endoplastic reticulum (RER).

On top of these microvilli, a glycocalyx is present, which creates a stagnant fluid layer consisting of proteoglycans and glycosaminoglycans to promote lubrication [18].

Those cells have well-developed cell–cell junctional complexes including tight junctions, adherens junctions, gap junctions and desmosomes [19]. The basal lamina supports the mesothelial cells at the basal surface. It consists of a layer of extracellular matrix with a thickness less than 100 nm, which is mainly composed of collagen type IV and laminin. The collagen type IV fiber network stabilizes the basal lamina, whereas laminin interacts with the mesothelial cells via β1 integrins. However, binding of mesothelial cells to the basal lamina is not strong and even minor injuries can cause cellular detachment [16]. Submesothelial stroma, also called interstitium, is composed of collagen type I fibers, laminin, fibronectin, proteoglycans, glycosaminoglycans, fibroblasts, adipocytes, blood and lymph vessels and nerves [20]. The composition and thickness of interstitium varies with age and presence of disease [17]. The sub-mesothelium is highly perfused and innervated and is considered important for the

evaluation of peritoneal fibrosis markers, which is why it is used in experimental models.

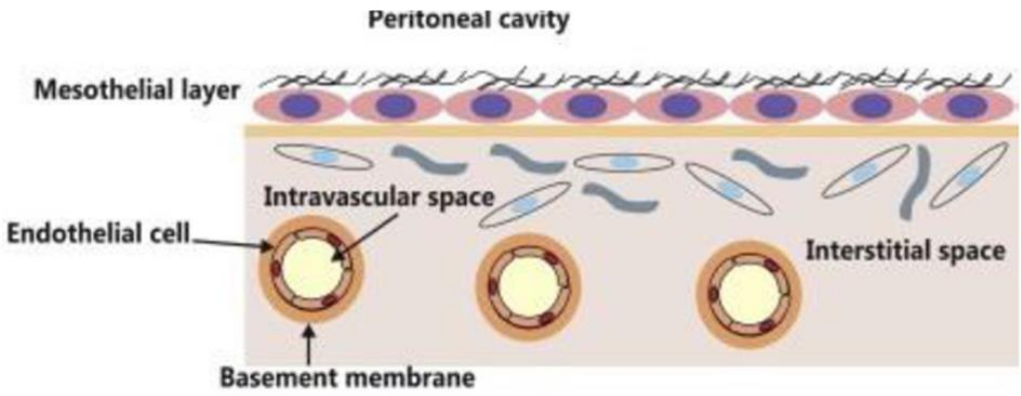

Figure 2- Graphical representation of the peritoneal membrane from the histological point of view. There are: the layer of epithelial cells in close contact with each other, the basement membrane that separates the first from the sub-mesothelium (richly vascularized) [11].

The vascularization of the peritoneal membrane differs according to the serous layer taken into account: the parietal one is supplied by the branches of the iliac, lumbar, intercostal and epigastric arteries; while the visceral one is supplied by the branches of the arteries of the splanchnic system. These arterial vascular structures branch into arterioles that form a large anastomotic network [21]. Instead, venous drainage is guaranteed by the veins: superior mesenteric and inferior mesenteric, which, following the course of the portal vein, drain the blood to the liver.

It is also of vital importance that a microvascular perfusion suitable for the organism's requirements is maintained. It is influenced by various factors: physical (hyperthermia and pressure) and chemical.

The permeability of the peritoneal membrane depends on that of the capillaries, the blood perfusion rate and the diffusivity of the solutes within the interstitial tissue. This is how the so-called “Effective peritoneal surface area” (EPSA) is configured, which is fundamental for the transport of molecules [8]. The peritoneum is a heteroporic membrane, through which the solutes are transported by diffusion and convection mechanisms that depend on the EPSA, the permeability of this area and the transmembrane pressure and which are closely linked by the concentration gradient.

Diffusion can be simple or facilitated, i.e. mediated by transporters, and does not require the use of the ATP molecule, since it occurs according to gradient, but is very selective towards low molecular weight molecules. Convection, finally, has the ability

to remove molecules with a higher molecular weight and consists in the entrainment of solutes which occurs together with ultrafiltration. It is secondary to the hydrostatic pressure, to which the water is subjected, dragging solutes with it.

4. The three pore model

PD is a method that seems limited due to the modest transport capacity of the peritoneal membrane. Its real effectiveness and the rational use of PD continues to be closely linked to the use of adequate mathematical models, such as that of the three-pore model.

To improve the therapeutic treatment under consideration, mathematical and experimental models are used. They are identified in the Pyle-Popovich model and in the Rippe-Haraldsson model. The first, also called "Model with homogeneous pores", takes into account in depth the personal data and parameters such as: Creatinine Clearance (CrCl), Kt / V (where "K" stands for clearance, "t" for time and "V" for the volume of distribution of urea, necessary for the assessment of dialysis adequacy), the amount of protein catabolized by the patients (the nPCR, expressed in g / kg / day), the GFR (expressed in ml / min), the class according to the Peritoneal equilibration Test (treated later).

From these parameters, information is obtained in terms of D/P of urea, concentration of glucose and ultrafiltration, MTAC (Mass Transfer Area Coefficient) of urea, creatinine and glucose, and of permeability of the peritoneal membrane [22]. MTAC is equal to the membrane permeability product for a given solute and the effective surface area. The mass transfer area coefficient is the inverse of the diffusive resistance

and represents the maximum diffusive clearance that could be obtained in the absence of both convection and accumulation of the solute in the dialysate [23].
The simulation of the results of dialysis adequacy and of the therapeutic target is guaranteed in two ways: the "Regimen", in which a hypothetical dialysis treatment is

prescribed and from it weekly results are obtained such as CrCl, Kt / V, UF and absorption of glucose, regardless of the type and volume of dialysis solution [22]; the "Optimise", on the other hand, is used to obtain a nutrition target, UF and Kt / V, outlining four prescription methods and guaranteeing results in terms of day and night dialysate volume and clearance [22] .
The three-pore model (TPM) of peritoneal transport, proposed by Rippe-Haraldson describes the capillary membrane as a primary barrier that determines the amount of solute it carries into the interstitium and into the peritoneal cavity [24].
Given the theoretical and applicative complexity, currently few mathematical models are used for the rational prescription of PD.
Only the Pyle-Popovich and Rippe-Haraldsson models (three-pore model) have been made available thanks to the creation of partially simplified software [25-27].
Some concepts are common to all these application models. In both models the peritoneal membrane is considered to have a minimal thickness and with three types of cylindrical pores (hence the name), arranged in parallel (Figure 3).
The three-pore model has proved to be one of the most similar to the physiological condition of the peritoneum. In fact, according to the conceptual basis of the theory, PD exploits diffusive, convective transport and osmosis via the highly vascularized peritoneal membrane [28].
The small pores are represented by interendothelial gaps (40-50 Å in diameter) through which small solutes can enter. Any pathological condition can determine an increase in capillary perfusion, as well as in the number of small pores and, consequently, an increase in the transport of small molecules. The large pores (with a diameter greater than 150 Å), on the other hand, correspond to gaps between endothelial cells of the venules capable of guaranteeing the transport of higher molecular weight particles, such as immunoglobulins; it seems that the components of the sub-mesothelial

interstitium influence its passage [8]. These gaps correspond to channels that are located between protein bridges suitable for cell adhesion.

Finally, the ultra-small pores (with a diameter smaller than 5 Å) are represented by AQP-1 (aquaporin-1) and localized at the endothelial level. They play an important role in the regulation of the osmotically active transport of solutes. In fact, it has been shown that 50% of the total transcapillary ultrafiltration (the so-called "UF coefficient") occurs through AQP-1[29]. In fact, the expression of AQP-1 in the plasma membrane of endothelial cells lining peritoneal capillaries and venules suggested it may have a role in water transport during PD. This hypothesis is confirmed by the development of experimental models of PD and their application to transgenic mice devoid of water pores. Here complete or partial deletion of AQP-1 gene resulted in a 50% decrease in net UF and a complete abolition of water permeability, when hypertonic glucose is used as osmotic agent [29-31]. This is the basis of the dialysis procedure, in which the glucose, contained in the solution used, guarantees an osmotic pressure gradient that allows the water molecules to pass through the ultra-small pores, contributing only to 1-2% of the coefficient of ultrafiltration. It is necessary to count moreover, the transendothelial transport system by means of intracellular membrane vesicles, present in high number in omental endothelial cells [32]. During dialysis, the permeability of the peritoneal membrane allows the transport of solutes and water inside and outside the peritoneal cavity. However, it is not easy to study this convective transport due to the fact that the ultrafiltration (time-dependent) and absorption by the lymphatic vessels (predominant mechanism) occur simultaneously. The first is supported by the osmotic and oncotic gradients that are established between the blood and the peritoneal cavity [33]. The second is given by the pressure exerted by the solution injected through the cavity. A hypothesis was developed to explain the simultaneous mechanism of ultrafiltration and absorption of intraperitoneal fluids (Figure 4). This mechanism, in fact, would occur in different areas: the absorption would take place between two areas of the peritoneal membrane suitable for ultrafiltration and, therefore, would serve to reduce the osmotic load and, subsequently, the volume of the fluid itself, with a speed determined by the intracavitary pressure of the fluid.

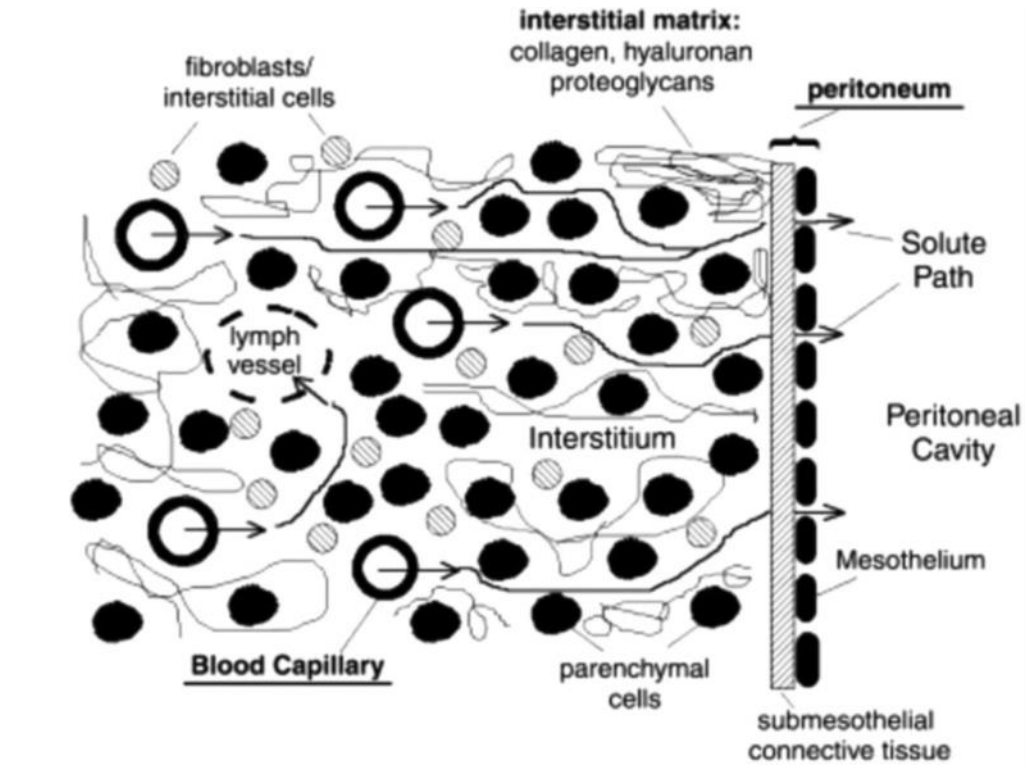

Figure 3- Representation of three types of pore on the endothelial membrane of capillaries that supply the peritoneal membrane. Distributed model describes the peritoneal barrier as blood and lymph capillaries spatially distributed within a peritoneal tissue space (made up of parenchymal cells, interstitial cells and matrix molecules) [25, 34].

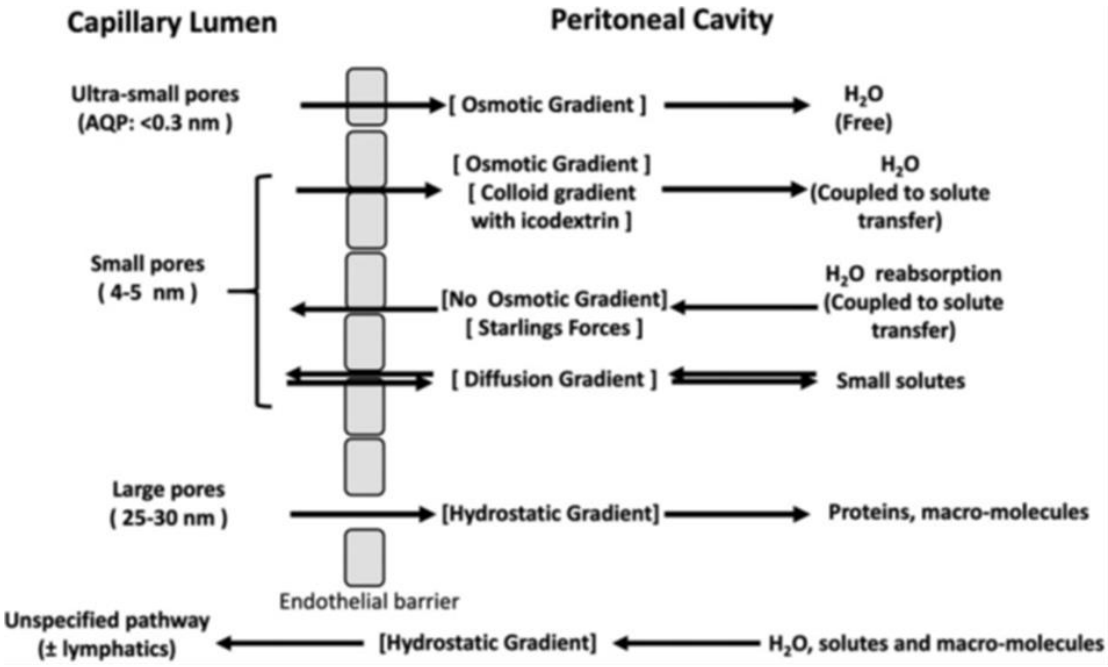

Figure 4- Graphical representation of the theory, according to which ultrafiltration and absorption occur simultaneously in adjacent areas of the peritoneal membrane, during dialysis [35].

In addition, the use of hyaluronic acid inside the dialysis solution allows to counteract the absorption process, reducing the speed and extent of the flow between adjacent areas of the peritoneal membrane [36]. This theory could bring an improvement in the dialysis quality in terms of time and frequency of exposure of the peritoneal surface to the solution, thus increasing the speed of transport of the molecules.

Furthermore, three pore model allows to understand how the peritoneal tissue can guarantee the "Sieving", the selectivity in the transport of solutes. The sodium sieving coefficient is influenced by numerous factors: it is low in patients undergoing peritoneal dialysis (due to a loss of Aquaporin-1 [37]. This parameter corresponds to the Na + measurement in the dialysate after at least 1 hour of dwell time during a high concentration 3.86% glucose/4.25% dextrose exchange [35]. The exchange is maximal between 1 hour and 2 hour and represents the rapid influx of free water into the peritoneal cavity via AQPs. The test is undertaken at 1 hour so as to minimize the amount of sodium diffusion through the small pores. It can also be expressed as the sodium sieving ratio:

$$1 - [Na+]t = 60\,min/[Na+]t = 0$$

The normal range is established from a cohort of 758 incident patients and is approximateky 0.07, range 0.055-0.085 [35].
Then sodium variations after 1 hour of dwell time are due to the water permeability through AQPs.
Furthermore, another factor that influences this selectivity is the Ultrafiltration rate, which, if low as for long-term peritoneal dialysis, determines an increase in the sodium "sieving" coefficient most likely due to the reduced convective transport of the molecules [37].

5. The transport status of the peritoneal membrane

A test has been implemented to evaluate the clearance ability of the peritoneal membrane. This is called Peritoneal equilibration test (PET), proposed by Twardowski in 1987 [38, 39].
Historically, it has been developed three types of tests, as shown in Table 1, using dialysate at different concentration of glucose and different dwell-time:

- traditional PET with 2.5% glucose dialysate for 4 hours;
- mini-PET with 3.86% glucose for 1 hour;
- mod-PET (modified) with 3.86% glucose for 4 hours.

These tests were compared on the basis of various parameters (D / P creatinine, D / D0 glucose and UF) and it was concluded that the first remains the most reliable test to perform, while the third is very useful to obtain information on free water transport and UF [40].
The D / P of a solute (such as creatinine and sodium) is an index of the rate at which equilibrium is reached between dialysate and plasma, while the D / D0 of glucose is based on the concentration of the glucose molecule in the dialysate before intracavitary administration and is closely linked to the fact that the glucose itself is absorbed by the plasma dialysate.
Based on the kinetic of D/P creatinine and D/D0 glucose it is possible to discriminate four different depuration profiles: high (H), high average (HA), low average (LA) and

low transporters (L) (Figure 5). This classification has clinical practice impact because it allows to refine the most appropriate therapy for PD patients. As shown in Table 2, low transporters can be well maintained in ways that allow for longer residence times, such as continuous ambulatory peritoneal dialysis (CAPD) [2, 41]. Conversely, fast transporters are generally good candidates for automated PD (APD) regimes that use shorter dwell times.

High transporters generally have a D/P creatinine greater than 0.80 [38, 39]. These patients achieve rapid and complete equilibrium of small solutes due to a larger functional surface area and greater membrane permeability [42, 43]. However, high transporters quickly lose their osmotic gradient and achieve poor ultrafiltration because glucose is rapidly absorbed into the blood. Therefore, high transporters have the highest D / P ratios for creatinine and urea, but the lowest D / D0 glucose. Unlike high transporters, low transporters have the lowest D / P ratios for creatinine and urea, where creatinine D / P is typically less than 0.55 [39].

These patients achieve a slower and less complete equilibrium for small solutes. On the other hand, low transporters have a high D / D0 glucose ratio due to the slower transport of glucose across the peritoneal membrane. As a result, they can support their osmotic gradient for longer periods and thus obtain a better ultrafiltration [44]. Patients who are high average or low average transporters have moderately high or moderately low diffusion and ultrafiltration features [44]. However, it is important to remember that these cut-offs may vary based on geographic area, PD time and other factors related to the tests or population studied [2].

	Membrane test			
	Classic PET[46]	Modified PET[a] (SPA)[93]	Mini-PET[b]	Double mini-PET[43]
Membrane characteristic	2.27% 4 h	3.86% 4 h	3.86% 1 h	1.36% and 3.86% 2 × 1 h
Solute transfer	Yes	Yes	Yes (at 1 h)	Yes (at 1 h)
Ultrafiltration capacity	Yes	Yes		Yes (at 1 h)
Sodium dip (free water transport)		Yes	Yes	Yes (Also calculates the proportion of UF via AQP and small pores)
Osmotic conductance				Yes
Net fluid reabsorption				
Effective lymphatic reabsorption		Yes (Calculated from instilled macromolecule)		
Protein Clearance		Yes (Uses proteins of different molecular weights)		

Table 1- Summary of different peritoneal function tests and the membrane characteristics they measure [35].

Transport Type	D/P Creatinine	Solute Clearance	Ultrafiltration	Preferred Regimen
High (Fast)	>0.80	Excellent	Poor	APD regimens (eg, NIPD, CCPD, PD Plus)
High-average	0.65-0.80	Adequate	Adequate	Any regimen
Low-average	0.55-0.64	Adequate/ Inadequate	Good	Standard dose CAPD
Low (Slow)	<0.55	Inadequate	Excellent	High dose, longer dwell CAPD (or hemodialysis)

**PET: Peritoneal equilibration test; APD: Automated Peritoneal Dialysis; NIPD: Nightly intermittent PD; CCPD: Continuous cyclic PD; CAPD: Continuous ambulatory PD*

Table 2- Table representation of the stratification (obtained by PET) of patients based on the D / P parameters of Creatinine, Solute Clearance, UF and related type of dialysis treatment suitable for the

types of transport. https://advancedrenaleducation.com/wparep/article/transport-status-classification-and-implications

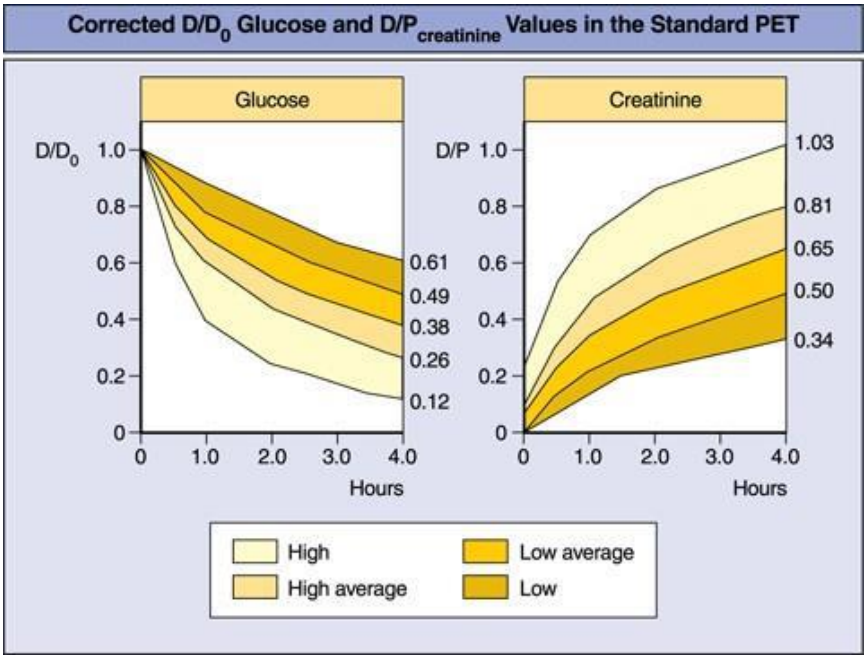

Figure 5- Graphical representation of the permeability curves based on the D / D0 parameters of Glucose and D / P of Creatinine and contextual classification of the patients into the four categories mentioned [45].

6. Peritoneal Dialysis: Role of AQP-1

The transport of water molecules across the peritoneal membrane occurs by means of a transcellular mechanism thanks to the presence of ultra-small pores. These are to be identified in the so-called Aquaporins, of which Aquaporin-1 (AQP-1) is predominant in the kidney and red blood cells, but above all in the mesothelial cells and in the sub-mesothelium (especially in the endothelial cells of the capillaries and post-capillary venules) [46].

AQP-1 is a membrane channel specific for water molecules and is a homotetramer of ~ 28 kDa, of which each subunit consists of six transmembrane domains arranged in

an alpha-helix, and delimits a central hourglass-shaped pore (about 3 Å in diameter) (Figure 6). Crystallographic studies have investigated the function of this channel, attributing to it a diffusion speed of three billion water molecules per second [47].

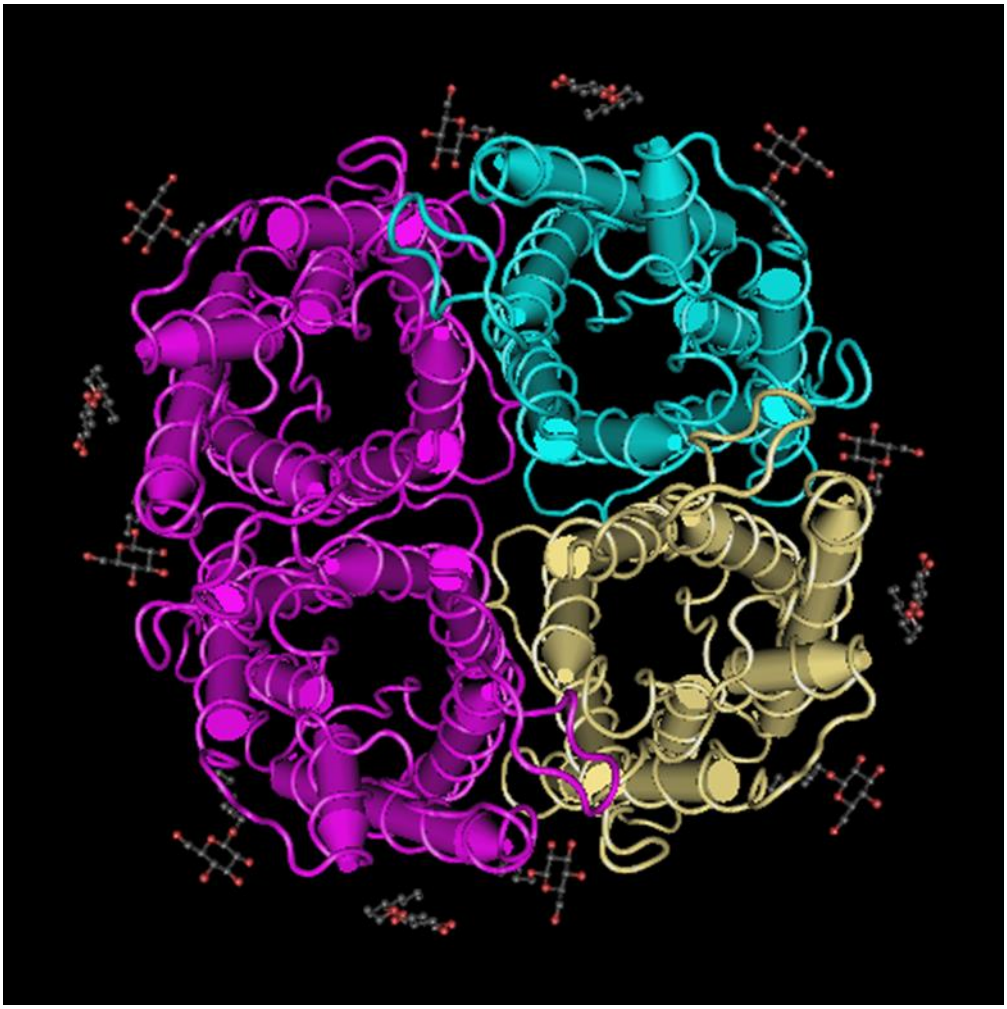

Figure 6- Crystal structure of AQP-1 water channel [48].

Furthermore, it has been observed that AQP-1 knockout mice show a reduction in osmostically induced water transport and that, therefore, these channels play an important role in the transport of water molecules during the dialysis procedure [49] towards the peritoneal cavity, but not in the absorption and alterations of the peritoneal tissue.

The important function of AQP-1 expressed in the endothelial cells of the peritoneum was demonstrated for the first time in a rat model [50]; the inhibition of AQP-1 by HgCl2 in rats induced a reduction of 60-80% in transcellular water flow and an inhibition of Na + sieving. While the expression and function of AQP-1 in endothelial cells is well demonstrated, the expression in mesothelial cells has long been debated [46].

Despite this, a constitutive expression of AQP-1 in human peritoneal mesothelial cells has been demonstrated by other authors. AQP-1 is reported to be abundantly present in human peritoneal mesothelial cells and is released via exosomes into dialysis fluids during PD [51].

The observation that mesothelial AQP-1 closely correlates with ultrafiltration of water and with sodium sieving during PD [51], suggests that mesothelial AQP-1 significantly contributes to its efficiency.

Hence the consideration of AQP-1 as a target to modulate the transport of water in dialysis and to obtain a better peritoneal exchange capacity. It is possible to study the function of AQP-1 by means of the PET which measures the volume of the dialysate together with the sodium concentration [52]. From it is possible to obtain an estimate of the free volume of water (the so-called “Water Free Fraction”) by subtracting from the total volume of water passing through the ultra-small pores. The sodium concentration is calculated with the ratio between the sodium concentration in the dialysate and the plasma.

A recent study proposed that the efficiency of peritoneal dialysis depends on ultrafiltration, the ability to remove excess water from the body [53]. Among patients starting treatment with peritoneal dialysis, there is broad variability in ultrafiltration. Such variability influences dialysis prescriptions and outcomes, but its causes are poorly understood. Variation in the gene encoding aquaporin-1, has been proposed as one contributing factor. In fact, a common variant in AQP-1 was associated with decreased ultrafiltration, then high transporter patient, and an increased risk of death or technique failure among patients treated with PD [53].

In condition of UF failure, the expression of AQP-1 tends to increase at the level of peritoneal tissue (perhaps as a compensatory mechanism, but in any case not sufficient to counteract the effect of fibrosis and subsequent sclerosis) [54].

This regulation has been carefully studied and it has been deduced that it can also be influenced by some molecules. Among them, corticosteroids certainly stand out: the gene, which codes for AQP-1, contains in the promoter region the elements of responsiveness to the steroids themselves [55] and its activation by the receptors of the latter leads to an increased sodium sieving and obviously UF through ultra-small pores. For this reason, the research for molecules that act as agonists of AQP-1 themselves has been proposed, in such a way as to increase the flow of water through them [56].

A derivative of Arilsulfonamide (AqF026) associated with furosemide enhances the function of AQP-1 by 20% [57]. Finally, it was hypothesized to monitor the free transport of water and the "sieving" of sodium to assess the severity of peritoneal fibrosis: the water molecules would most likely interact with type I collagen fibers, present at the interstitium level of sub-mesothelium and this would result in a reduction in the water flow through the mesothelium [58].

During dialysis exchange, both ultra-small and small pores contribute to the transport of water molecules, which occurs in the first two or three hours diluting the sodium concentration in the dialysate. [59, 60]. In the long term, the ultrafiltration rate is reduced and an equilibrium is established between the sodium of the intraperitoneal fluid and the serum: all this happens after the total absorption of glucose in the vascular compartment. Furthermore, as regards the transport of other solutes, it is necessary to deal with calcium and magnesium. Calcium, in fact, given its concentration in the dialysate slightly higher than that of the plasma, reaches the lumen of the vessels; the same goes for magnesium. Potassium, on the other hand, is not contained in the dialysis solution and for this reason the predominant mechanism for the transport of this electrolyte is certainly diffusion [61]. Usually, in the fluid used during peritoneal dialysis, there is lactate which acts as a "buffer", being absorbed into the blood and converted into bicarbonate. This process reduces the loss of bicarbonate, which is removed from the plasma during PD [62].

7. Changes of peritoneum during Peritoneal Dialysis

Peritoneal dialysis is limited in time. Usually this technique is efficient for 2.5 - 3 years representing a good bridge towards kidney transplantation. PD failure is usually associated to severe histopathological changes of the peritoneal membrane. Conventional dialysis solutions are mainly made up of highly concentrated glucose and so for have a low biocompatibility with the peritoneal membrane, given their osmolality, their lactate content, glucose degradation products (including formaldehyde, Acetaldehyde, glyoxal, methylglyoxal, 3-deoxy-glucosone, 3,4-deoxyglucosone-3-ene and 5-hydroxymethylfuraldehyde), their acid pH (it would have two effects: the first, the reduction of the fibrinolytic activity and the second, the increasing of coagulation activity) and AGEs ("Advanced glycation end-products") [63].

Glucose is reported to stimulate the secretion of pro-inflammatory molecules by the mesothelial cells, including the TGF-β1 "Transforming growth factor-β1", the MCP-1 "Monocyte chemoattractant protein-1" (through the stimulation of TLR-4 / MyD88 / NFkB) and fibronectin [64, 65].

As additional factor, the osmolality of the solution (358-510 mOsm / kg) reduces the proliferation of the mesothelium and increases the production of the TGF- β1. TGF-β1, therefore, stimulates fibrogenesis, angiogenesis (through the secretion of VEGF, Vascular endothelial growth factor) and reduces ultrafiltration in experimental models from rodents [63].

The Renin-Angiotensin System also appears to be involved in this fibrotic process, enhancing the secretion of TGF-β1 and fibronectin and increasing the production of ROS "Reactive oxygen species" [66, 67]. TGF-β1, induces the synthesis of alpha-SMA (Alpha-Smooth Muscle Actin), an additional marker of tissue fibrosis and contractility of fibroblasts [63].

Epithelial cells of the peritoneal membrane are induced by dialysis fluid to produce and release factors that regulate coagulation and fibrosis like t-PA (Tissue Plasminogen Activator) and PAI-1 (Type 1 Plasminogen Activator Inhibitor) [68]. t-

PA plays a role in the deposition of elements of the extracellular matrix, but PAI-1 is considered the most important factor involved in fibrogenesis, as well as the bFGF "Basic Fibroblast Growth Factor", produced by the mesothelium on stimulation of lactate [68].

Further factors involved are certainly the degradation products of glucose, including 3,4-DGE (3,4-dideoxyglucosone-3-ene) (which would seem to determine an alteration of the division of mesothelial cells and an increase in the release of VEGF) and methylglyoxal.

As a result of this inflammation/fibrosis, the mesothelial cells almost completely disappear and the remaining acquire a cuboidal shape, while the lamina propria is thickened and neo-vascularized.

This is closely related to the action of MMP-2, matrix metalloproteinase, which destroys the peritoneal membrane. The angiogenesis is related to the production of type IV collagen by mesothelial cells, an important scaffold for the construction of blood vessels, induced by the release of VEGF [69].

The Advanced glycation end-products (AGEs) accumulate at the epithelial, sub-mesothelial level and in the thickness of the vessel walls and contain and interact with their receptor (RAGEs, expressed in these same tissues), causing an increase in the production of IL-6, VEGF, VCAM-1 and inducing apoptosis [70].

At histology, the peritoneal membrane thickness is characterized by deposition of collagen type I fibers inside the sub-mesothelium layer, and increased and branched vasculature as proven by positivity to CD-31, GLS-1 (Glutaminase-1) and VEGF-A (Vascular Endothelial Growth Factor-A), important for angiogenesis, proliferation and migration of endothelial cells (Figure 7) [71].

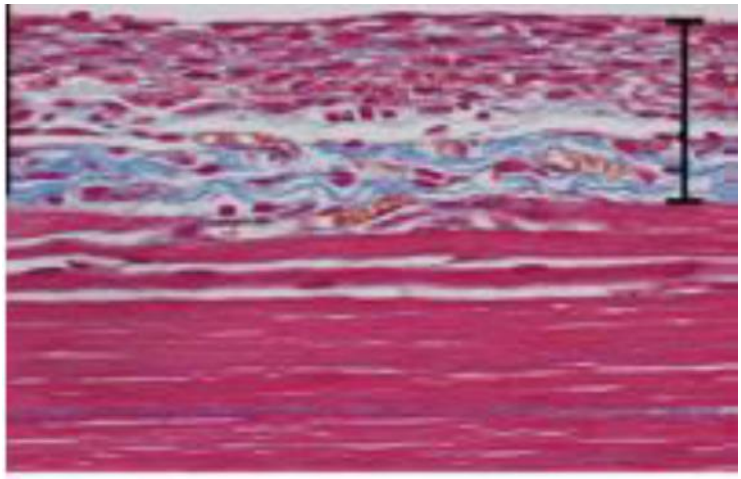

Figure 7- Representation of the histo-pathological analysis of peritoneal membrane tissue, which describes the thickening of the tissue (both of the epithelial and sub-mesothelial components) [71].

An additional damage at vessels level is the hyalinization of the walls of capillaries and post-capillary venules which undergo a process of hyalinization (PHV, Peritoneal Hyalinizing Vasculopathy) with thickening of the basement membrane that induces the narrowing and/or occlusion of the vascular lumen leading to ultrafiltration failure (Figure 8).

This alteration is most likely due to the increase in synthesis and the reduction of the extensibility of type 4 collagen fibers, as a result of the cross-linking that the AGEs themselves are able to form [72].

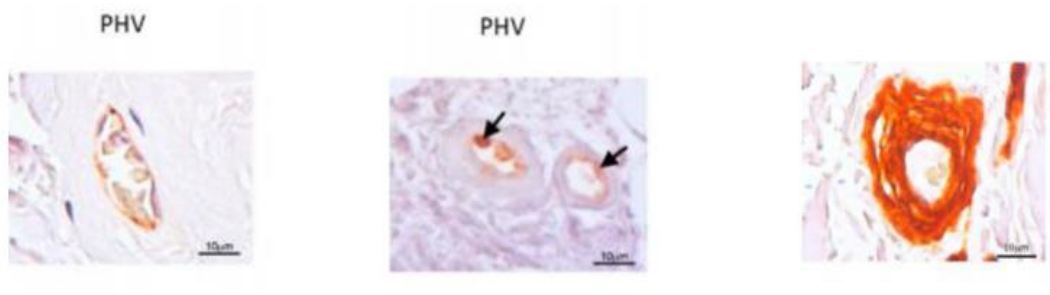

Figure 8- Graphic representation of the pathological analysis of the sub-mesothelial vascular structures during PHV. On the left, there is a reduced CD-31 immunohistochemical positivity in endothelial cells; in physiological conditions there is a more intense positivity. In the center, there is a positivity to the nuclear Smad3 factor in the endothelial cells; in physiological conditions it is not present. On the right, staining that highlights the pathological deposition of type 4 collagen molecules to the basement membrane [72].

Finally, chronic exposition to conventional dialysates results in a process that is called "Mesothelial-to-Mesenchymal transition" (MMT), which corresponds to a real epithelial to mesenchymal transition (EMT). The MMT process normally occurs in some pathological conditions such as wound healing and in tumor progression [73]. It occurs reversibly in the early stages of peritoneal fibrosis and, during this process, mesothelial cells lose their polarity and their epithelial phenotype due to the lack of E-cadherin synthesis [74] (Figure 9).

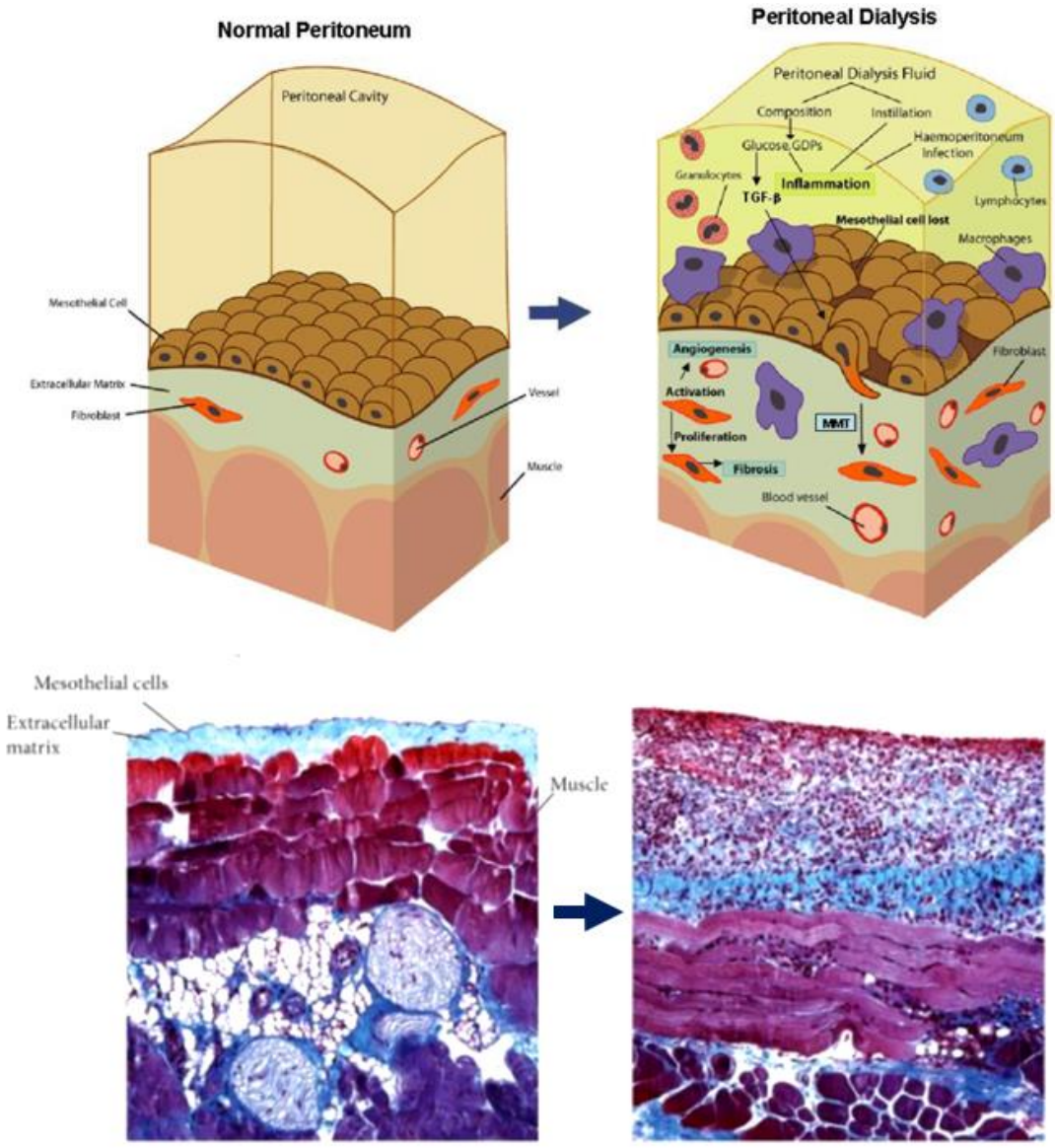

Figure 9- Graphical and histological representation of the Mesothelial-Mesenchymal Transition. On top left, normal mesothelial tissue can be seen, in the absence of alterations in the basement membrane and sub-mesothelial interstitium. On top right the elements of the dialysis fluid together with infections and haemoperitoneum recruit inflammation cells (such as granulocytes and macrophages) which produce and secrete TGFβ-1, inducing fibrosis. The Mesothelial-Mesenchymal Transition leads to the transformation of mesothelial cells into fibroblasts that lay extra-cellular matrix (the sub-mesothelial layer is thickened) and stimulate angiogenesis. Below the corresponding histological condition [75].

The overall changes in the epithelial component of the peritoneal membrane is compensated by the acquisition of mesenchymal functions, including deposition of extracellular matrix (in particular deposition of collagen fibers type I and IV) and is associated with the action of IL-6, in turn released on the effect of IL-17A. Furthermore, IL-17A could be a pharmacological target able to slow down the MMT process [76]. On the other hand, cell migration within the sub-mesothelial tissue is favored by the destruction of the basement membrane by the secretion of Metalloprotease-2 and 9 by various cytotypes (fibroblasts, endothelial cells and inflammation cells).

One of the clinical correlate of an aberrant activation of the mechanism of fibrosis is the EPS (Encapsulating Peritoneal Sclerosis), which corresponds to massive fibrotic state of the peritoneal membrane [77]. When EPS is diagnosed the peritoneum function is definitely impaired both for toxins clearance and for ultrafiltration.

The changes in the peritoneal membrane over time cause a transition to different forms of UF failure. Four types of UF failure have been identified [78], the most common form being high EPSA (also referred to as type 1), which is mainly related to neoangiogenic alterations of the peritoneal membrane. The presence of poorly formed capillaries appears to be the cause of a state of increased transport of solutes and water with consequent exhaustion of the osmotic gradient and reduction of Ultrafiltration [79]. A remedy to this complication could be found in the suspension of peritoneal dialysis for a period of 4 weeks [80] or the use of icodextrin or even the pharmacological inhibition of the Renin-Angiotensin-Aldosterone system through ACE-I (Angiotensin converting enzyme) or Sartans [81].

Type two relates to the low osmostic conductance to glucose, with reduced transport of water molecules through Aquaporin-1 and secondary reduction of sodium sieving. In fact, it has been noted that there is actually functional damage, the cause of which is perhaps attributable to oxidative stress and to non-enzymatic glycosylation [82]. For this reason, a possible therapeutic strategy would consist in the administration of drugs that up-regulate the gene expression of Aquaporins-1 [78].

The third type of UF failure corresponds to low EPSA secondary to peritoneal fibrosis and to histological changes of the vessels and above all to Encapsulating Peritoneal

Fibrosis [83]. Therefore, the slowdown as well as the prevention of EPS can be important for restoring this type of UF failure. In conclusion, the fourth type of UF failure corresponds to the increase in the rate of absorption of fluids from the peritoneal cavity, through the lymphatic vessels, and the absence of UF, while using icodextrin, is to be considered an indirect method for diagnosing this condition.

An accredited pathophysiological hypothesis concerns the effect of TGF-β1 on lymphangiogenesis [84]. In this regard, Bethanechol is a cholinergic drug, whose pharmacodynamics involve the capillary structures of the lymphatic vessels, guaranteeing the contraction of the stomata that connect the surface of the peritoneum with the subsomesothelial system and reducing the lymphatic flow [85].

In this context, various strategies have been introduced to deal with the toxicity of glucose and its products. This represents one of the primary objectives of the research that is taking place recently and above all of the following project which aims to outline the strategies for better preserving the peritoneal membrane.

8. Strategy to preserve peritoneal membrane: role of Antioxidants and glucose sparing solutions

The dialysis solutions are not bio-compatible with the peritoneal membrane and trigger a process of oxidative stress and production of ROS (Reactive oxygen species).

For this reason, the suppression of the release of the ROS could improve the quality and duration of the dialysis procedure, thus also presenting a systemic effect with the reduction of cardiovascular risk and damage to the renal parenchyma (especially in ESKD patients). A dietary restriction in terms of salt and water and proper administration of diuretics, for example, could limit the introduction into the peritoneal cavity of solutions with high concentrations of glucose. In fact, it has been observed that, both *in vitro* and *in vivo*, this method significantly reduces the fibrotic and neoangiogenic process [86].

Furthermore, oxidative stress can be reduced by improving the composition of the dialysis solution: starting with a more physiological pH, a higher concentration of

bicarbonate, a lower concentration of AGEs and glucose degradation products, as in solutions composed by icodextrin [86].

Control of lipidemia and blood pressure can also positively affect the function of the peritoneal membrane. In fact, icodextrin manages to have this effect. EPA (Eicosapentaenoic acid) at a dosage of 1.8g for three months has been shown to reduce oxidized LDL and, therefore, the atherogenic risk [87]. Vitamin E (Alpha-tocopherol), with a dosage of 800 I.U./die, and statins also reduce the tendency of LDL to oxidation [88] and can be administered in combinations to obtain a synergistic effect. The statins are defined as pleiotropic, since, in addition to restoring the lipid profile in a more specific way, they perform an anti-inflammatory activity and inhibit MMT and hyalinizing vasculopathy of the sub-mesothelial interstitium [88].

On the other hand, the oral administration of Vitamin C (Ascorbic acid) has a further beneficial effect on hemoglobin levels, so as to be able to normalize the blood count in patients with chronic renal failure. Another molecule can also be introduced per os, the so-called N-Acetyl-Cysteine (or simply NAC), which is defined as an important "radical scavenger".

In fact, in addition to its anti-inflammatory function (inhibition of IL-6 release), at a dosage of 1200mg for two months it negatively affects the production of ROS, activating glutathione and cysteine [89] and thus determining a reduction in the concentrations of oxidative biomarkers such as MDA (Malondialdehyde) and AOPP (advanced oxidation protein products). MDA can be used as a peroxidation index, while the AOPP represents the advanced oxidation products of proteins under the effect of cellular myeloperoxidase. Given its importance, it can be used to prevent EPS, thanks to its functional stability, within the dialysis solution [90]. In addition to these molecules, it is also necessary to include polyphenols, which, taken with the diet, have antioxidant, anti-inflammatory, neuroprotective, cardioprotective properties, act as chelators of heavy metals, as inhibitors of cancerization, as inhibitors of glycation processes and slow down cellular aging, even if at high concentrations they can cause cytotoxicity especially towards isolated primary mesothelial cells, the HPMCs.

They are responsible for the reduction of ROS by acting on the cytotoxic products of the Amadori reaction (a glucose isomerization between an aldose and a ketose), which

are useful for the regulation of the expression of pro-inflammatory genes (such as NFkB) and of iNOS (enzyme with pro-oxidant action) [91]. Polyphenols inhibit apoptosis in the mesothelium, through the inactivation of Caspases 3 and 7, and reduce both the levels of Annexin-V (used to identify cells in an apoptotic state) and those of p53 (modulator of apoptosis), induced by Reaction of Amadori. Among them, tannic acid, resveratrol, quercetin and gallic acid certainly stand out.

Resveratrol is a polyphenolic phytolexin contained in some wines, but especially in vegetables such as peanuts, tea and berries [92]. Quercetin, on the other hand, is part of the flavonoids and is contained in onions, broccoli, apples, grapes, wine and tea. Its function is first of all "radical scavenging", but its anti-inflammatory activity and that relating to the inhibition of the glycation process (especially at the level of the DNA molecule) have also been noted. On the other hand, gallic acid is found in grapes, berries, tea, wine and berries [93] and, in addition to the basic properties already listed, it also plays an antibacterial and antiviral role.

The efficacy of a derivative of gallic acid in direct intra-peritoneal administration was studied: Epigallocatechin gallate.

This molecule significantly counteracts the consequences of high concentrations of methyl-glyoxal, inhibiting the MAPK signal and the nuclear translocation of NFkB [93], stimulated by AGEs. Inhibitory effects were also recorded on MCP-1 (Monocyte Chemoattractan Protein-1) and VEGF.

Finally, tannic acid, mainly contained in wine, grapes, plants and tea, has all the basic functions of polyphenols, but accentuated.

Additional drugs, which can be used for the same purpose, are Beta-mimetics and, with similar effects, Ambroxol [94]. However, unlike polyphenols, they have an indirect antioxidant effect.

Indeed, the peritoneal membrane physiologically secretes a small amount of liquid, named peritoneal surfactant. This derives not only by the passive leakage of fluid from the blood-stream but also from the secretion of the content of lamellar bodies, from the mesenchymal cells. The surfactant works as a lubricant for the peritoneal layers and as also anti-microbial activity. [95]. Beta-mimetics stimulate the production and

secretion of peritoneal surfactant, while Beta-blockers can cause the onset of peritoneal sclerosis in patients undergoing dialysis [96].

Instead, Ambroxol is a very lipophilic molecule, used mainly as an expectorant mucolytic, and, from a pharmacodynamic point of view, it induces synthesis, secretion, but also a reduction in the catabolism of the molecules constituting the peritoneal surfactant (such as Phosphatidyl-choline), it also has an anti-inflammatory and antioxidant function; these last two effects are secondary. Even the administration of Zinc (in the form of ZnSO4) has shown a role in the prevention of fibrosis at the level of the murine peritoneum: among the effects, the reduction of glucose transport across the membrane, the inhibition of the "MMT" process certainly stand out, and, consequently, of the cell migration process. From a molecular point of view, in fact, ZnSO4 inhibits the formation of ROS, which is the basis of the epithelial to mesenchymal transition phenomenon, by activating the NRF2 antioxidant pathway [97].

The same applies to Astaxanthin, a natural carotenoid, that is found in the cell membrane and consists of two annular structures, each of which has a hydroxyl and ketone group [98]. These functional groups attribute a high antioxidant capacity to the extent to be defined the most powerful antioxidant ever isolated [99] Astaxanthin reduces the proportion of spindle-shaped cells expressing 8-Ohdg (8-hydroxy-2'-deoxyguanosine), another oxidative biomarker), the expression of MCP-1 (as well as that of its miRNA), and of α-SMA positive cells [100].

An enzyme, DPP-4 (Dipeptidyl-peptidase IV), takes part in the pathogenesis of peritoneal fibrosis, which intensifies its activity due to the high glucose concentrations of the dialysate. DPP-4 is a transmembrane glycoprotein, which has the active site in its extracellular domain, and is important for the catabolism of Incretins and their analogues; it is also involved in the expression of genes that code for proteins involved in the processes of inflammation, fibrosis and oxidative stress [101].

For this reason, the use of DPP-4 inhibitors (including Sitagliptin) can negatively affect these elements, preventing peritoneal dialysis from being ineffective in the long term. The signal transduction pathways, influenced by this enzyme, involve SMAD3 (an up-regulator of Snail, previously mentioned and stimulator of TGF-β1 production

and secretion), NFkB / MyD88 (activator of the free radical generator) [102], VEGF, CD45 (marker of inflammatory cells which appear to be reduced).

Studies, carried out by administering molecular hydrogen (H2) inside the peritoneal cavity, have shown that H2 can slow down fibrogenesis by down regulating the PTEN depending signaling cascade, thus being considered for its possible therapeutic implications [103].

The implementation of the generation solutions defined as “double-chamber” since glucose, stored at acid pH, is separated from lactates and bicarbonates to prevent the formation of Degradation Products of glucose [104]. This allows for greater stability of the sugar [105]. The new dialytic solutions are represented in the Table 3.

Secondly, amino acid-based solutions, stored at pH 6.6, can be used, taking advantage of their osmotic properties and reducing the glucose concentration. Despite their unclear biocompatibility, they can stabilize the metabolic state of the patient, but they are not free from side effects such as azotemia and metabolic acidosis [106].

Two other molecules with "osmo-metabolic" function have also been identified: L-carnitine and Xylitol, in fact, reduce cardiovascular events in both diabetic and non-diabetic patients and improve the metabolic state of carbohydrates and lipids [107].

L-Carnitine, which has a molecular weight of 161.2 Da, is a shuttle necessary for the transport of fatty acids and acetic acid across the inner mitochondrial membrane. Among the chemical properties, we certainly include its high solubility and stability in water [108], osmotic efficacy, its biocompatibility with the peritoneal membrane and "radical-scavenging".

L-carnitine, added to the dialysis fluid rich in glucose, prevents histological alterations of the mesothelium and sub-mesothelial vascular structures [109] and the reduction of AQP-1 gene expression [110].

Furthermore, like the previous amino acid-based solutions, it can attenuate insulin resistance and maintain diuresis [111]. Xylitol, on the other hand, with a molecular weight of 151.2 Da, is a five-carbon alcohol that has less efficient osmotic functions than L-carnitine, but is still important for stabilizing UF and guaranteeing glycemic control [112]. It also neutralizes free radicals and nitric oxide and increases the concentrations of Reduced Glutathione (GSH) and the activity of antioxidant enzymes,

directly and indirectly reducing oxidative stress [113]. Dialysis solutions containing both molecules have been developed and tested *in vitro* and it was concluded that they are effective in maintaining the integrity of the mesothelial cell, in reducing the production and release of pro-inflammatory cytokines [114] and in preventing the effects of high glucose concentration.

In the present study we tested the effects of a novel formulation of PD solution, developed by an Italian company, leader for the production of new dialysis solutions. This solution is composed by a particular combination of L-Carnitine and Xylitol. In fact, the osmo-metabolic agents may be used alone or in combination in order to maximize their therapeutic effects. This combination was tested to evaluate *in vivo* the potential effects against the aging parameters of the peritoneal membrane induced by conventional solutions (fibrosis, angiogenesis, MMT), validating the results obtained from *in vitro* studies [114].

	GLUCOSE- BASED PD SOLUTIONS								
	Physioneal 40®			Dianeal PD4®			BicaVera®		
mMol/L	LOW	MEDIUM	HIGH	LOW	MEDIUM	HIGH	LOW	MEDIUM	HIGH
Sodium	132	132	132	132	132	132	134	134	134
Calcium	1.25	1.25	1.25	1.25	1.25	1.25	1.75	1.75	1.75
Magnesium	0.25	0.25	0.25	0.25	0.25	0.25	0.5	0.5	0.5
Chloride	95	95	95	95	95	95	104.5	104.5	104.5
Glucose	75.5	126	214	75.5	126	214	83.25	126.1	235.9
Xylitol	-	-	-	-	-	-	-	-	-
Lactate	15	15	15	40	40	40	-	-	-
Bicarbonate	25	25	25	-	-	-	34	34	34
Icodextrin	-	-	-	-	-	-	-	-	-
Aminoacids	-	-	-	-	-	-	-	-	-
L-carnitine	-	-	-	-	-	-	-	-	-
Osmolarity *(mOsmol/L)*	344	395	483	344	395	483	358	401	511
pH	7.4	7.4	7.4	5–6.5	5–6.5	5–6.5	7.4	7.4	7.4

	GLUCOSE- FREE PD SOLUTIONS		GLUCOSE-SPARING PD SOLUTIONS					
	Extraneal®	Nutrineal®	− L-CARNITINE			+ L-CARNITINE		
mMol/L	Icodextrin 7.5%	Amino acids 1.1%	LOW	MEDIUM	HIGH	LOW	MEDIUM	HIGH
Sodium	133	132	134	134	134	134	134	134
Calcium	1.75	1.25	1.75	1.75	1.75	1.75	1.75	1.75
Magnesium	0.25	0.25	0.5	0.5	0.5	0.5	0.5	0.5
Chloride	96	105	103.5	103.5	103.5	103.5	103.5	103.5
Glucose	-	-	27.7	27.7	83	27.7	27.7	83
Xylitol	-	-	46	98.6	125	46	98.6	125
Lactate	40	40	35	35	35	35	35	35
Bicarbonate	-	-	-	-	-	-	-	-
Icodextrin	7.5 (%)	-	-	-	-	-	-	-
Aminoacids	-	87.16	-	-	-	-	-	-
L-carnitine	-	-	-	-	-	1.24	1.24	1.24
Osmolarity *(mOsmol/L)*	284	365	351.9	404.5	486.2	351.9	404.5	486.2
pH	5–6	6.6	5.5 ± 0.5	5.5 ± 0.5	5.5 ± 0.5	5.5 ± 0.5	5.5 ± 0.5	5.5 ± 0.5

Table 3- Composition of PD solutions commercially available and widely used for the treatment. On the top are represented the conventional solutions with more side effects compared to the alternative solutions, on the bottom [114].

9. Role of Oleuropein (Ole) on mesothelial cells and different diseases

Oleuropein (Ole) is a molecule abundant in the mediterranean diet. From a structural point of view, it is defined as a secoridium (particular form of iridoid, which corresponds to a secondary metabolite present in plants) and is characterized by three subunits: hydroxytyrosol (a polyphenol that performs the function of a powerful antioxidant and of active principle), helenoic acid (a secoridium) and a molecule of Glucose [115] (Figure 10). Oleuropein represents 96.9% of the total phenols extracted from olive leaves, the remaining part is represented by hydroxytyrosol, the form in which it is metabolized [116] (Figure 10).

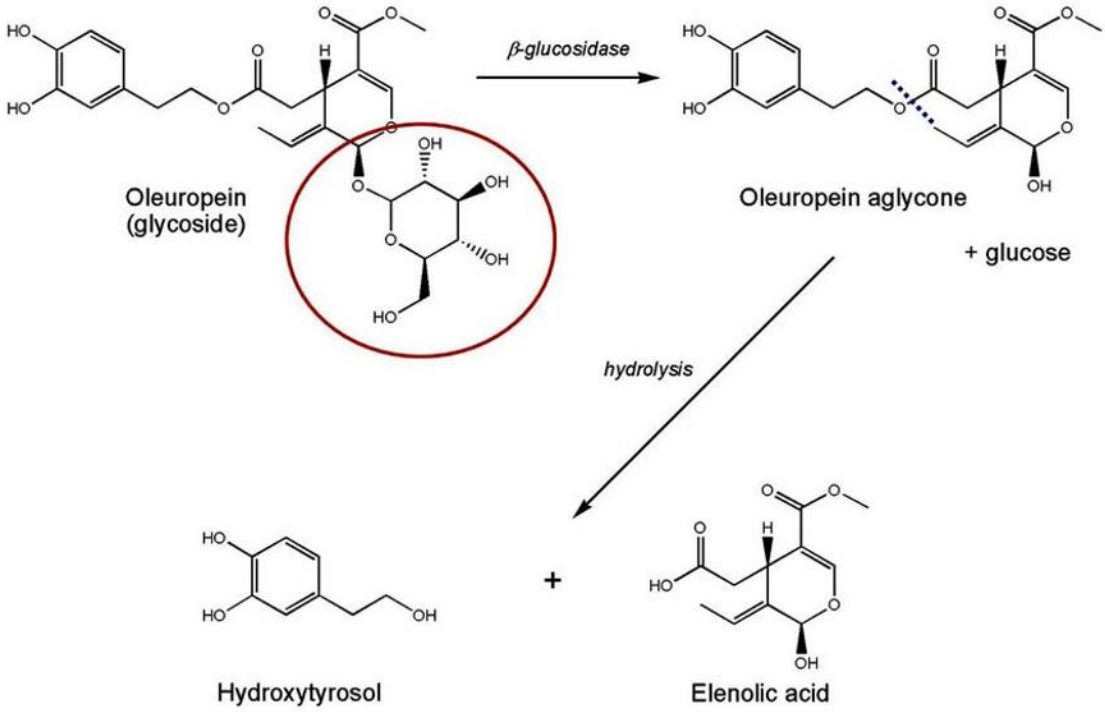

Figure 10- Metabolism of Oleuropein [117].

Its quantity inside the fruit varies according to the degree of ripeness: the more ripe a fruit is, the greater the reduction in the concentration of Oleuropein in it will be. The Ole is rapidly cleaved, due to the breakdown of the glycosidic bond, and from this originate a free glucose molecule and the oleuropein aglycol, which through the β-glucosidase is transformed into a helenoic acid (in its dialdehyde and decarboxymethyl form, the "HyEDA") linked to hydroxytyrosol [118].

Immortalized mesothelial cells co-treated with both TGF-β1 and Oleuropein maintain the integrity of the intercellular epithelial structures and preserve the migration capacity [119].

Ole co-treatment inhibits the SMAD3 dependent pathways [120]). In addition, Ole themselves can increase the expression of genes encoding epithelial markers both directly and indirectly due to the presence of overlapping between the intracellular signaling pathways: especially E-cadherin, whose transcription factor is activated, while its co-repressor (the SNAIL protein, already mentioned) is translocated outside the cell nucleus, inhibiting its action.

Ole has antioxidant, antiplatelet, hypotensive, antirheumatic, antipyretic properties [121]. Furthermore, its antitumor and antimicrobial activities are known [122-124]. *In vitro* studies performed on cancer cells show that this molecule is able to counteract the transdifferentiation process of mesothelial cells, as well as angiogenesis, and to inhibit all those mechanisms underlying the fibrotic phenomenon [119].

In vivo studies demonstrate the antioxidant activity of the molecule, capable of reducing the levels of the final products of oxidative stress and lipid peroxidation in various organs including the liver of mice and rats subjected to stress induced by Arsenic and Bisphenol A [116, 119, 125].

In addition, it attenuates the progression of myocardial infarction in rat models that simulate heart disease, thanks to its remarkable antioxidant, anti-inflammatory, hypotensive and vasodilatory properties [126-128].

Ole, reduces the inflammatory state and the consequent fibrosis in the liver and heart in induced pathological models [129], and reduces the infiltration of leukocytes, glomerulosclerosis and glomerular hypertrophy in diabetic rats [130].A study

demonstrates its action against progression to Diabetic Nephropathy, protecting the kidney from apoptosis, oxidative stress and inflammatory response [131].

STUDY 1

Setting up a method for in vivo-imaging of peritoneal membrane during PD exchange

1. Intravital Microscopy: use of Multiphoton Microscopy (2PM)

Intravital microscopy of living tissues is possible with conventional confocal microscopy, but this
method is limited by the relatively low tissue depth and the high photo-toxicity. Intravital multiphoton microscopy (MPM) is an advanced technique that offers 3D images and high resolution movies of dynamic cellular and subcellular processes. Thanks to the deeper laser penetration and less phototoxicity, MPM allowed researchers to verify important questions regarding human and animal physiology, becoming the gold standard approach for *in vivo* imaging.

The concept of MPM was first described in the 1930s by Maria Göppert-Mayer [132], but it started to be used for biological imaging about 50 years later. The term "two-photon" microscopy rather than "multiphoton" is sometimes preferred because most studies performed so far have used two-photon excitation.

MPM exploits two low-energy photons arriving almost simultaneously on the sample and uses a long wavelength laser exciting in the near infrared range (700-1000 nm). The two photons alone have the half of the energy compared to the single photons used in one-photon excitation and the resulting fluorescence emission is comparable with that generated in one-photon event. Since the energy of photon is inversely proportional to the wavelength, in two-photon excitation the wavelength used should be approximately twice than one photon excitation [133-135]. The Figure 11 shows a simplified jablonsky diagram for one-photon and two-photon excitation fluorescence.

MPM exhibits several advantages compared to conventional microscope methods. First, the laser
penetration in the tissue is higher in consequence of less light scattering, allowing to image in the
tissue up to 150-200 μm [134]. This represents a depth capacity 3-4 times more than confocal

microscopy [136]. In optically transparent organs, such as brain, MPM permits the imaging with higher depth [137, 138]. Hence the idea of exploiting MPM for morphological and functional studies on the parietal peritoneum as there are very few references in the literature. Second, the phototoxicity is less thanks to the two low-energy photons arriving on the sample. In this way it is possible to image continuously over the time, especially when thick samples are visualized, including brain slices, embryos and living organs [139]. Third, the out of focus is reduced, and the fluorescence is high only in the focal plane because the excitation energy drops proportionally to the square of the distance to the focal point. Therefore, the photobleaching is reduced, the necessity of a pinhole is avoided, and more sensitive detectors can be used to collect the fluorophore emission [140, 141] (Figure 12).

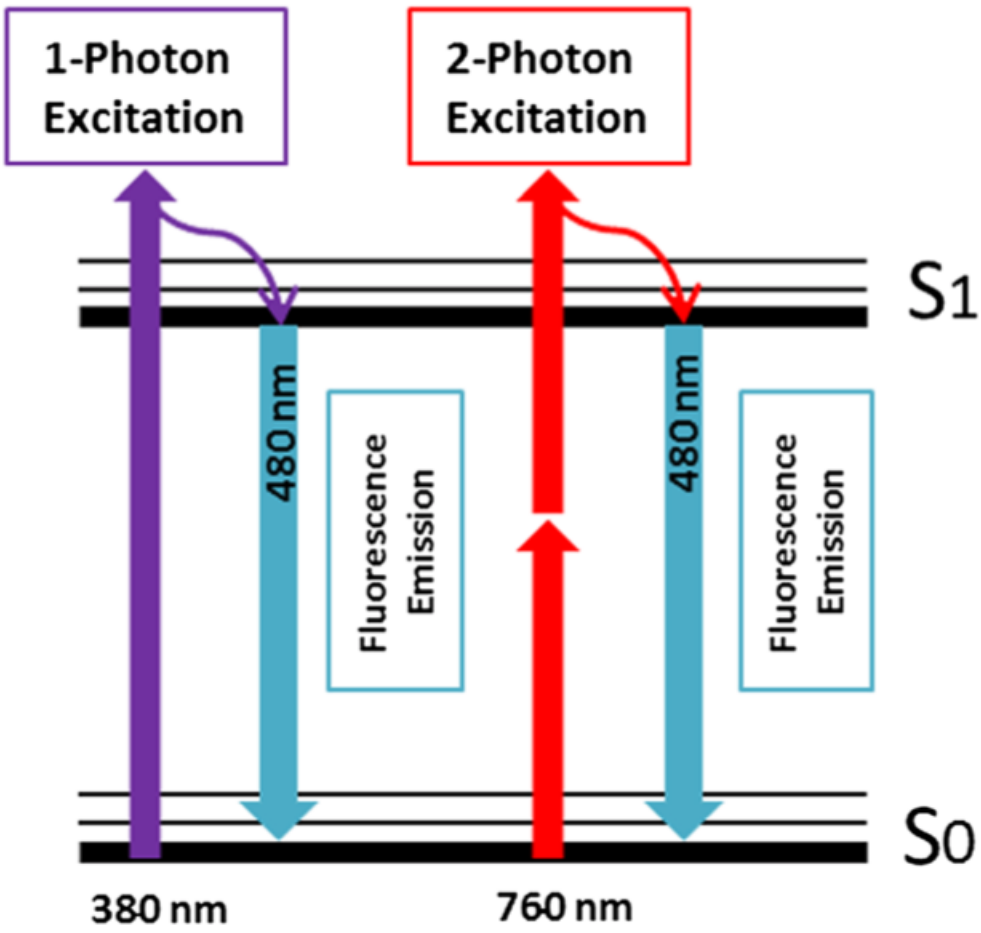

Figure 11- Simplified Jablonsky representation for one-photon and two-photon excitation.

One-photon excitation occurs after the absorption of a single photon which provides sufficient energy to reach the excited state (S1). Two-photon excitation is provided by the simultaneous absorption of two photons of lower energy. The subsequent fluorescent emission of one-photon and two-photon excitation is comparable [133].

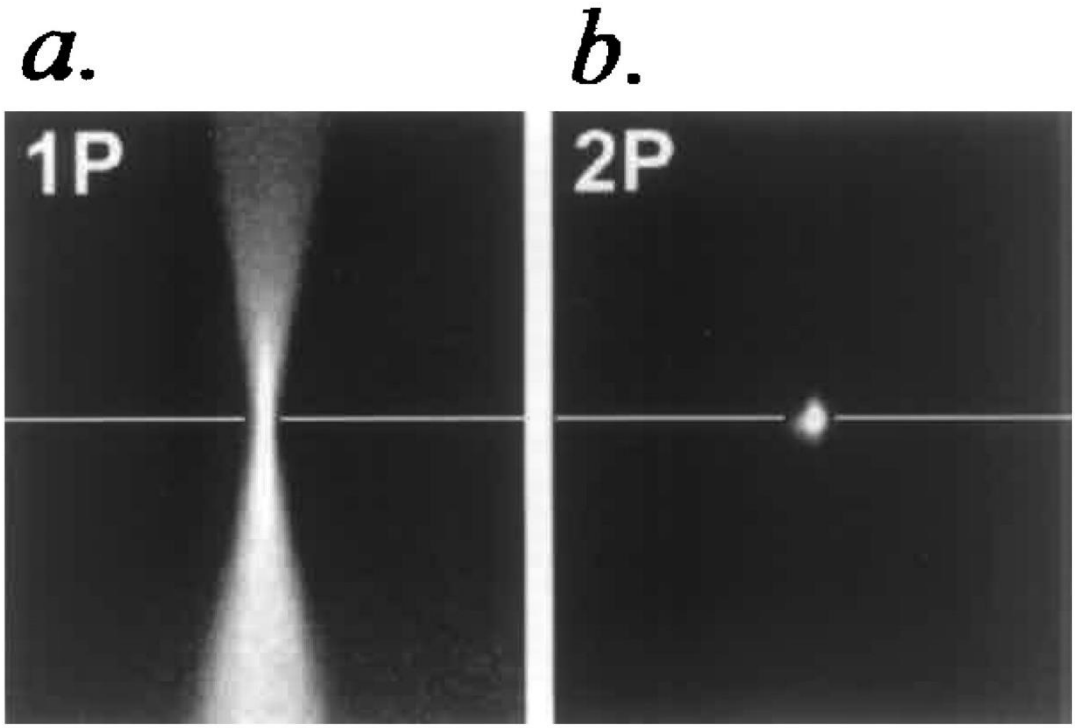

Figure 12- Localization of fluorescence by one-photon and two-photon excitation.
In one-photon excitation (a) the fluorescence spreads far from the focal plane, requiring a pinhole to reject all the out of focus. Two photon microscopy (b), instead, emits fluorescence only at the focal plane, represented by the line, reducing photobleaching and avoiding the necessity of a pinhole [142].

As consequence of these improvements, MPM permits to capture dynamic events in organs of living animals, still incorporating the complexity of hormonal factors and metabolites with subcellular resolution, becoming the technique of choice for intravital imaging. As largely shown in literature, the application of MPM gave the opportunity to increase the knowledge of many organs, such as brain [143], skin [144], liver [145], heart [142] and kidney [146] as well as investigations in immunology [147] and cancer fields [148]. The peritoneum, in particular, presents a very intricate structure with different cell types that are difficult to analyze with conventional techniques since they

may show changes when removed from the physiological body. For this reason, the imaging of living organs with MPM overcomes the limits shown by confocal microscopy and offers the unique opportunity to extend the knowledge of human pathophysiology, with the future perspective to evaluate efficient treatment strategies.

2. Surgical procedures and isolation of the Peritoneum

All animal procedures were approved by authorization from the Italian Ministry of Health, n. 889/2020-PR, 29/09/2020 and by the Animal Ethics Committee (CESA) of Biogem, a genetic research institute located in Ariano Irpino (Avellino, Italy), where most of the experimental activities were carried out. Following dialysis treatment, male rats (Wistar, wild type) were anesthetized by intraperitoneal injection of 160 mg of Thiobutobarbital (Inactin) per kg of body weight [149]. Analgesia followed by subcutaneous injection of Butorphanol at a concentration of 0.03 mg / kg.

After making an incision at the base of the neck, the tracheostomy was performed and the jugular vein was isolated for the insertion of a polyethylene catheter, PE50 (2Biological instruments), useful for intravenous infusion of the fluorophores listed below.

Subsequently, the animals were shaved abdominally and placed on a homeothermic table to maintain the body temperature at 37 ° C [149]. After dissection of the abdominal skin, a longitudinal incision was made along the linea alba (Figure 13) with the aim of externalizing the peritoneum as best as possible, obtaining a small flap, turned upside down so as to have the parietal peritoneum superficially, continuously hydrated with isotonic saline solution. The peritoneum flap on which *in vivo* imaging was performed using multiphoton microscopy was fixed by sutures (Figure 14), to achieve better stability during acquisition. A gauze soaked in saline was placed inside the abdomen for constant perfusion of the peritoneum and to keep the abdominal organs in place. The animals were placed sideways on the microscope stage so as to have the peritoneum flap in front of the 20x objective of the multiphoton microscope [150], using inverted arm approach (Figure 14).

This inverted approach, which requires the positioning of the microscope objective below the flap of peritoneum, was generally preferred since it provides more stable conditions and minimize the movements due to breathing and heartbeat (Figure 15).

Throughout the duration of the experiment, mean arterial blood pressure was monitored by the carotid artery following cannulation (with polyethylene tube, PE50, 2Biological instruments) using the BP-1 Pressure Monitor Recorder, 2Biological instruments, connected to a Power Lab System (Adinstruments). The pressure transducer was previously calibrated using a pharmaceutical pressure manometer. Arterial blood samples were also taken using the Epoc blood system analysis reader (Siemens) for the analysis of the various physiological parameters (pH, pO2, pCO2, electrolytes). In addition to pressure, body temperature was monitored using a thermometer with a rectal probe. All this in order to keep the animal's state of well-being and its general health conditions under control. At the end of the experiment, the animals were sacrificed under deep anesthesia by asphyxiation with CO2, according to the National guidelines.

(a)

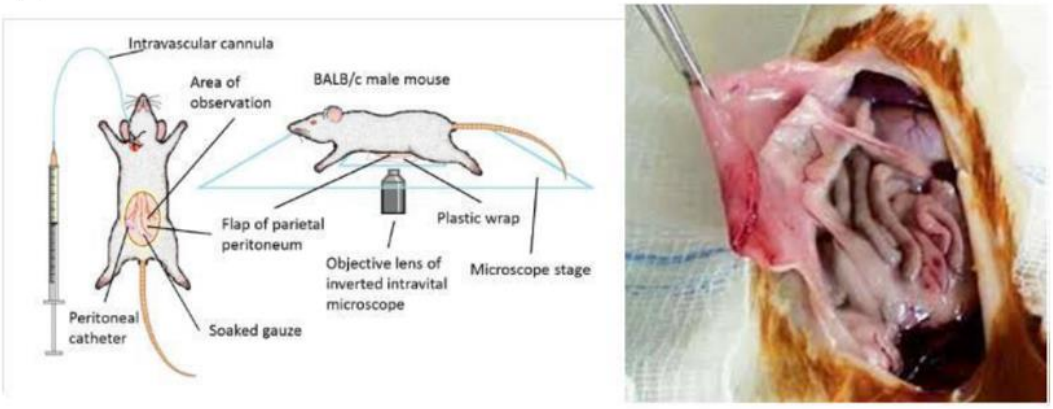
Intravascular cannula
Area of observation
BALB/c male mouse
Flap of parietal peritoneum
Plastic wrap
Objective lens of inverted intravital microscope
Microscope stage
Peritoneal catheter
Soaked gauze

(b)

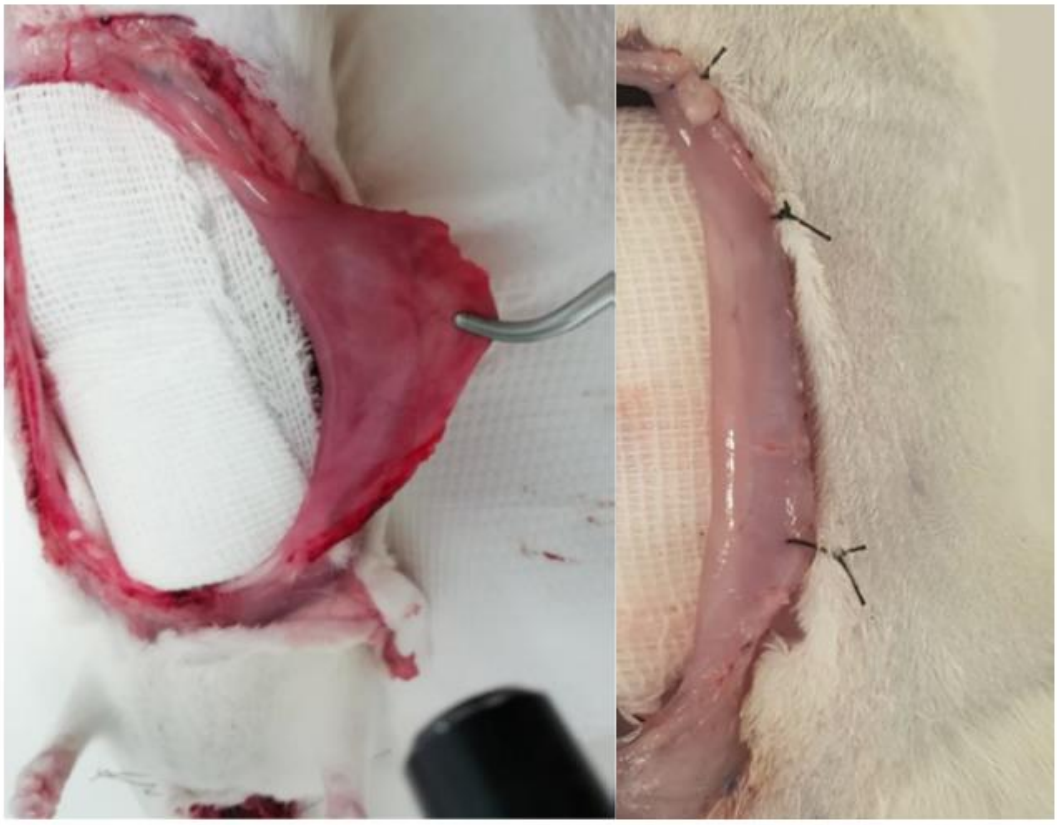

Figure 13- Surgical preparation for *in vivo* imaging using multiphoton microscopy starting from a protocol present in literature [150] (a). Details of the isolation of the parietal peritoneum in the rat (b) and in the mouse (c).

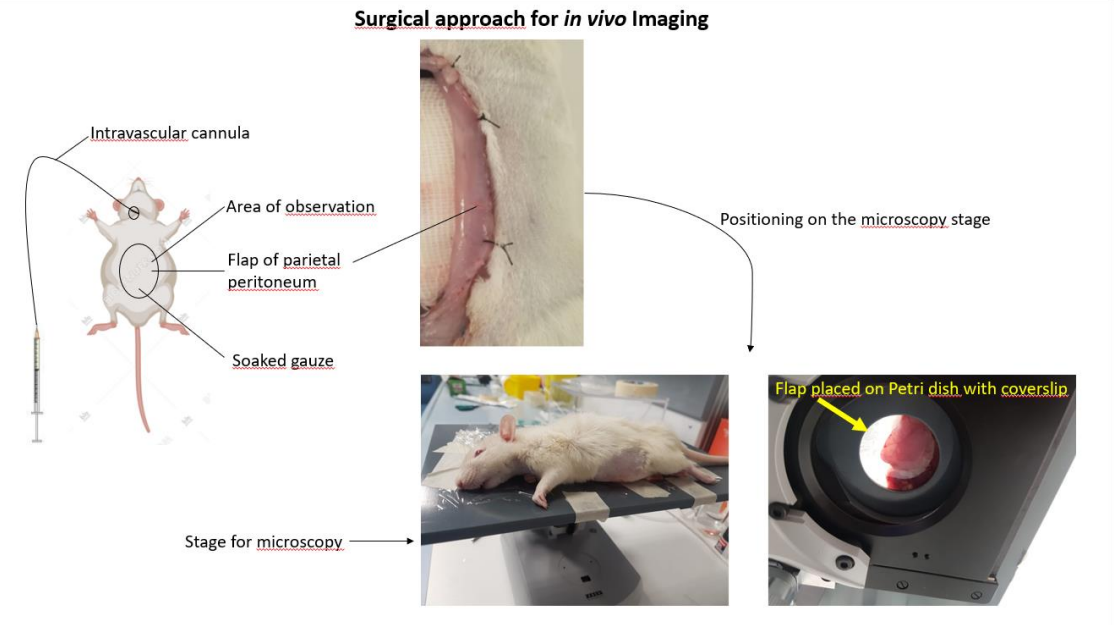

Figure 14- Surgical approach for *in vivo* imaging and positioning of the animal on the microscopy stage.

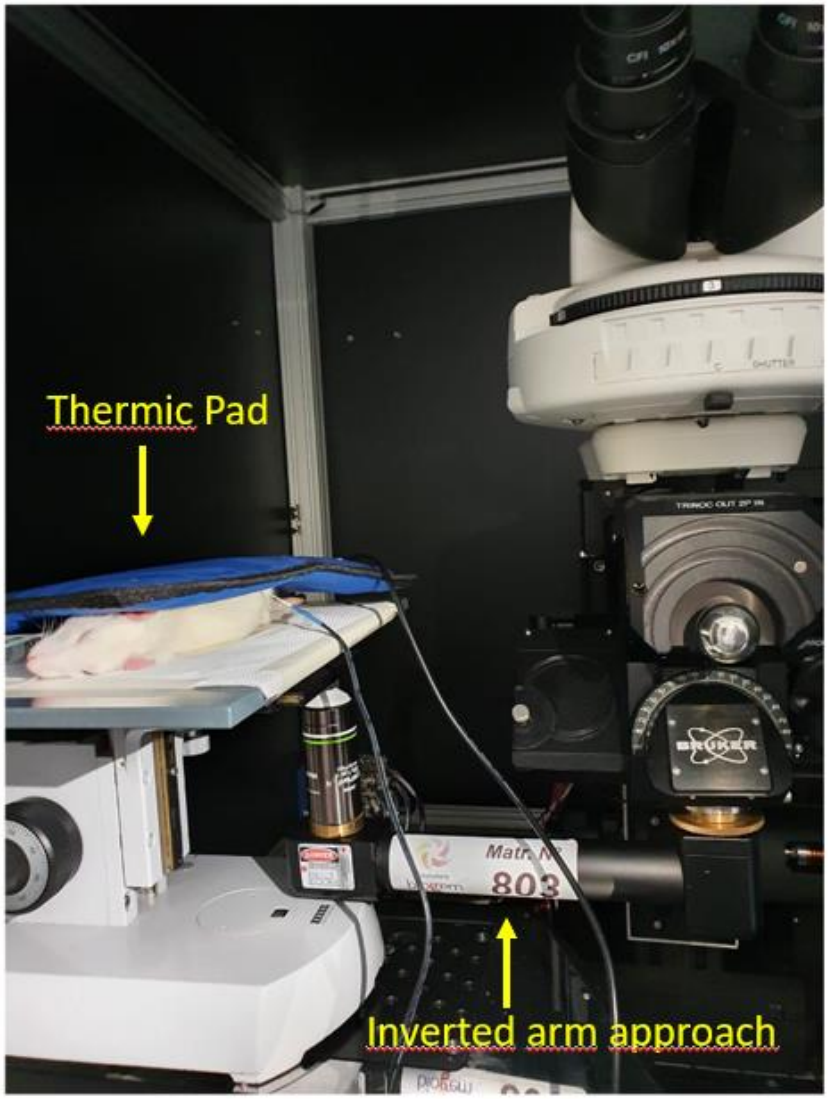

Figure 15- Representation of the inverted approach for *in vivo* imaging. The arm was connected to the microscope from a side and holds the objective facing up from the other side. The animals covered by a heating pad were placed on microscope stage with the exteriorized peritoneum immersed in warm saline solution. The imaging of the parietal peritoneum was performed from below to reduce the animal movements.

The fluorophores used, infused iv in animals using PE50 polyethylene catheters were the following:

- FITC- Dextran 500 kDa (FD500S, Sigma): single intravenous bolus of 100 µL of the solution at a concentration of 10 mg / mL for peritoneal vessel imaging [151].
- Hoechst 33342 (H1399, Invitrogen): single intravenous bolus of 100 µL at a concentration of 3 mg / mL, to detect cell nuclei [152].

These fluorophores are used in order to evaluate the morphological and physiological parameters of the peritoneum listed below:

- red blood cell velocity,
- blood pressure,
- hematocrit,
- capillary diameter,
- blood flow rate,
- microvascular density,
- macromolecule permeability and transport,
- fibrosis and angiogenesis,
- cellularity.

3. Use of Multiphoton microscopy (MPM)

Two-photon microscopy (2PM) was performed using an upright Ultima Investigator 2-photon
microscope (Bruker, MS, USA) equipped with a 20X objective XLUMPlanFL20XW NA 1.0
(Olympus, Japan) and supplemented by a converter arm (Inverterscope, LSM TECH, USA) to allow inverted imaging (Figure 16). The microscope was controlled by Prairie View software. Ti-Sapphire laser (Mai Tai® DeepSee™, Spectra-Physics, USA) was tuned for excitation wavelengths of 800 and 900 nm for *in vivo* experiments. For the detection of green channel, emitted light between 500 and 550nm was recorded using Hamamatsu model H10770PB-40 GaAsP-detector. For the detection of red channel

and blue channel light between 570 and 620 and between 435 and 485nm, respectively, were recorded using Hamamatsu model R3896 multi-alkali detectors. The images were collected at 512x512 resolution and the pixel dwell time was 2.8 µs, zoom 1.0x.

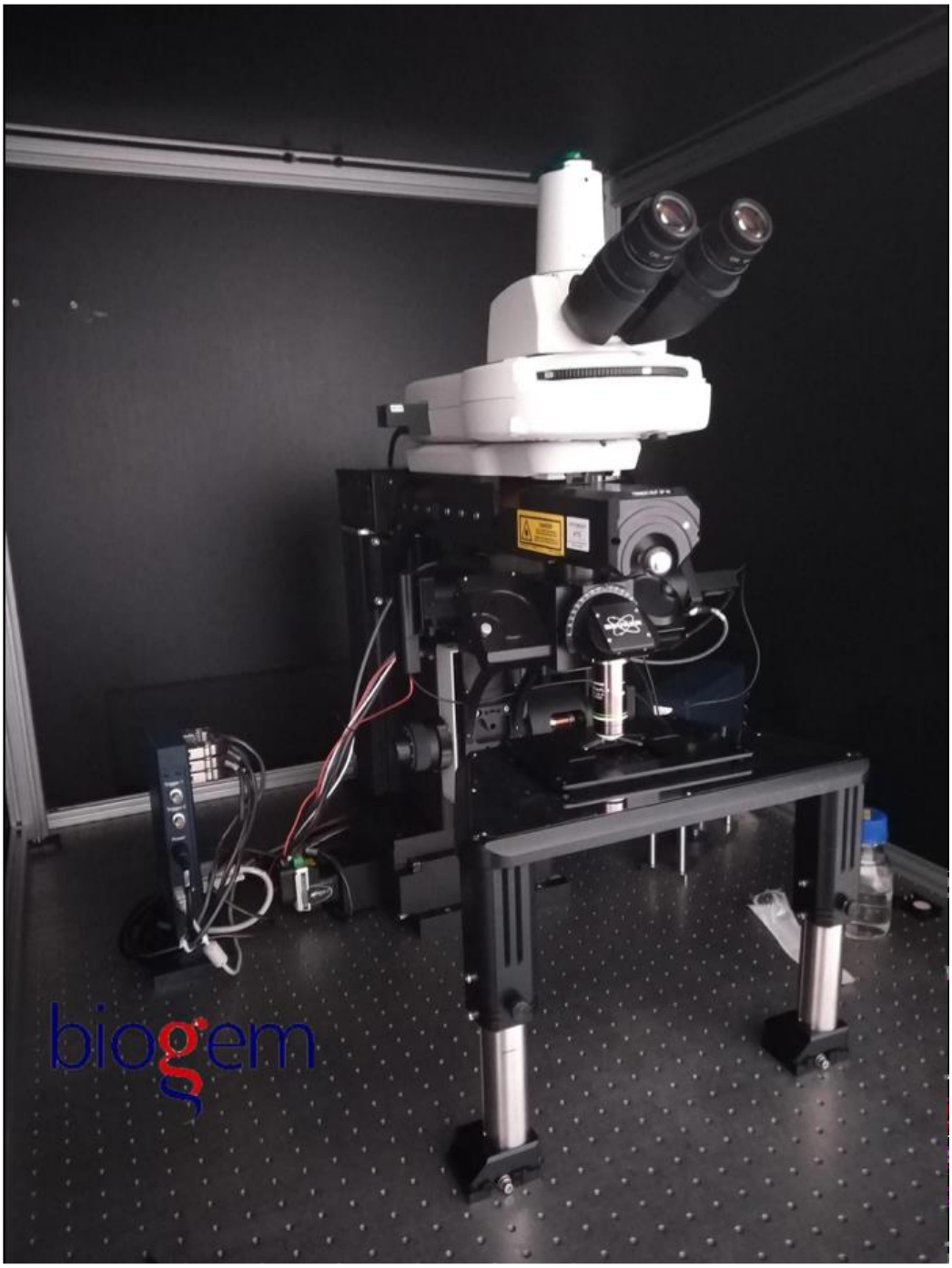

Figure 16- Two-photon microscopy of the intravital microscopy facility at Biogem Scarl.

4. Results

Multiphoton microscopy as an innovative technology for the morphological study of the parietal peritoneum

The innovative experimental approach of multi-photon microscopy has made it possible to develop an *in vivo* imaging method that allows to detect the different vessels of the microcirculation that supply the peritoneum (arterioles, capillaries, postcapillary venules), but also the well-structured layer composed of mesothelial cells and the underlying cellular and fibrotic composition of the sub-mesothelial space (Figure 17).

The z-stack, the continuous acquisition along the z axis, from the surface to the below layers of the membrane, represented a useful support for the study of the morphology of the parietal peritoneum, as nothing is known in the literature (Figure 18).

Starting from the output of the z-stack it was possible to obtain 3D models of the entire studied structure using different plugins available on Fiji (3D viewer, Clear Volume, 3D script).

The 3D rendering was found to be informative for the morphological description of the full thickness peritoneal membrane (Figure 19).

By exploiting the potential of multiphoton microscopy it was possible to classify the different vessels of the microcirculation that supply the peritoneum. This distinction was made on the basis of the caliber of the vessels and made possible the subsequent functional analysis on the characteristics of the vessels in the different osmolarity conditions of the exchanged liquid (Figure 20).

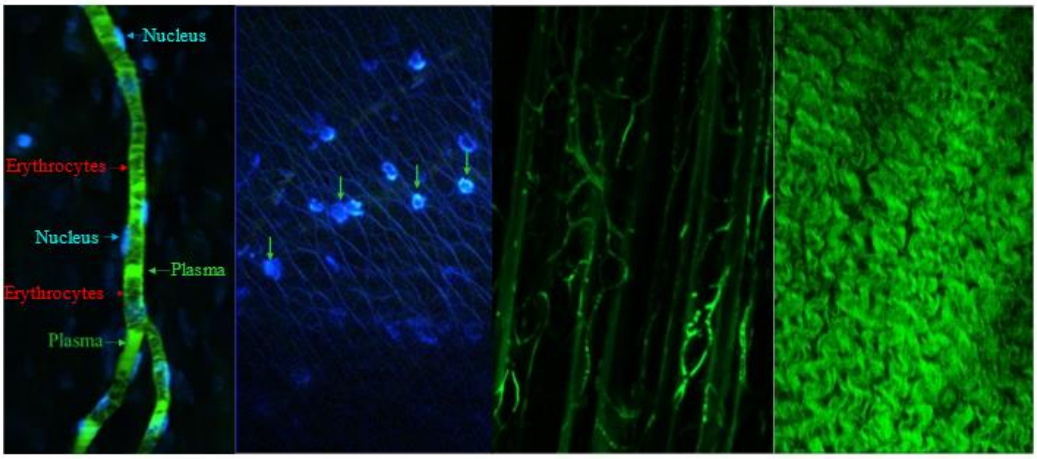

a. Peritoneal capillary with the characteristic shading of erythrocytes.

b. Nuclei of mesothelial cells which rest on a dense framework of collagen fibers in the area sub-mesothelial

c. Vascular network

d. Thickened collagen fibers in the fibrotic event

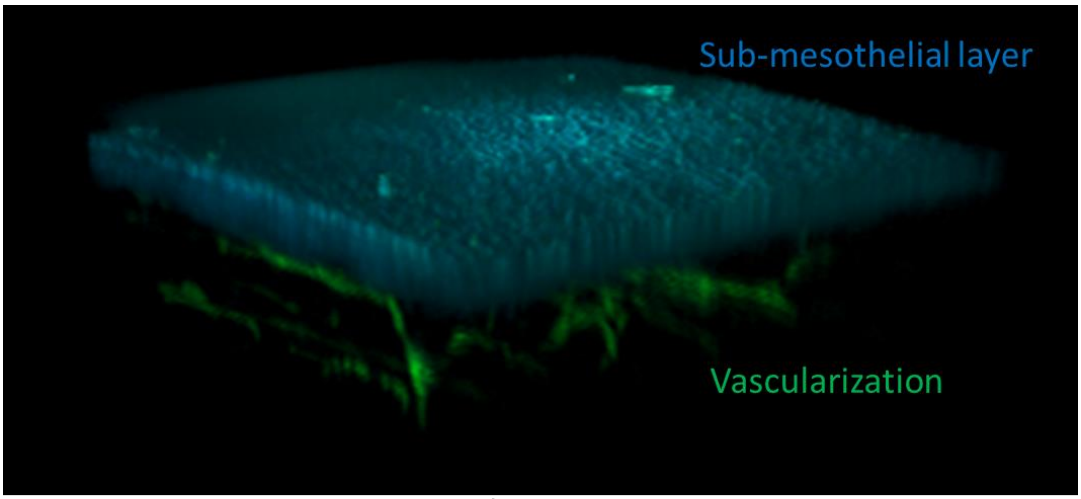

3D reconstruction of the peritoneal membrane

Figure 17- Multiphoton microscopy applied for the morphological study of the parietal peritoneum**.**

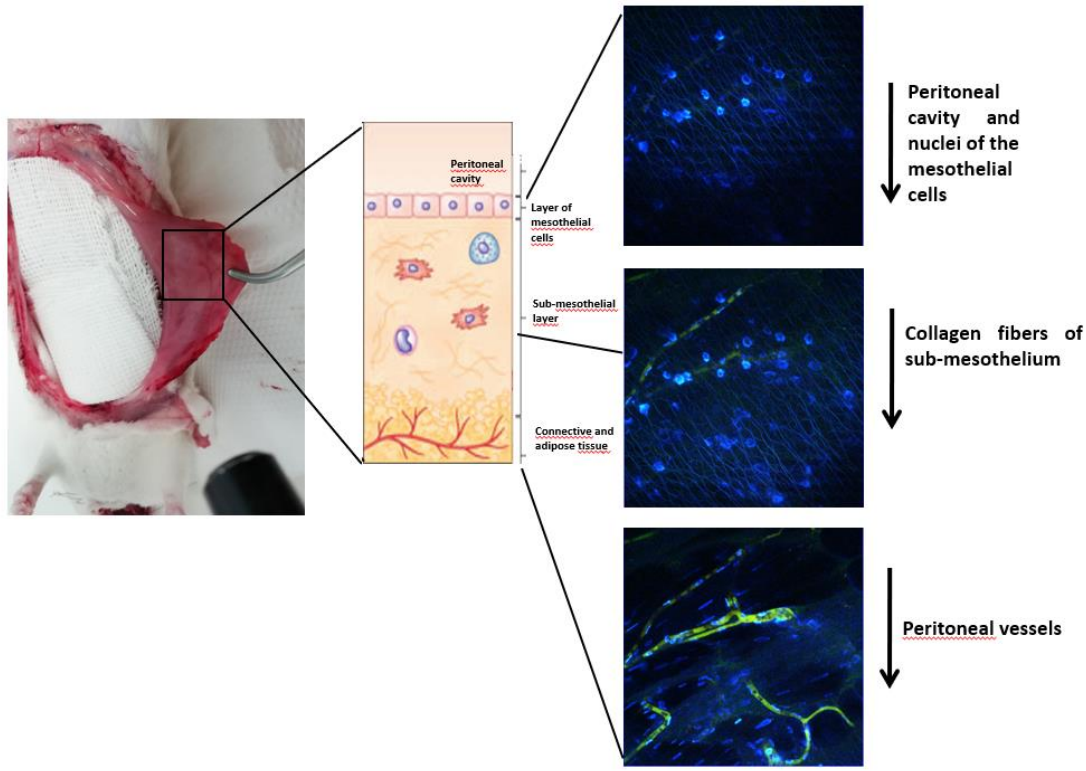

Figure 18- Z-stack as an informative tool for morphology of parietal peritoneum.

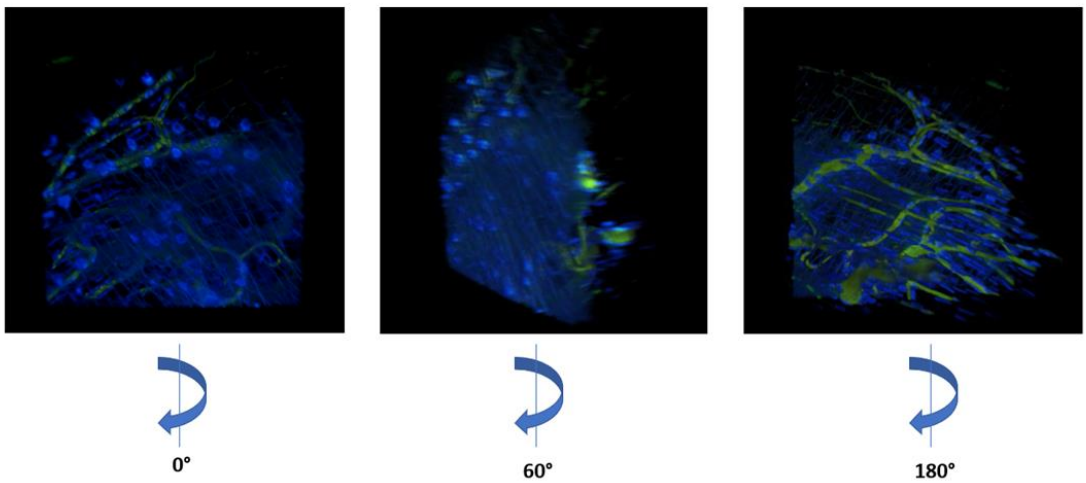

Figure 19- 3D rendering of full thickness parietal peritoneum.

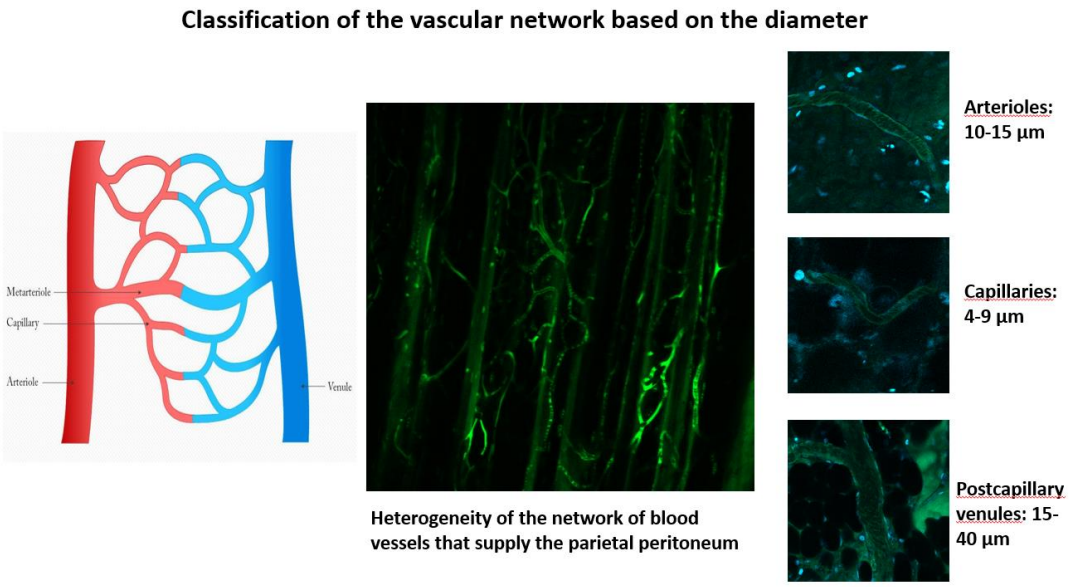

Figure 20- *In vivo* imaging on vascular network of peritoneal membrane.

STUDY 2

Oleuropein preserves the peritoneal membrane in an *in vivo* experimental model of peritoneal dialysis

1. Aim of the study

Given the remarkable and multiple therapeutic properties of the molecule, well documented in literature, the aims of the following experimental project were:

- To evaluate the *in vivo* effects of Oleuropein, following conventional dialysis treatment on animal models, on aging parameters of the parietal peritoneum: fibrosis, vascularization (neoangiogenesis) and cellularity;

- To verify the biocompatibility of Oleuropein and any beneficial therapeutic effects;

- To evaluate the exchange and filtration performance and the ability to protect mesothelial cells and microcirculation vessels from damage.

Using fluorescent probes to simultaneously mark the peritoneal vessels, it was possible to distinguish them into arterioles, capillaries and venules thanks to the real time determination of their diameters and to mark the pericytes, the mesothelial cells, the interstitial components of the sub-mesothelium (thus measuring the density of collagen fibers). This allowed to study the morphology of the parietal peritoneum using various microscopy "tools": the Z-stack with the consequent 3-D rendering, the Time-series, the Linescan. In fact, among the advantages of its use, two-photon fluorescence microscopy was useful due to its efficient characteristics: greater penetration into the tissues, obtaining in this way more information in terms of sample depth, less photo-damage (production of ROS and destruction of intracellular macromolecules were avoided), simultaneous absorption of two photons, whose source is represented by a laser, less energy absorbed by the fluorophores which will allow a rapid process of excitation [133, 149, 152] and image acquisition.

2. Materials and Methods

Experimental models to investigate the mechanisms behind the senescence of the peritoneal dialysis consist in the intraperitoneal infusion of high glucose content dialysis solutions [153-158]. According to this protocol, Wistar male rats were subjected to dialysis treatment by intraperitoneal (IP) injection without the need for drainage, for 15 days, once a day, following a light gas anesthesia with isoflurane.
After making the IP injection, the animals were placed inside the cage and kept with access to food and water ad libitum. To monitor the state of the animals, in addition to daily checks, body weight was analyzed. Dialysis treatment was performed only on wild type animal models, with preserved kidneys function. This allowed no problem in handling the dialysate load. Animals were used in the juvenile phase, after weaning, of 2-3 months of life, to have a better response to the maneuvers performed during dialysis treatment and especially during surgery. 3.86% glucose concentrated solutions were used.

a. Experimental model

The following experimental work was based on the study of the biocompatibility of a molecule extracted from olive leaves, the Oleuropein (Ole), at a concentration of 30 mg / kg diluted in saline or 3.86% dialysis solution, injected i.p. a few minutes before dialysis treatment [119, 159-162].
The concentration of Ole is the same used in the literature in *in vitro* studies on mesothelial cells. For the activation and stabilization of the molecule used in the treatment, it was necessary to use the immersion Sonicator, through the action of ultrasound. The molecule was then activated by mild sonication (20 Hz) for 5 minutes.
Four groups of animals were considered:

- Sham-operated (n = 3), daily infusion (10 mL) of 0.9% physiological solution;
- Sham-operated + Ole (n = 4), daily infusion (10 mL) of 0.9% physiological solution + Ole 30 mg / kg;

- 3.86% (n = 3), daily infusion (10 mL) of dialysis solution with a high concentration of glucose (3.86%, Physioneal 40, Baxter);
- 3.86% + Ole (n = 4), daily infusion (10 mL) of dialysis solution with a high concentration of glucose (3.86%, Physioneal 40, Baxter) + Ole 30 mg / kg.

10 mL corresponds to the maximum volume allowed for intraperitoneal administration according to the international guidelines. The intraperitoneal administration of dialysis solution at a concentration of 3.86% was used to induce the fibrotic state of the peritoneum and the Ole for the consequent inhibitory response. Instead the administration of physiological solution was used to mimic the normal physiological state of the membrane.

b. Evaluation of peritoneal membrane morphology

Typical morphological changes of the peritoneal membrane include fibrosis and neoangiogenesis [163]. The degree of fibrosis is closely related with the components of the dialysis solution. For this purpose acquired images were analyzed using Fiji, image analysis software, and the Angio Tool software very useful for the morphological and functional analysis in the post-processing phase.
Using Angio Tool the vascularized area is expressed as the percentage density of the vessels in a precise ROI, region of interest. A further vascular parameter considered was the evaluation of the number of nodes (branching) between the vessels.
In order to analyze parameters of angiogenesis were developed two methods using different computational machine learning tools: Ilastik and Angio Tool. First, acquired images were segmented using Ilastik algorithm, an open-source software that is able to make image classification thanks to an assisted machine learning program. The software is based on the concept that its predictions are based on the input drawn by the user as short brush. It uses a Random Forest classifier that calculate the image features (color, shape, texture) to segment the image of choice in well-established classes.

A training phase of the program is required to give inputs to a small set of representative images. In this way the software is capable to classify other images with similar features never analyzed before, ensuring reproducibility and reliability [164].
Ilastik was used for the pre-processing of the images before the use of the vessel density plugin from Fiji.
For the training phase with Ilastik were used 15 images. Images were segmented in two classes (vessels and background) to create segmentation masks where each pixel was assigned to two possible values depending on their assignment by the algorithm.
For image classification, ROIs as short brushes were placed in all two compartments, then a simple segmentation was created (Figure 21 b).
The final segmentation obtained with Ilastik, despite the training of the software with multiple images, was not very reliable for the analyzes to be carried out as shown in the Figure 21 c.
For this reason a new approach was developed based on software created specifically for analysis on vascular networks, Angio Tool. In fact, the use of the Angio Tool software, useful for morphological and functional analysis on blood vessels, returns precise measurements of the density of the vessels by area and the number of branches (branching) in the vessels of the microcirculation.
Angio Tool is a quick and reproducible image analysis tool, developed as a Fiji plugin for quantification of microvascular networks in microscopic images [165, 166].
Angio Tool computes the branching index and several other morphometric parameters such as total explant area, average and total vessel length, number of endpoints, vessel density and average lacunarity. Two parameters have been chosen in this project: vessel density and number of branching point.
The basic analysis flow implemented by the software includes segmentation, skeletonization and analysis of vasculature. Opening an image Angio Tool identifies vessel profiles according to the software's preset parameters. The output is represented by an overlay that represents the area encompassing all vessels, a skeletal representation of the vascular network and the computed branching points inside this area (Figure 22 c). These outputs are saved together with an excel file containing the

analysis parameters and the computed results. For the segmentation execution performance, Angio Tool was chosen as the software of choice for vessel analysis.

The fibrosis, on the other hand, was analyzed by making Z-stacks of the recorded images. It is a microscopy tool able to scan the tissue along the z axis. The ability of the microscope laser to scan tissues with a thickness of up to 150 µm was exploited. The thickness of the peritoneal layers, in microns, was used to quantify the degree of peritoneal fibrosis, a direct consequence of the dialysis treatment.

The phenomenon of the Second Harmonic Generation (SHG) was used. The power of the laser at 900 nm is able to excite the collagen fibers type I that make up the sub-mesothelial layer in the form of auto-fluorescence.

SHG is a MPM tool that uses a laser source inducing a second-order nonlinear polarization in the

sample and emits at double harmonic frequency. SHG was first used in 1980s to image rat tail tendon, then it started to be exploited to detect the morphology of thick samples [167]. SHG presents several advantages compared with histological approaches. First, since it is associated only at types I and III collagen fibers, it offers great specificity of the signal detected. Indeed, no SHG signal is detectable in non-fibrillar type IV collagen [168]. Second, SHG has an endogenous 3D resolution that is proper of MPM, permitting 3D reconstructions useful for the analysis and avoiding variations due to variable thickness of the samples. Third, SHG only requires fresh unlabeled samples and no particular preparation is needed. Moreover, quantification of fibrosis using SHG can benefit the MPM advantages, like higher tissue penetration especially in thick samples and less light dispersion [169, 170].

For vascular analysis, a single bolus, 100 µL, of the high molecular weight (500 KDa) marker FITC-Dextran was injected into the isolated and cannulated jugular vein of anesthetized animals to visualize *in vivo* the intravascular distribution of the probe. Scans were carried out in different ROIs by exciting the fluorescent molecule at 800 nm.

To optimize the morphological overview, an intravenous bolus of 100 uL of the Hoechst 33342 marker at a concentration of 3 mg / mL was performed, for the staining of cell nuclei, useful for counting of mesothelial cells.

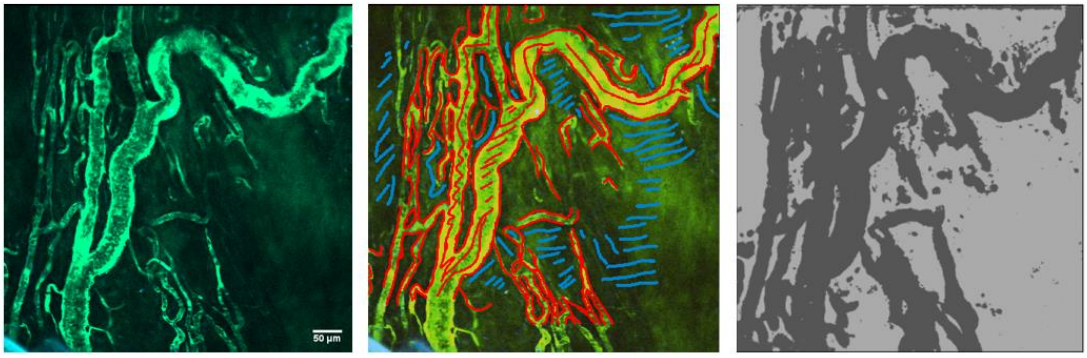

a b c

Figure 21- Vessels analysis using Ilastik segmentation.

a. Original acquired image before the segmentation.
b. For image classification several ROIs drawn as short brushes of different color were placed in two compartments: red for vessels, blue for background.
c. Output of segmentation made by Ilastik after the images training. Segmentation masks were created and for each pixel two possible values were assigned depending on their assignment by the algorithm. The final segmentation was not very reliable, in fact small vessels crossed with each other were classified as same big vessel. For this reason it was preferred to use Angio Tool for subsequent analysis on vessels.

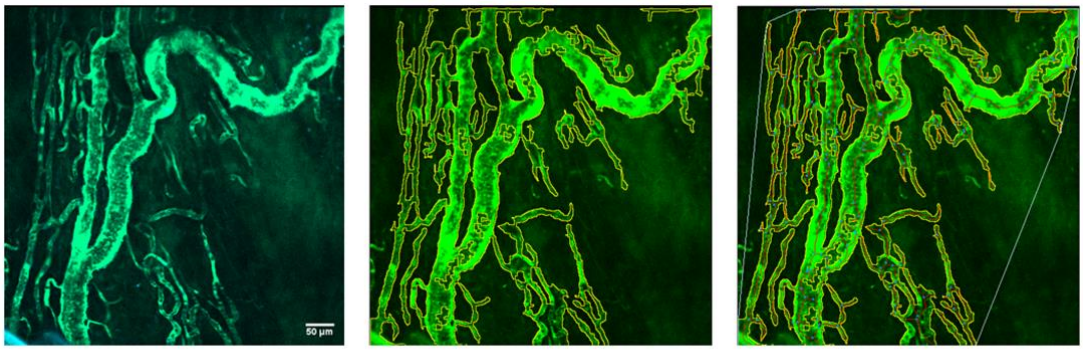

a b c

Figure 22- Vessels analysis using Angio Tool software

a. Original acquired image before the segmentation made by Angio Tool.
b. Identified vessels are demarcated with an outline on the displayed image which dinamically updates its shape in response to adjustments done using the controls included in the analysis tab of software. Once the outline overlay matches the vessels in the displayed image, the analysis was carried out. In the control tab was possible to adjust different parameters such as
c.

diameter, shape, and was possible also to fill holes and to remove small particles inside the image.

d. The resulting image indicates the area encompassing all vessels, a skeletal representation of the vascular network (in yellow) and the computed branching points inside this area (blue points).

c. *Ex vivo* evaluation of fibrosis

The histological protocol was carried out on cross sections of the parietal peritoneum which were fixed in the Bouin, fixative of choice for the peritoneum. In fact, the Bouin fixative was used to avoid the loss of mesothelial cells and of the layers of the sub-mesothelial extracellular matrix during the different steps of histology [171, 172].
The tissue was then fixed and subsequently embedded in paraffin using special steel molds (Bio Optica, 07-MBM6) so as to be able to orient the organ without encountering major difficulties.
Plastic grids were used to mount the paraffin block and to facilitate subsequent microtome cutting procedures. The biopsies of parietal peritoneum were cut into 4 µm sections with microtome and stained with Masson's Trichrome (Bio Optica, 04-010802). The thickness of the tissue was determined using the optical microscope, Zeiss Axioplan 2, and the software for imaging Zen 3.3 Blue edition.
The peritoneal thickness of each animal was calculated by the mean of measurements, at least 5, taken from one extreme to the other of the biopsy considering the specificity of the staining to the collagen layer affected by the fibrotic state**.**

d. Peritoneal ultrafiltration and analysis of transport status of membrane

In this study the PET test was performed to analyze the transport status of the peritoneal membrane. The test was performed by infusing 10 mL of 4.25% dialysis solution (Stay-safe, Fresenius) by intraperitoneal injection. For the intraperitoneal injection with the beveled side facing away from the animal, the needle was inserted through the peritoneal wall at the lower quadrant of the abdomen at a ~10 degree angle and almost parallel with the vertebral column to avoid perforation of abdominal organs. Immediately after the infusion, 1 mL of dialysate was taken to be used in

subsequent analysis, D0. For this purpose a cannula needle for intravenous injections 18G was left in place, provided with a metal core inside a plastic catheter. In fact, the metal core was removed during the withdrawal maneuver to avoid piercing the internal organs. The catheter, on the other hand, has been suitably punctured to facilitate the collection as the extremity is easily blocked. The details of the procedure are shown in the Figure 23.

After 1 hour of dwell time inside the abdomen, the drainage fluid was withdrawned by making an abdominal cut and using a syringe with a 21G needle. The total abdominal peritoneal fluid was collected and the drained volume was measured.

Blood samples taken from the cannulated carotid artery and dialysate from the abdomen were used for the Pet test. The samples were centrifuged at 3000 rpm for 10 minutes to remove any debris in the case of the dialysate and to obtain plasma in the case of the blood sample.

The Net Ultrafiltration value was obtained from the difference between the drainage volume and the infusion volume, demonstrating the dialysis capacity of the membrane after 15 days of treatment [29, 173-175].

Also as parameters for peritoneal solute transport were calculated dialysate-to-dialysate (D/D_0) for glucose and dialysate-to-plasma (D/P) ratios for creatinine and Na+. Values of plasmatic creatinine were corrected and normalized for plasmatic glucose [35, 176].

Na+ concentration in dialysate (Na+ sieving) was determined for the transcellular water transport (TCWT) and to analyze the UF failure threshold set with the value of 5 mM [35], considering the difference between the concentration of Na+ before and after the dwell time of 1 hour.

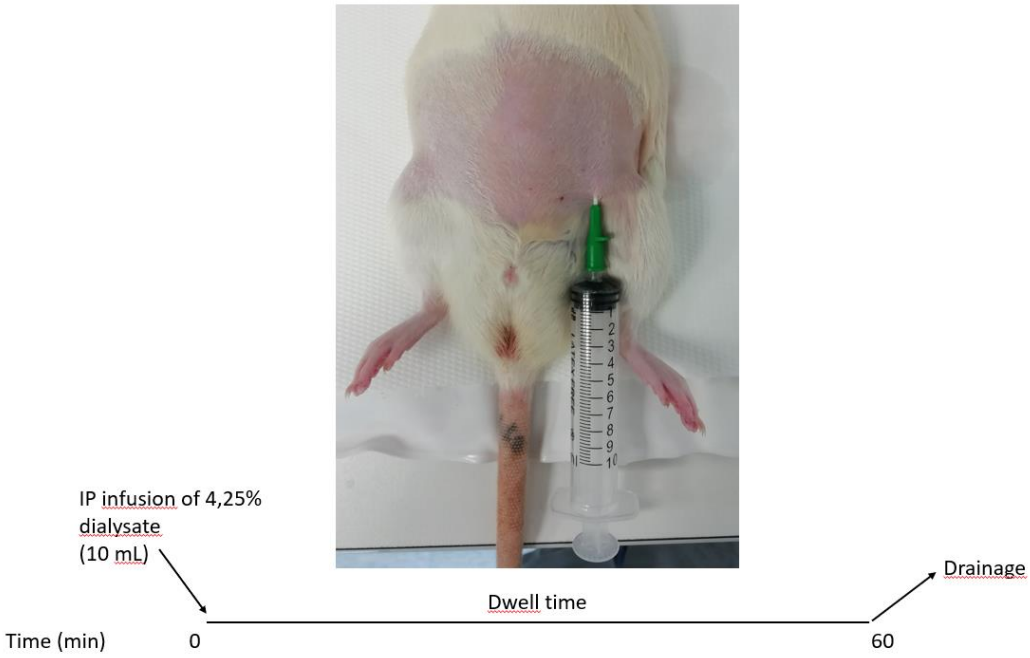

Figure 23- Details for the PET test protocol.

e. Statistical analysis

The data was shown as means of the measurements ± SEM (standard error of the mean). Multi-parametric analysis, comparing more than two groups, were performed through the Anova Test, followed by Tukey's multiple comparison test to analyze differences between two interested groups. A probability value (p value) $p < 0.05$ was considered statistically significant. GraphPad Prism 8 software was used for statistical data analysis.

3. Results

a. Treatment with Ole reduces the fibrosis induced by high concentrate glucose dialysate

The chronic treatment of peritoneal dialysis carried out on Wistar rats by daily infusion of dialysate with a high concentration of glucose (3.86%) showed a significant increase in the fibrotic state of the peritoneum, inhibited by treatment with the molecule with remarkable antioxidant properties, Ole (Figure 24 a). The difference founded between the two groups of treated animals (Sham-operated and 3.86%) which received an infusion of saline 0.9% and dialysis solution, respectively, was significant (Figure 24 a).

Single measurements were carried out for at least 15 measurements per each animal (Figure 24 b) in different ROIs, to have a fair number of measurements and to cover a large part of the flap of the isolated peritoneum during the acquisition. Using the image analysis software, Fiji, and specifically the 3D viewer plugin, it is possible to obtain 3D models of the membrane (Figure 24 c).

Furthermore, by carrying out measurements on the percentage of collagen fibers compared to the background, a significant difference was founded between animals treated with the dialysate 3.86% compared to Sham-operated (Figure 22 d). Considering this parameter, the antifibrotic effect of the molecule in the group of animals subjected to dialysis was described (Figure 24 d).

The density of collagen fibers was measured using 10 different stack frames of 5 different z-stack for each animal to derive this ratio of density to background using the threshold tool from Fiji, considering the following formula:

$$\frac{Fibrosis}{(Fibrosis+\boldsymbol{Background})} * 100$$

Here the most compact collagen layer in the treated group with dialysate was evident (Figure 24 e). The density of fibers of collagen in the 3.86% group was more abundant compared to sham group and was visible the reduction effect of Ole. Also the

composition of collagen fibers was different: it was well compacted and organized in the 3.86% group, compared to the other groups.

(a)

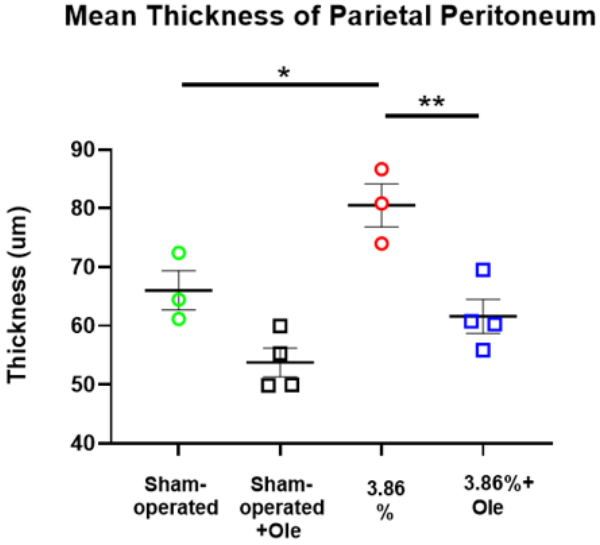

Test details	Mean 1	Mean 2	Summary	Adjusted P Value
Sham-operated vs. Sham-operated+Ole	66.03	53.76	ns	0.0692
Sham-operated vs. 3.86%	66.03	80.52	*	0.0432
Sham-operated vs. 3.86%+Ole	66.03	61.59	ns	0.7351
Sham-operated+Ole vs. 3.86%	53.76	80.52	***	0.0005
Sham-operated+Ole vs. 3.86%+Ole	53.76	61.59	ns	0.2620
3.86% vs. 3.86%+Ole	80.52	61.59	**	0.0061

Figure 24- Effect of Oleuropein on the thickness of parietal peritoneum.

(a) Reproduction of the thickness of the peritoneal membrane in µm. Significant difference between the group receiving the dialysate and between the latter group and the sham-operated group. Mean thickness of parietal peritoneum. Values of thickness in µm were obtained from the number of frames of the z-stack where were detactable the signal of collagen and the step size of z-stack, 0.3 µm. Data are presented as mean±SEM, p value<0.05, using ordinary one-way analysis of variance (ANOVA) with Tukey's multiple comparison test.

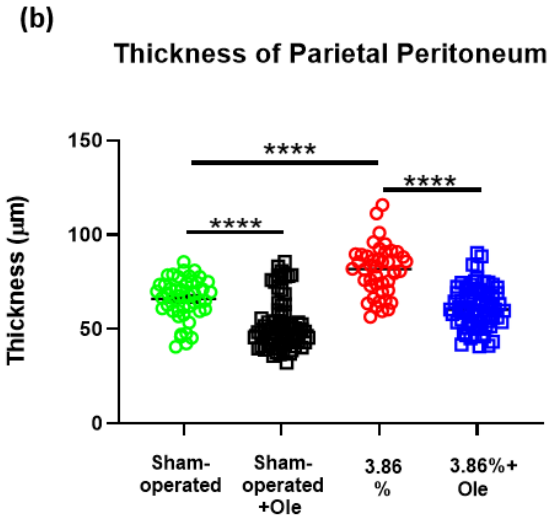

Thickness (µm)

Test details	Mean 1	Mean 2	Summary	Adjusted P Value
Sham-operated vs. Sham-operated+Ole	65.90	52.61	****	<0.0001
Sham-operated vs. 3.86%	65.90	80.82	****	<0.0001
Sham-operated vs. 3.86%+Ole	65.90	61.56	ns	0.2660
Sham-operated+Ole vs. 3.86%	52.61	80.82	****	<0.0001
Sham-operated+Ole vs. 3.86%+Ole	52.61	61.56	***	0.0002
3.86% vs. 3.86%+Ole	80.82	61.56	****	<0.0001

Figure 24- Effect of Oleuropein on the thickness of parietal peritoneum.

(b) Single measurements carried out on several ROIs, at least 15 per each animal. Data are presented as mean±SEM, p value<0.05, using ordinary one-way analysis of variance (ANOVA) with Tukey's multiple comparison test.

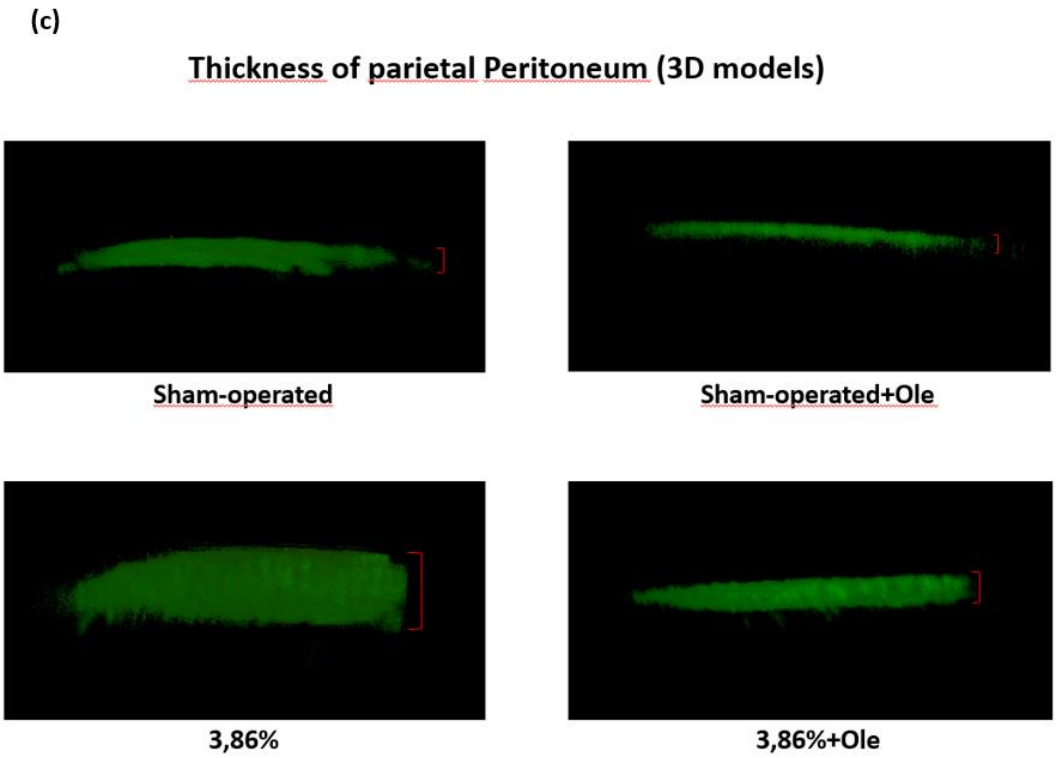

Figure 24- Effect of Oleuropein on the thickness of parietal peritoneum.

(c) 3D reconstruction of the fibrotic state of the sub-mesothelial layer in the different groups of rats subjected to treatment.

(d)

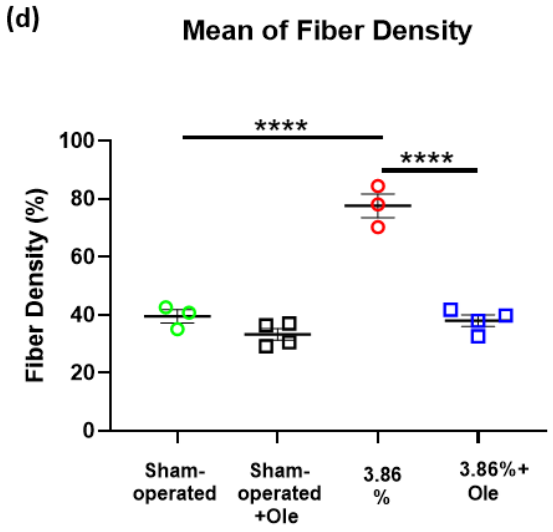

Fiber Density (%)

Test details	Mean 1	Mean 2	Summary	Adjusted P Value
Sham-operated vs. Sham-operated+Ole	39.50	33.27	*	0.0405
Sham-operated vs. 3.86%	39.50	77.61	****	<0.0001
Sham-operated vs. 3.86%+Ole	39.50	38.04	ns	0.9198
Sham-operated+Ole vs. 3.86%	33.27	77.61	****	<0.0001
Sham-operated+Ole vs. 3.86%+Ole	33.27	38.04	ns	0.1205
3.86% vs. 3.86%+Ole	77.61	38.04	****	<0.0001

Figure 24- Effect of Oleuropein on the thickness of parietal peritoneum.

(d) Percentage ratio of density of fibrosis to background. Data are presented as mean±SEM, p value<0.05, using ordinary one-way analysis of variance (ANOVA) with Tukey's multiple comparison test.

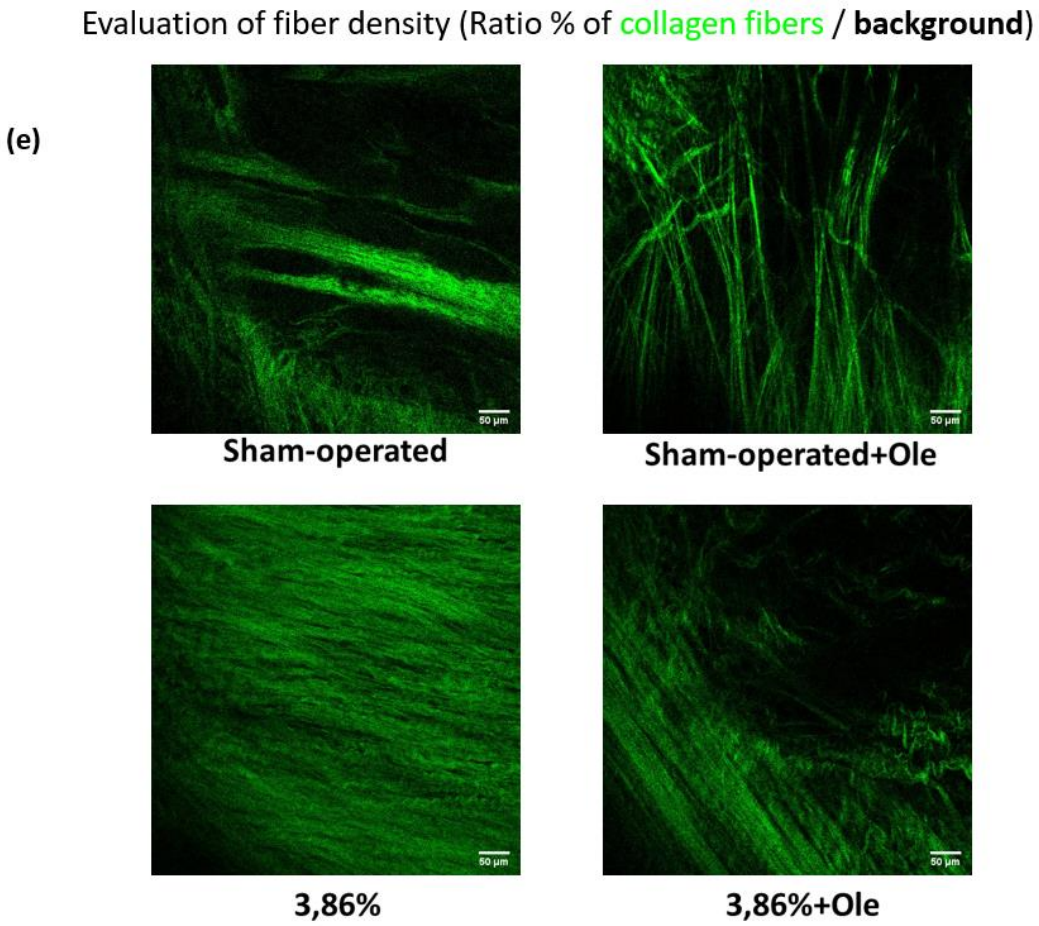

Figure 24- Effect of Oleuropein on the thickness of parietal peritoneum.

(e) Organization of collagen type I detected with SHG in the different treated groups. Scale bars, 50 µm.

b. Ex vivo evaluation of fibrosis confirmed in vivo measurements

The *ex vivo* approach confirmed the data obtained with multiphoton microscopy technology. In fact, the different measurements per area carried out on the biopsies showed a significant increase of the fibrotic layer in the dialysis group (Figure 25 a) The thickening was peculiar because of the presence of numerous nuclei, probably of cells recruited in the inflammatory phenomenon (Figure 25 b).

The anti-fibrotic effect of the Ole was significant with the relative reduction of the thickening of the sub-mesothelial layer (Figure 25 a).

(a)

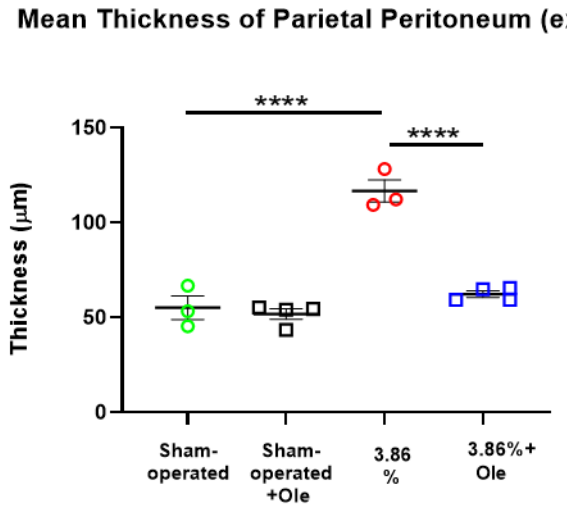

Thickness (µm)

Test details	Mean 1	Mean 2	Summary	Adjusted P Value
Sham-operated vs. Sham-operated+Ole	55.23	51.85	ns	0.9341
Sham-operated vs. 3.86%	55.23	116.7	****	<0.0001
Sham-operated vs. 3.86%+Ole	55.23	62.28	ns	0.6279
Sham-operated+Ole vs. 3.86%	51.85	116.7	****	<0.0001
Sham-operated+Ole vs. 3.86%+Ole	51.85	62.28	ns	0.2675
3.86% vs. 3.86%+Ole	116.7	62.28	****	<0.0001

Figure 25- *Ex vivo* evaluation of thickness of parietal peritoneum.

(a) Ole had an anti-fibrotic effect on dialytic group after 15 days of treatment. Range of significativity: p value<0.05. Data are presented as mean±SEM, p value<0.05, using ordinary one-way analysis of variance (ANOVA) with Tukey's multiple comparison test.

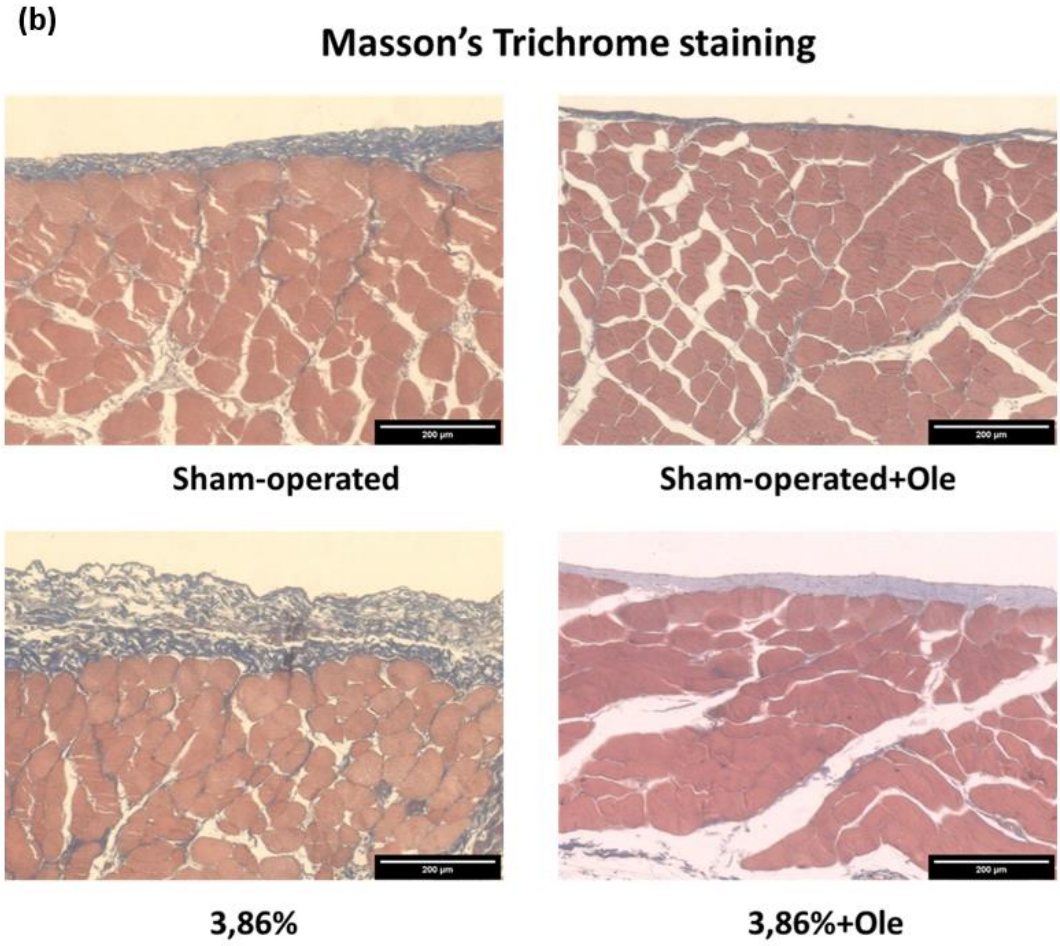

Figure 25- *Ex vivo* evaluation of thickness of parietal peritoneum.
(b) Masson's Trichrome staining confirm the thickenig induced by the high concentration of glucose inside the dialysate. Scale bars, 200 µm.

c. PET test: evaluation of better dialytic capacity of membrane induced by Ole

In order to have a greater robustness of the functional data, the number of animals enrolled in the treatment was increased: n=6 for sham-operated group, n=8 for sham+Ole group, n=6 for 3.86% group, n=8 for 3.86%+Ole group.

Functional analysis of the peritoneal membrane revealed improved ultrafiltration in the sham + Ole group compared to the dialysis group (Figure 26 a).

This result might be the consequence of Ole's effect on inflammation and angiogenesis and is in line with the data in the literature.

The further parameters analyzed, referring to clinical practice (D / D0 glucose, D / P creatinine, D / P Na +) did not show any significant data (Figure 26 b) except that considering the Na + sieving (Figure 26 c). Here, no significativity was obtained between the groups analyzed, but considering the average values, the UF failure condition was highlighted in the groups that took dialysis solution for 15 days both with and without the addition of Ole.

In fact, in the clinic, reference is made to the value of 5 mM as the limit below which there is the condition of functional deficit of the membrane and therefore a slowed flow of water into the peritoneal cavity through AQPs [35].

(a)

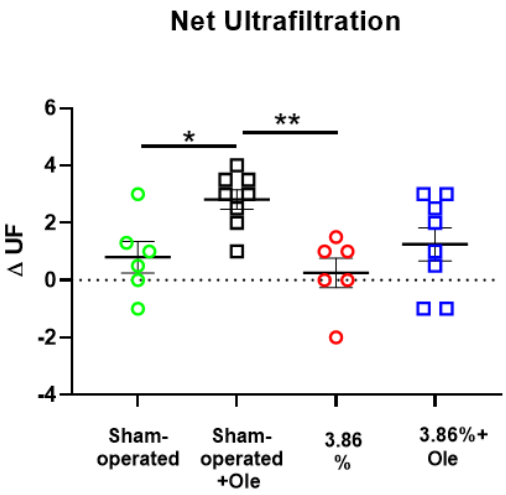

ΔUF

Test details	Mean 1	Mean 2	Summary	Adjusted P Value
Sham-operated vs. Sham-operated+Ole	0.8000	2.813	*	0.0455
Sham-operated vs. 3.86%	0.8000	0.2500	ns	0.8896
Sham-operated vs. 3.86%+Ole	0.8000	1.250	ns	0.9225
Sham-operated+Ole vs. 3.86%	2.813	0.2500	**	0.0079
Sham-operated+Ole vs. 3.86%+Ole	2.813	1.250	ns	0.1147
3.86% vs. 3.86%+Ole	0.2500	1.250	ns	0.5160

Figure 26- Evaluation of dialytic capacity of membrane:

(a) Net ultrafiltration.

Data are presented as mean±SEM, p value<0.05, using ordinary one-way analysis of variance (ANOVA) with Tukey's multiple comparison test.

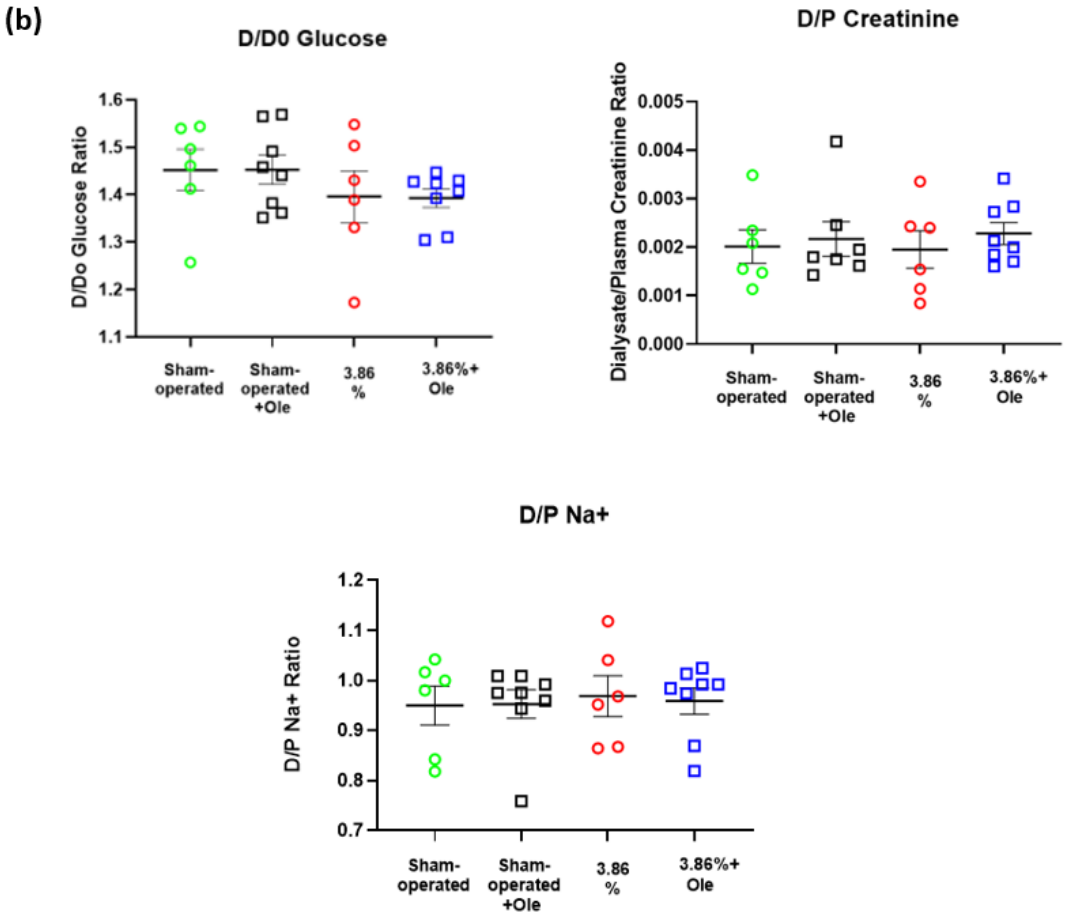

Figure 26- Evaluation of dialytic capacity of membrane:

(b) Clinical parameters used for functional analysis of peritoneal membrane.

Data are presented as mean±SEM, p value<0.05, using ordinary one-way analysis of variance (ANOVA) with Tukey's multiple comparison test.

(c)

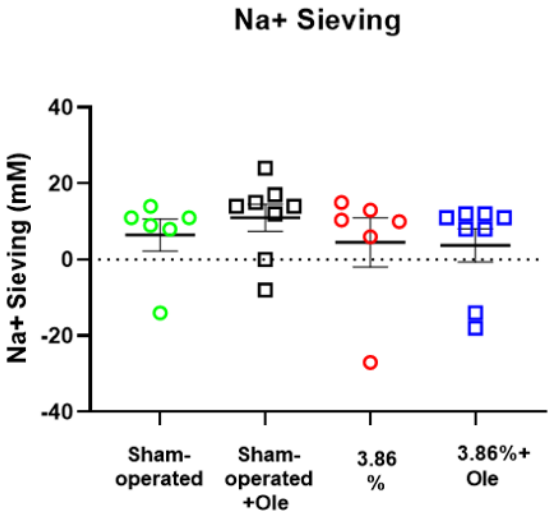

Na+ Sieving

Test details	Mean 1	Mean 2	Summary	Adjusted P Value
Sham-operated vs. Sham-operated+Ole	6.500	11.00	ns	0.9019
Sham-operated vs. 3.86%	6.500	4.567	ns	0.9925
Sham-operated vs. 3.86%+Ole	6.500	3.750	ns	0.9748
Sham-operated+Ole vs. 3.86%	11.00	4.567	ns	0.7627
Sham-operated+Ole vs. 3.86%+Ole	11.00	3.750	ns	0.6380
3.86% vs. 3.86%+Ole	4.567	3.750	ns	0.9993

Figure 26- Evaluation of dialytic capacity of membrane:

(c) Influx of free water into the peritoneal cavity considering the parameter of Na+ sieving.

Data are presented as mean±SEM, p value<0.05, using ordinary one-way analysis of variance (ANOVA) with Tukey's multiple comparison test.

d. Angiogenic effect of the 3.86% dialysate inhibited by Oleuropein

AngioTool was chosen as the software of choice for vessel analysis.

The analysis on the vessels showed a significant angiogenic effect induced by the hyperosmotic solution inhibited by the Ole, due to the anti-angiogenic potential reported in the scientific literature (Figure 27 a) [177, 178]. The further parameter analyzed, the density of the vascular nodes (branching), shows a significant increase in the nodes induced by the dialysate inhibited by the effects of the Ole (Figure 28 a).

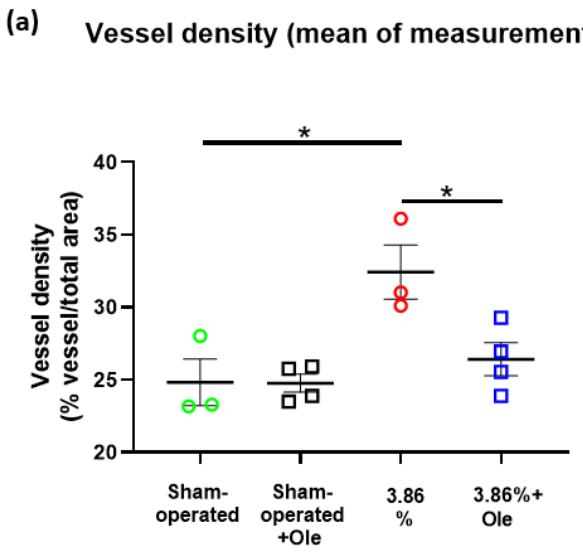

Test details	Mean 1	Mean 2	Summary	Adjusted P Value
Sham-operated vs. Sham-operated+Ole	24.83	24.76	ns	>0.9999
Sham-operated vs. 3.86%	24.83	32.42	*	0.0130
Sham-operated vs. 3.86%+Ole	24.83	26.42	ns	0.8175
Sham-operated+Ole vs. 3.86%	24.76	32.42	**	0.0081
Sham-operated+Ole vs. 3.86%+Ole	24.76	26.42	ns	0.7615
3.86% vs. 3.86%+Ole	32.42	26.42	*	0.0338

Figure 27- Anti-angiogenic effects of the Ole.

(a) Ole significantly reduced the angiogenic effects induced by the high concentrations of glucose as a consequence of thickening of peritoneal membrane and then of the need for greater vascularization to nourish the tissue.

Data are presented as mean±SEM, p value<0.05, using ordinary one-way analysis of variance (ANOVA) with Tukey's multiple comparison test.

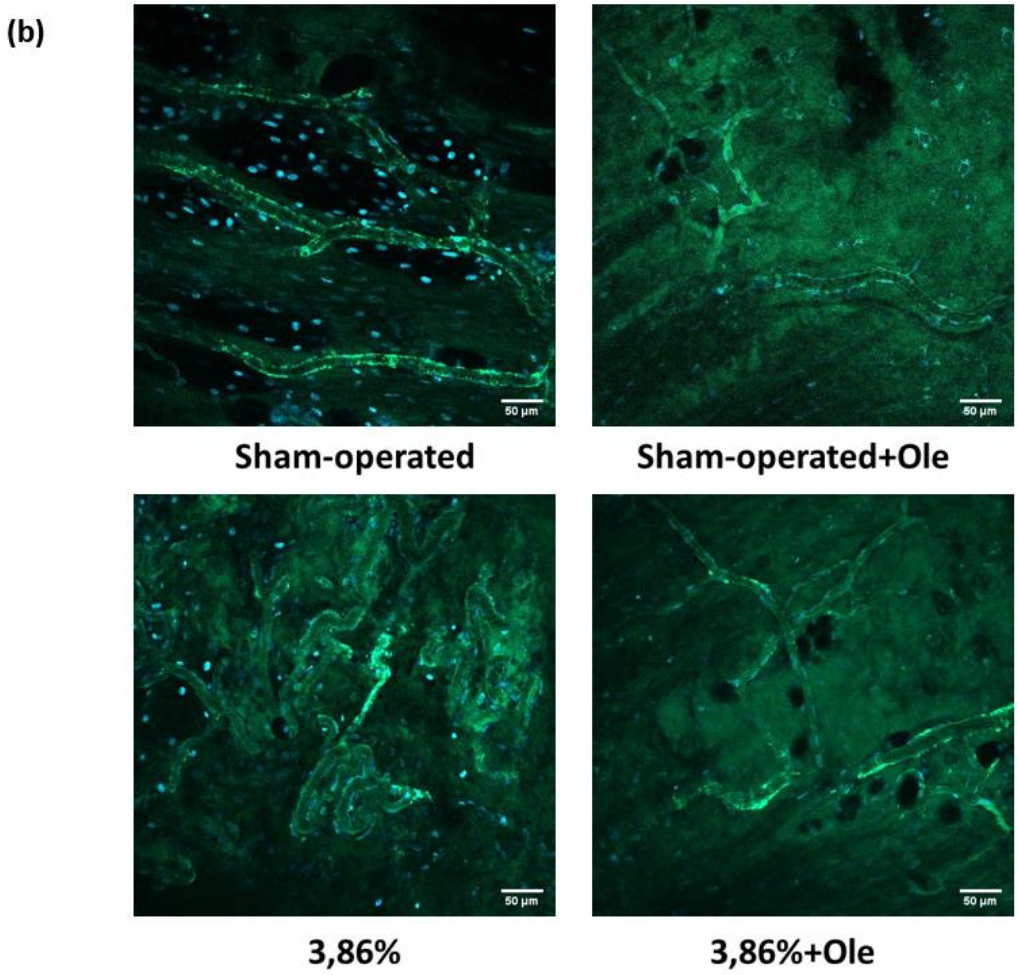

Figure 27- Anti-angiogenic effects of the Ole.

(b) 2PM acquisitions showing the conditions of vascular density in the different groups of animals. Scale bars, 50 µm.

(a)

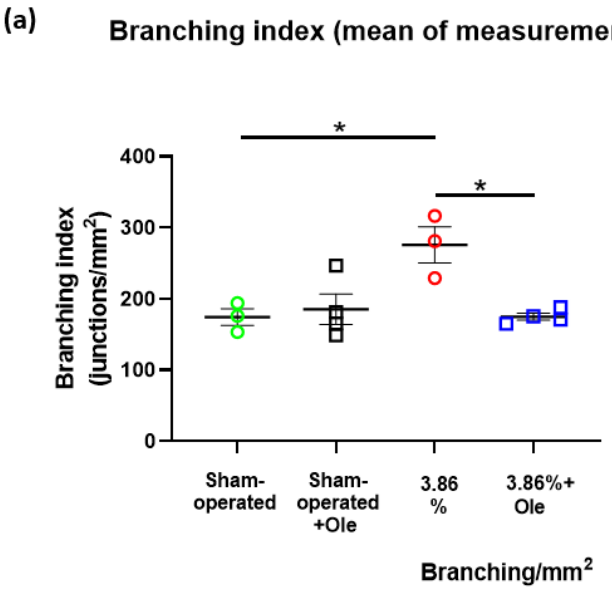

Test details	Mean 1	Mean 2	Summary	Adjusted P Value
Sham-operated vs. Sham-operated+Ole	174.5	185.5	ns	0.9691
Sham-operated vs. 3.86%	174.5	275.7	*	0.0148
Sham-operated vs. 3.86%+Ole	174.5	174.9	ns	>0.9999
Sham-operated+Ole vs. 3.86%	185.5	275.7	*	0.0196
Sham-operated+Ole vs. 3.86%+Ole	185.5	174.9	ns	0.9649
3.86% vs. 3.86%+Ole	275.7	174.9	*	0.0100

Figure 28- Branching index measured with AngioTool software.

(a) The use of Angio Tool software returns the output of vascular density which increased due to the angiogenesis induced by the dialysate and is significantly reduced thanks to the daily infusion of Ole. Data are presented as mean±SEM, p value<0.05, using ordinary one-way analysis of variance (ANOVA) with Tukey's multiple comparison test.

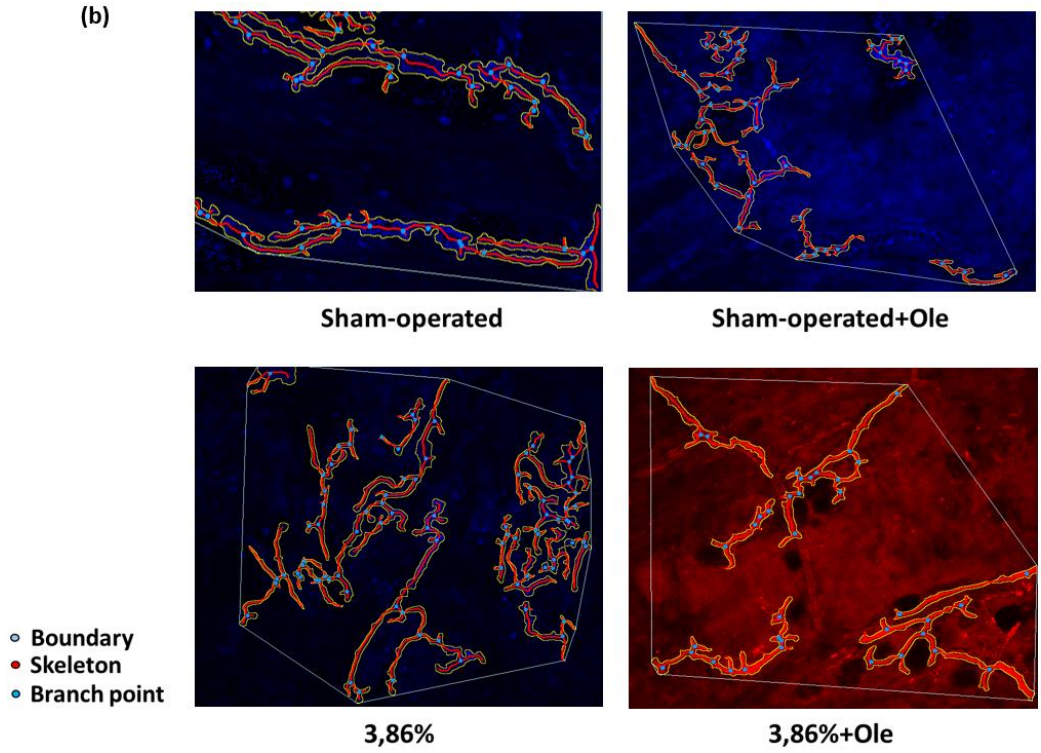

Figure 28- Branching index measured with AngioTool software.

The use of Angio Tool software returns the network of vascular branching points **(b)** which increased due to the angiogenesis induced by the dialysate and is significantly reduced thanks to the daily infusion of Ole. The software returns other outputs used during the vascular analysis: the area encompassing all vessels, a skeletal representation of the vascular network.

e. Ole reduces the proliferative effects induced by high glucose concentrations

Chronic treatment with 3.86% dialysate induced a significant increase in a further aging parameter of the peritoneal membrane, cellularity. The use of marker Hoechst for cell nuclei allowed identification of cells during *in vivo* imaging. The images were acquired using the superficial focal plane where there is the layer of mesothelial cells before the sub-mesothelium. The use of Fiji image analysis software allowed the counting of cells by area, using the analyze particle plugin.

Before this to remove background the images were pre-processed using different filters with Fiji, the Pure Denoise and the enhance contrast command.

Here the segmentation performed using Ilastik led to a better background removal performance than in the analysis performed in the vessels (Figure 29).

Using analyze particles plugin it was possible to substract background, to adjust threshold, to fill holes inside cells, to separate attached cells and to exclude counting on edges. The plugin was able to provide an output represented by an overview of the cells to be counted and the relative count (Figure 30). This analysis was made on several images, at least 10-15 images from different ROIs per each animal.

This analysis showed an increase in cellularity, understood as the number of nucleated cells, induced by the dialysate, probably indicative of the EMT process. This effect was significantly inhibited with the treatment of Ole. This result confirmed the data obtained from *in vitro* studies [119] (Figure 31).

Figure 29- Segmentation with Ilastik.

a. Original acquired image of nuclei before the segmentation.
b. For image classification several ROIs drawn as short brushes of different color were placed in two compartments: blue for nuclei, yellow for interstitium.
c. Output of segmentation made by Ilastik after the image training.

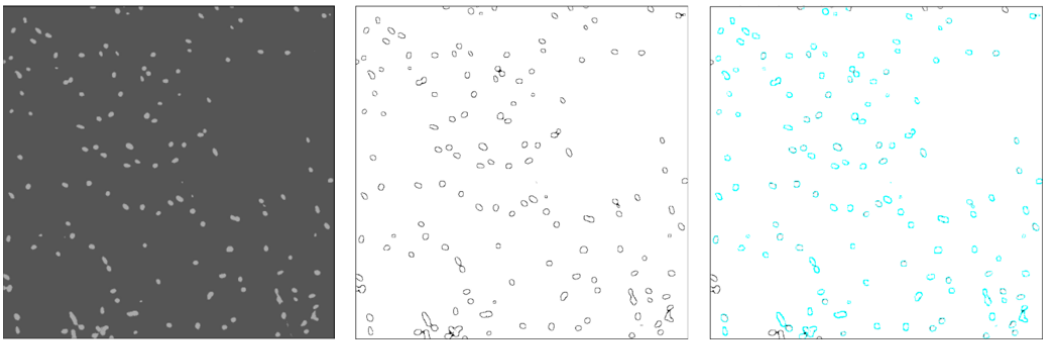

a b c

Results

	Area	Mean	StdDev	Min	Max	IntDen	RawIntDen
162	40	255	0	255	255	10200	10200
163	1	255	0	255	255	255	255
164	31	255	0	255	255	7905	7905
165	45	255	0	255	255	11475	11475
166	18	255	0	255	255	4590	4590
167	52	255	0	255	255	13260	13260
168	2	255	0	255	255	510	510

Summary

Slice	Count	Total Area	Average Size	%Area	Mean	IntDen
3202.png	168	6189	36.839	1.055	255	9394.018

d

Figure 30- Counting of nucleated cells with Fiji.

a. Mask generated from Ilastik.
b. Adjustments with Fiji software: substract background, fill holes, conversion to mask, watershed (separation of nucleated cells attached each other).
c. Generation of overlay masks with analyze particles plugin.

d. Outputs of the plugin: overview of the nucleated cells to be counted and the relative count.

(a) **Counting of nucleated cells/total area (mean of measurements)**

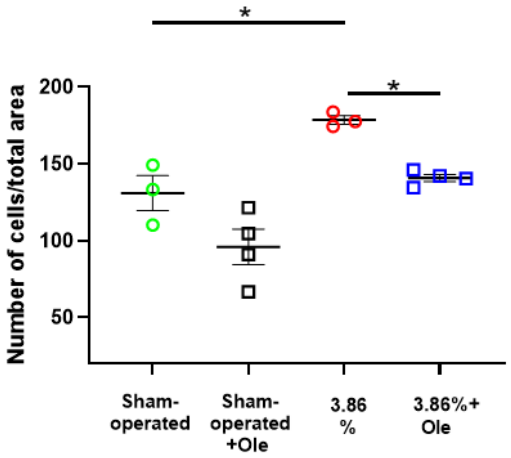

Nucleated cells/total area

Test details	Mean 1	Mean 2	Summary	Adjusted P Value
Sham-operated vs. Sham-operated+Ole	131.0	95.99	ns	0.0642
Sham-operated vs. 3.86%	131.0	178.6	*	0.0183
Sham-operated vs. 3.86%+Ole	131.0	140.8	ns	0.8480
Sham-operated+Ole vs. 3.86%	95.99	178.6	***	0.0002
Sham-operated+Ole vs. 3.86%+Ole	95.99	140.8	*	0.0111
3.86% vs. 3.86%+Ole	178.6	140.8	*	0.0443

Figure 31- Antiproliferative effect of the Ole

(a) The proliferative increase of mesothelial cells induced by the dialysate is significantly reduced by the Ole that inhibits the EMT process, as demonstrated by in vitro studies.

Data are presented as mean±SEM, p value<0.05, using ordinary one-way analysis of variance (ANOVA) with Tukey's multiple comparison test.

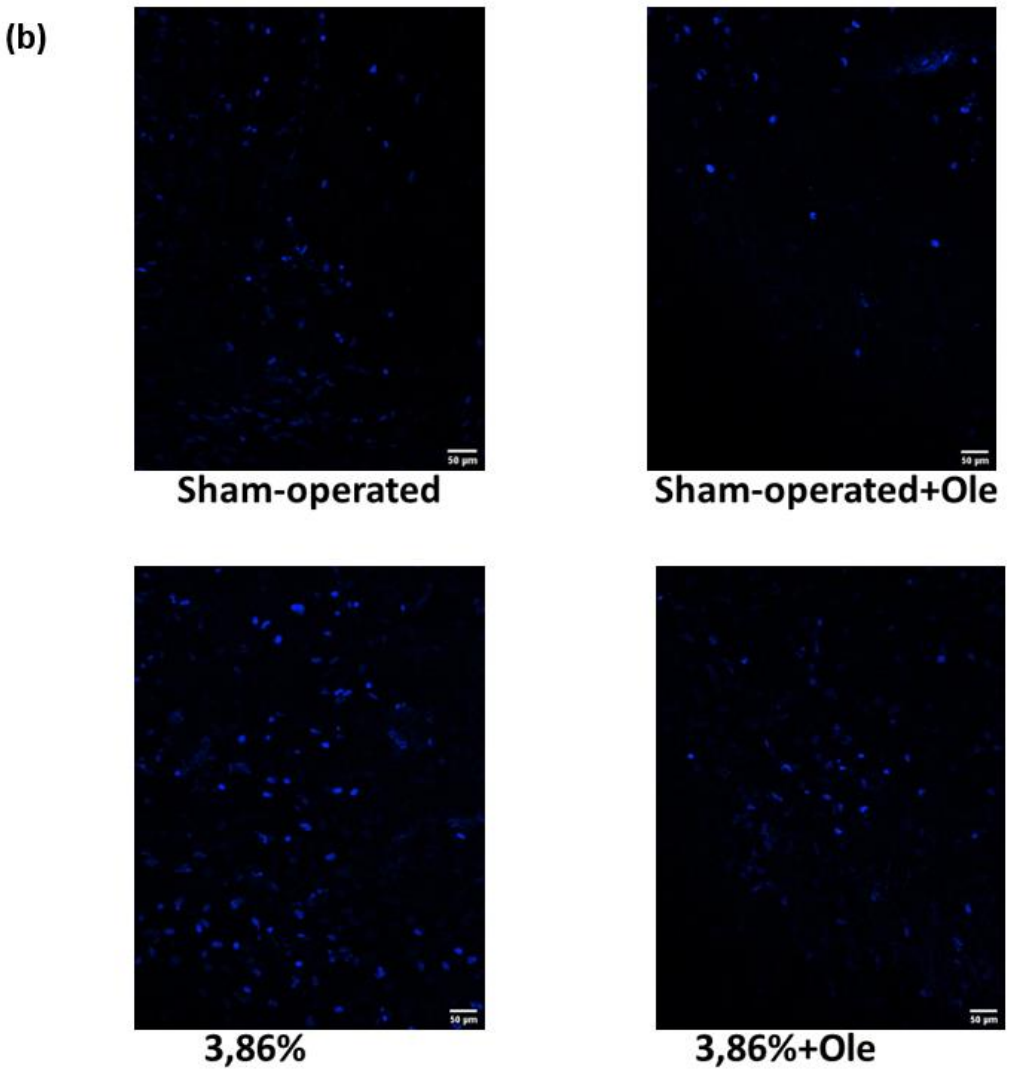

Figure 31- Antiproliferative effect of the Ole

(b) 2PM acquisitions showing the density of nucleated cells in the different groups of animals. Scale bars, 50 µm.

STUDY 3

The role of glucose sparing solution on peritoneal membrane

1. Glucose sparing solution treatment

In the present study we tested the effects of a novel formulation of PD solution, developed by an Italian company, leader for the production of new dialysis solutions. This solution is composed by a particular combination of L-Carnitine and Xylitol. In fact, the osmo-metabolic agents may be used alone or in combination in order to maximize their therapeutic effects. This combination was tested to evaluate *in vivo* the potential effects against the aging parameters of the peritoneal membrane induced by conventional solutions (fibrosis, angiogenesis, MMT), validating the results obtained from *in vitro* studies [114].

The tested solution was composed by: Glucose (1.5% w/v), Xylitol (2% w/v), Carnitine (0.02% w/v). This solution was chosen for the treatment considering the osmolarity similar to that of the conventional dialysis solution, 486 mOsm / L versus 483 mOsm / L.

Three groups of animals were considered:

- Sham-operated (n = 4), daily infusion (10 mL) of 0.9% physiological solution;
- 3.86% (n = 4), daily infusion (10 mL) of dialysis solution with a high concentration of glucose (3.86% Physioneal 40, Baxter);
- Glucose sparing solution (n = 5), daily infusion (10 mL) of solution with a combination of osmo-metabolic agents (Xylitol and Carnitine).

10 mL corresponds to the maximum volume allowed for intraperitoneal administration according to the international guidelines. The intraperitoneal administration of dialysis solution at a concentration of 3.86% was used to induce the fibrotic state of the peritoneum and the glucose sparing solution for the consequent inhibitory response. Instead the administration of physiological solution was used to mimic the normal physiological state of the membrane.

The treatment was performed only on wild type animal models, with intact kidneys in which there is no difficulty in filtration and drainage processes, trying to mimic the

peritoneal fibrotic state induced by dialysis solutions with a high glucose concentration (3.86%). Animals were used in the juvenile phase, after weaning, of 2-3 months of life, to have a better response to the maneuvers performed during the treatment and especially during surgery. For this purpose, the animals in housing, specifically male rats of the Wistar strain, were subjected to dialysis treatment by intraperitoneal (IP) injection without the need for drainage, for 15 days, once a day, following a light gas anesthesia with isoflurane. After making the IP injection, the animals were placed inside the cage and kept with access to food and water ad libitum. To monitor the state of the animals, in addition to daily checks, body weight was analyzed daily. After 15 days of treatment, the animals underwent surgical preparation for *in vivo* imaging and the protocol for carrying out the Pet test.

At the end of the experiment, the animals were sacrificed under deep anesthesia by asphyxiation with CO2, according to the National guidelines.

The endpoints considered for this type of project were the follows:

- Anti-fibrotic effect of alternative dialysis solution;
- Anti-angiogenic effect of glucose sparing solution;
- Effects on dialytic capacity of peritoneal membrane induced by the alternative dialysis solution.

2. Results

a. Treatment with glucose sparing solution prevents the fibrosis induced by chronic 3.86% glucose dialysate

The chronic treatment of peritoneal dialysis carried out on Wistar rats by daily infusion of dialysate with a high concentration of glucose (3.86%) showed a significant increase in the fibrotic state of the peritoneum. Similar treatment with Xylocore solution of the same osmolality but lower glucose concentration (1.5%) and containing carnitine and xylitol as additional osmo-metabolic agents had comparable as control level of collagen deposition (Figure 32).

The difference between the two groups of treated animals (Sham-operated and 3.86%) which received an infusion of saline 0.9% and dialysis solution, respectively, was significant (Figure 32).

Using the image analysis software, Fiji, and specifically the 3D viewer plugin, it was possible to obtain 3D models of the membrane (Figure 33). 3D rendering described well the condition of fibrotic state in different groups enrolled in the treatment and the specific condition of increased thickness of the sub-mesothelial layer induced by chronic treatment with the solution with a high concentration of glucose (Figure 33).

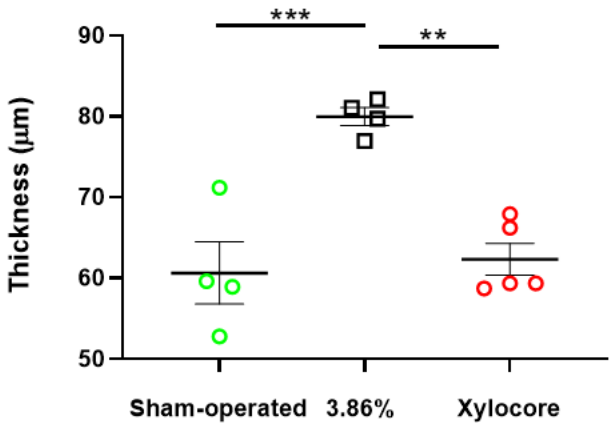

Thickness (µm)

Test details	Mean 1	Mean 2	Summary	Adjusted P Value
Sham-operated vs. 3.86%	60.63	79.96	***	0.0010
Sham-operated vs. Xylocore	60.63	62.31	ns	0.8807
3.86% vs. Xylocore	79.96	62.31	**	0.0013

Figure 32- Effects of Glucose sparing solution on the thickness of parietal peritoneum.

Reproduction of the thickness of the peritoneal membrane in µm. Values of thickness in µm were obtained from the number of frames of the z-stack where were detactable the signal of collagen and the step size of z-stack, 0.3 µm. Data are presented as mean ± SEM, p value<0.05, using ordinary one-way analysis of variance (ANOVA) with Tukey's multiple comparison test.

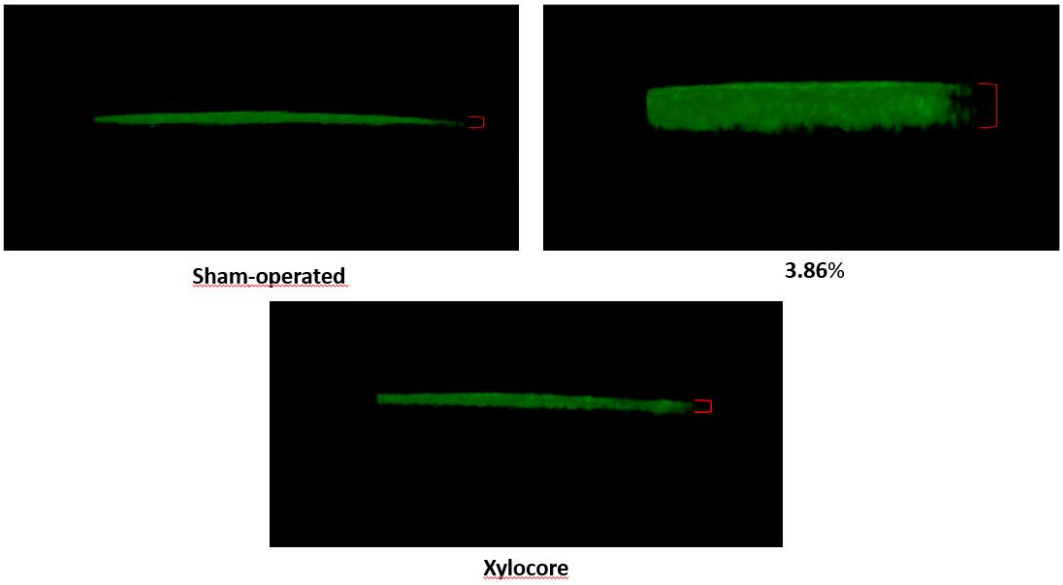

Figure 33- 3D reconstruction of the fibrotic state of the sub-mesothelial layer in the different groups of rats subjected to treatment.

b. Angiogenic effect of the 3.86% dialysate inhibited by Glucose sparing solution

For the segmentation execution performance, Angio Tool was chosen as the software of choice for vessel analysis.

The analysis on the vessels showed a significant pro-angiogenic effect induced by 3.86% glucose containing dialysate, but not by similar osmolar xylocore (Figure 34). The further parameter analyzed, the density of the vascular nodes (branching), shows a significant increase in the nodes induced by the dialysate inhibited by the effects of the alternative solution for PD treatment (Figure 35).

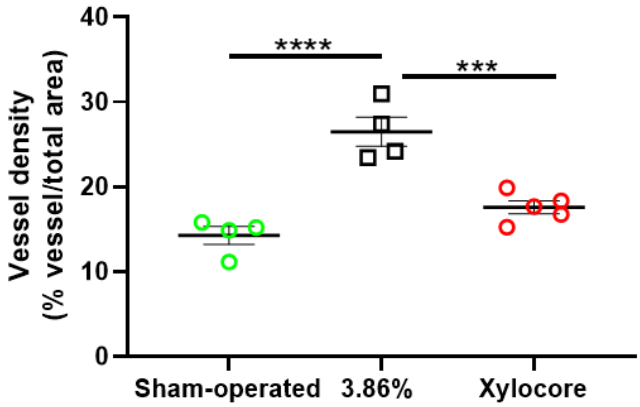

Vessel density

Test details	Mean 1	Mean 2	Summary	Adjusted P Value
Sham-operated vs. 3.86%	14.27	26.49	****	<0.0001
Sham-operated vs. Xylocore	14.27	17.58	ns	0.1619
3.86% vs. Xylocore	26.49	17.58	***	0.0008

Figure 34- Glucose sparing solution significantly reduced the angiogenic effects induced by the high concentrations of glucose as a consequence of thickening of peritoneal membrane and then of the need for greater vascularization to nourish the tissue.

2PM scans, at least 15, were done in different ROIs per each animal of the different groups of treatment. Data are presented as mean±SEM, p value<0.05, using ordinary one-way analysis of variance (ANOVA) with Tukey's multiple comparison test. On the graph are reported the mean of measurements on vessel density per each animal.

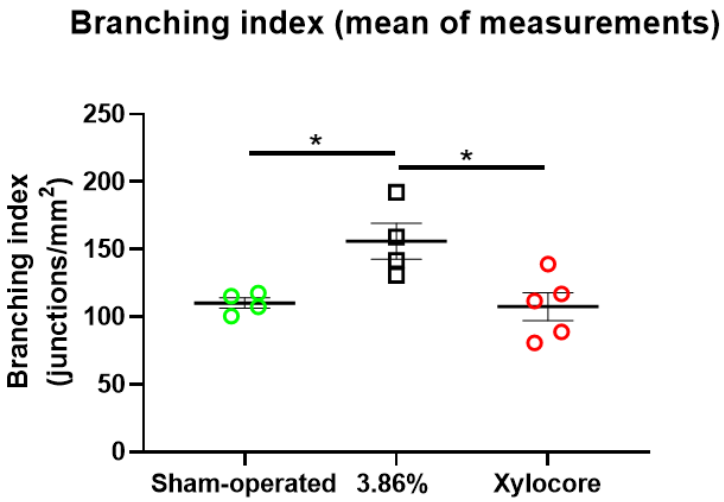

Branching index

Test details	Mean 1	Mean 2	Summary	Adjusted P Value
Sham-operated vs. 3.86%	110.2	155.9	*	0.0300
Sham-operated vs. Xylocore	110.2	107.5	ns	0.9810
3.86% vs. Xylocore	155.9	107.5	*	0.0169

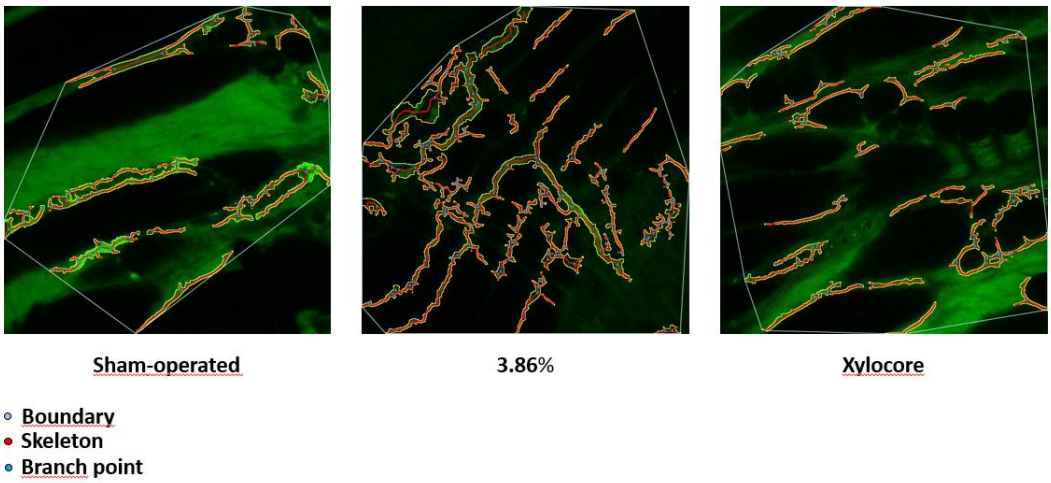

Figure 35- The use of Angio Tool software returned the network of vascular branching points which increased due to the angiogenesis induced by the dialysate and is significantly reduced thanks to the daily infusion of glucose sparing solution. Data are presented as mean±SEM, p value<0.05, using ordinary one-way analysis of variance (ANOVA) with Tukey's multiple comparison test.

c. Glucose sparing dialysate is associated to a tendency in the amelioration of functional parameter of peritoneal membrane

Functional analysis of the peritoneal membrane revealed a trend for a better ultrafiltration in the group treated with xylocore compered to 3.86% glcuose dialysate. (Figure 36). No difference was found for D / D0 glucose and D / P creatinine among the three groups (Figure 37).

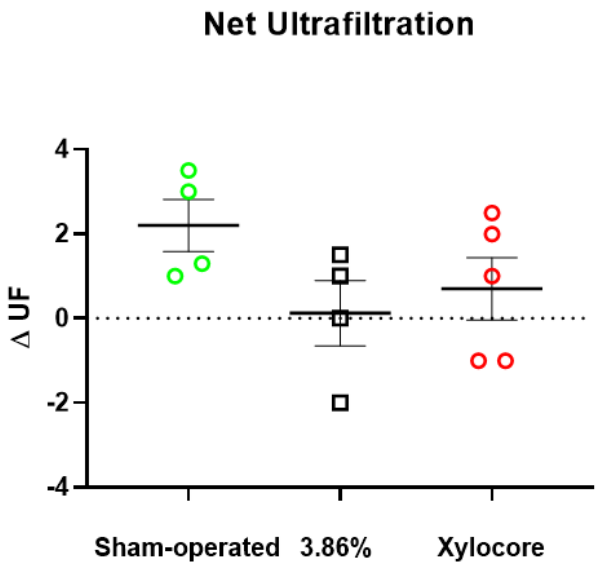

ΔUF

Test details	Mean 1	Mean 2	Summary	Adjusted P Value
Sham-operated vs. 3.86%	2.200	0.1250	ns	0.1744
Sham-operated vs. Xylocore	2.200	0.7000	ns	0.3367
3.86% vs. Xylocore	0.1250	0.7000	ns	0.8384

Figure 36- Evaluation of dialytic capacity of membrane: Net ultrafiltration. Data are presented as mean±SEM, p value<0.05, using ordinary one-way analysis of variance (ANOVA) with Tukey's multiple comparison test.

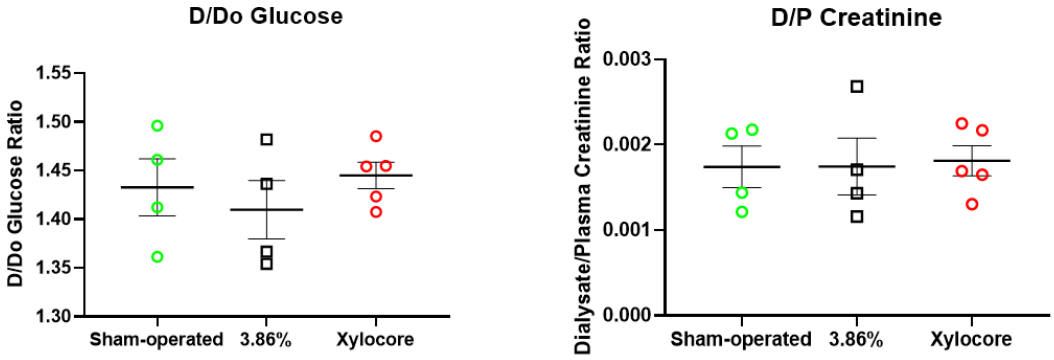

Figure 37- Evaluation of dialytic capacity of membrane: Clinical parameters used for functional analysis of peritoneal membrane. Data are presented as mean±SEM, p value<0.05, using ordinary one-way analysis of variance (ANOVA) with Tukey's multiple comparison test.

STUDY 4

2PM as an innovative tool for *in vivo* analysis of water permeability inside peritoneal vessels

1. Linescan tool for blood flow measurements

Multi-photon microscopy has high accuracy in measuring the flow in the vessels of the microcirculation. An innovative tool is represented by the Linescan that allows to acquire repetitive scans with very high spatial and temporal resolution within a region of interest. The Linescan tool is generally used in multiphoton microscopy experiments to assess the blood flow in tissues.

During the acquisition using the Prairie view software a Linescan path considering the lumen of different vessels of the microcirculation (arterioles, capillaries, post-capillary venules) was hand drawn (Figure 41).

After the iv bolus of the vessel marker (FITC 500 Kda, 10 mg/mL) during imaging it was possible to classify the vessels of the microcirculation based on the lumen diameter in real time. Furthermore, it was possible to notice the characteristic black shading of the erythrocytes (RBCs) in a background represented by the labeled plasma. In fact, the high spatial resolution, combined with the high temporal resolution of the linescans, allowed to capture the movement of the erythrocytes.

In the Linescan window the number of acquired lines was fixed to 3000 lines. Laser power and PMT gain of green channel were adjusted to avoid saturation of fluorescence signal.

The resulting output of the Linescan (Figure 38) represents a matrix in which the x axis is the space traversed by the RBCs (Δx) while the y axis is the temporal dimension (Δt). RBCs appear as black sloped bands with the relative slope of each band inversely correlated to the flow velocity [179-183]. The higher the slope the slower will be the flow.

Captured images had a resolution of 0.58 µm per pixel and a variable scanline period depending on the lenght of the traced path.

The analysis of the Linescan was performed with Fiji software. A linear ROI was drawn over each band and the slope angle (α) was measured, then the velocity was obtained by this formula:

$$RBCs\ velocity\ (mm/ms) = \frac{\Delta x}{\Delta t} = (cos(\alpha)*pixel\ size)/(sin(\alpha)*scanline\ period)$$

This experiment was set up with Prof. Sebastian Frische, (Department of Biomedicine, University of Aarhus (DK)), starting from the model of brain edema with IP infusion of milliQ water [184].

The tool of Linescan represented an innovative approach to measure the variations of blood flow inside the vessels of the microcirculation as the osmolarity of different solutions varied.

The flap of parietal peritoneum was used as an access door for drops of solutions (saline 0.9%, milliQ water, dialysate 2.3%(Stay safe CAPD/DPCA 19, Fresenius)).

A volume of 2 mL was added and then the acquisition was started for 10 minutes, the time limit for all the solution to be exchanged by the membrane.

During the 10 minutes of acquisition several measurements were made on vessels of different diameters.

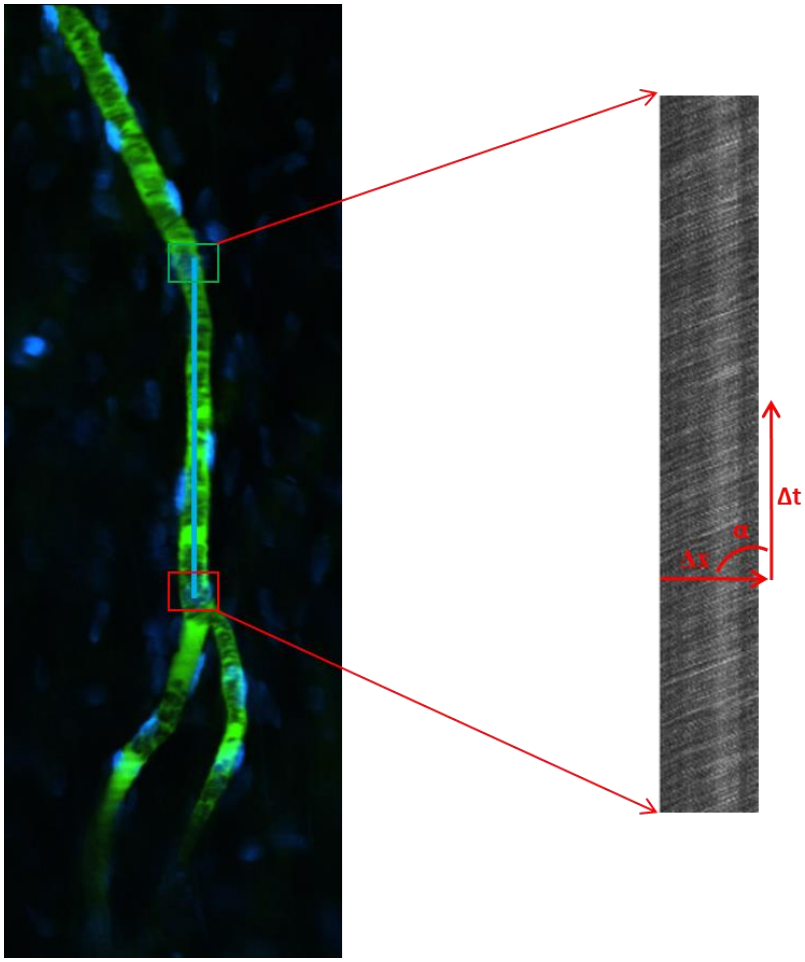

Figure 38- Representation of Linescan tool and measuring blood flow velocity**.**

2. Results

Linescan tool as an informative tool to study water exchange along the peritoneal membrane

Values of blood velocity were obtained using two approaches: first one using micron/pixel and scanline period values from metadata. Second one using angle obtained from Fiji and sine and cosine of this angle. The two values of velocity must be the same or similar. Details of Linescan are the follows: 3000 lines (number of lines), 9000 milliseconds (line period).

Adding 1-2 mL of solution and acquiring for 10 minutes the follows were the obtained data: velocity inside capillaries and arterioles using different solutions was the same,

but in the postcapillary venules the flow adding milliQ water increased twice. This was due for hemodilution and also explain the increased permeability of the venules. Also the velocity trend was like a wave, mainly in venules district, adding the milliQ water after 5 minutes of acquisition.

The phenomenon is not due to the increase in the diameter of the vessels, but to hemodilution and the greater permeability of the venules (Figure 39).

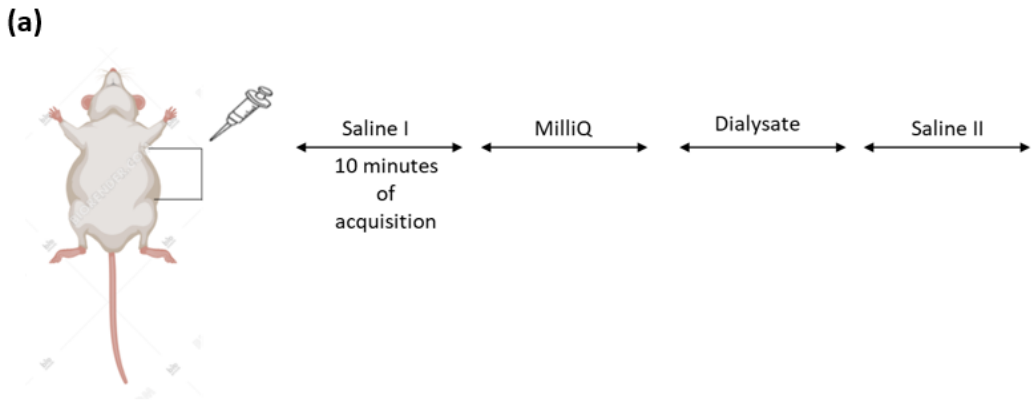

Figure 39- Measurements of blood flow using Linescan tool.

(a) Protocol for blood flow measurements.

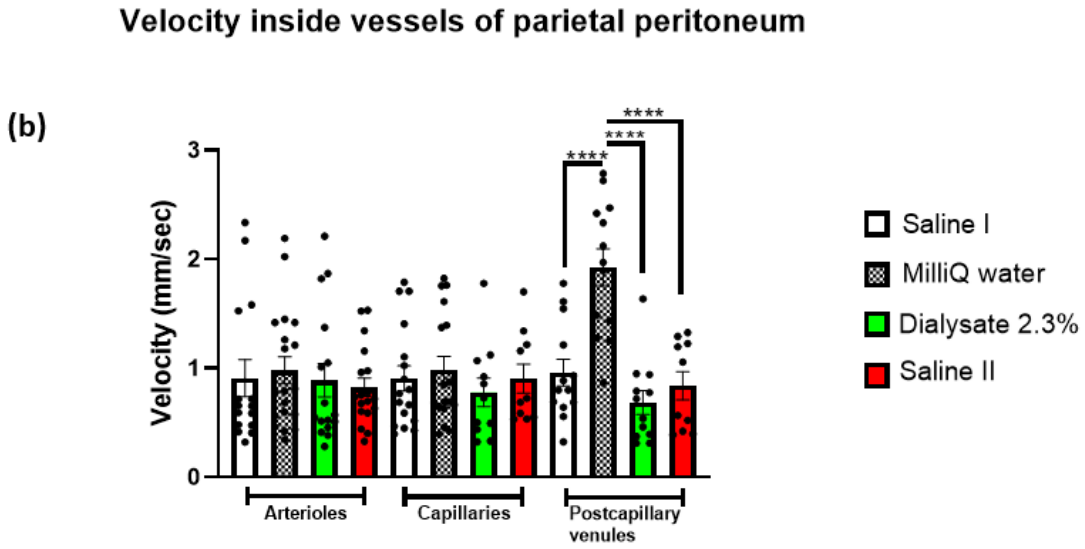

Mean velocity values (mm/sec)

	Arterioles	Capillaries	Venules
Saline I	0,90415	0,914732	0,958952
MilliQ	0,979714	0,98412	2,282854
Dialysate 2,3%	0,88374	0,777665	0,984919
Saline II	0,824794	0,902899	1,010148

Figure 39- Measurements of blood flow using Linescan tool.

(b) Graph reports the blood flow values and the relative increse in post-capillary venules district. Values are reported in mm/sec.

Data are presented as mean±SEM, p value<0.05, using ordinary one-way analysis of variance (ANOVA) with Tukey's multiple comparison test.

(c)

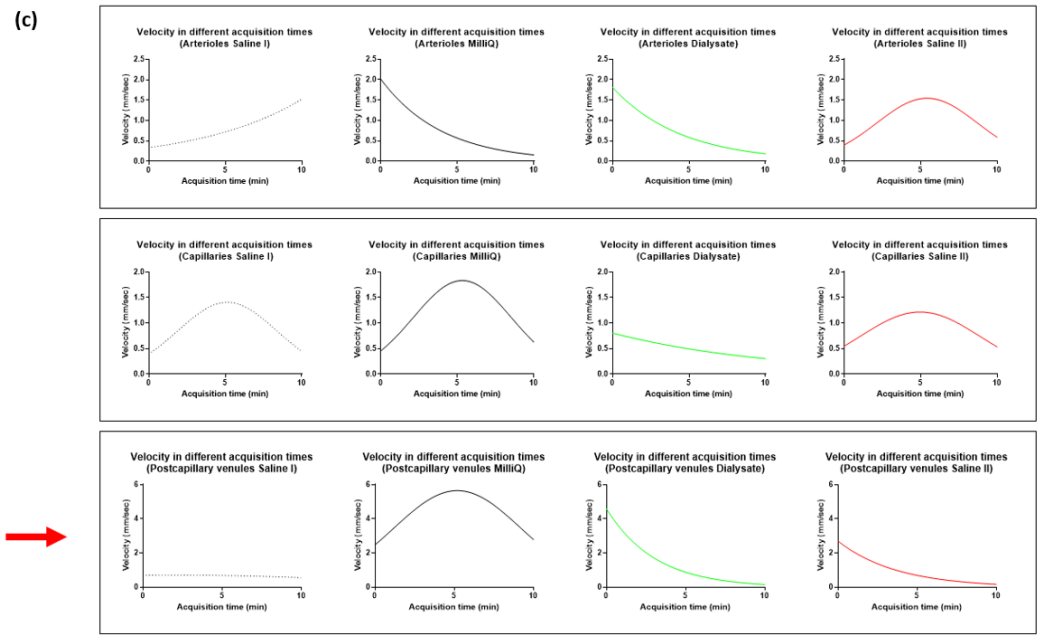

Figure 39- Measurements of blood flow using Linescan tool.

(c) The blood flow trend is like a wave, mainly in venules district, adding the milliQ water after 5 minutes of acquisition.

(d)

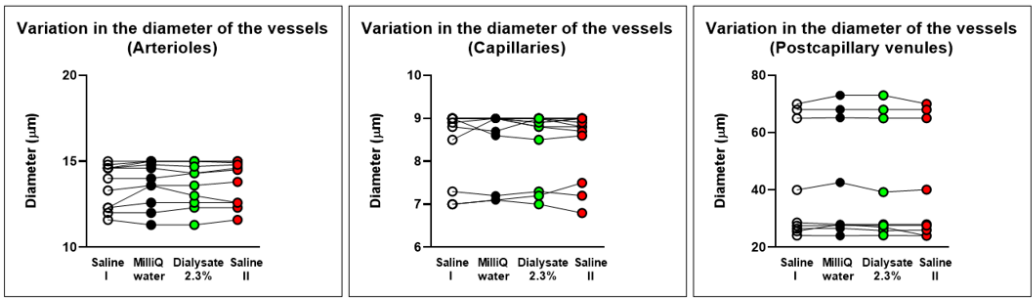

Mean Diameter values (µm)

	Arterioles
Saline I	13,55455
MilliQ	13,77273
Dialysate 2,3%	13,73636
Saline II	13,79091

Mean Diameter values (µm)

	Capillaries
Saline I	8,5
MilliQ	8,515885
Dialysate 2,3%	8,492303
Saline II	8,484615

Mean Diameter values (µm)

	Venules
Saline I	35,87692
MilliQ	36,38462
Dialysate 2,3%	36,19231
Saline II	35,84615

Figure 39- Measurements of blood flow using Linescan tool.
(d) The phenomenon is not due to the increase in the diameter of the vessels, but to hemodilution and the greater permeability of the venules.

10. Discussion

Multiphoton microscopy (MPM) is a powerful tool to study the physiology of living tissues in health and disease. Taking advantage from deep optical sections of tissues, it provides sharp images and high resolution movies of pathophysiological processes. Because of its great potential, MPM represents an advanced technique compared to confocal microscopy, allowing to investigate *in vivo* tissues and cellular compartments that were studied only *in vitro*. Starting from these applications and considering the absence of valid and reproducible *in vivo* systems in this study it is proposed a setting of a method to investigate *in vivo* all the component of the peritoneal membrane by mean of multiphoton microscopy.

Multiphoton microscopy allows *in vivo* evaluation of the microcirculation that supply the peritoneum and also to study the framework of mesothelial cells and their underlying layer of collagen fibers that contributes to the sub-mesothelial space.

We have implemented the surgical procedure in order to optimize the stability of a flap of parietal peritoneum to directly observe at the scope. With this approach the peritoneal membrane is evaluable at baseline condition and during exposure to dialysate solutions.

Our method allows to build 3d render of the peritoneal membrane, with the evaluation of all the single layers without the use of specific markers. In this way we could assess specifically the phenomena induced by the fibrotic process: the thickening of the sub-mesothelial interstitium and the greater density of the vascular network.

In vivo multi-photon microscopy allows the continuous acquisition of the movement of erythrocytes along the lumen of the vessels and has high accuracy in the measurement of blood flow.

The measurements of flow in the vessels of microcirculation (arterioles, capillaries, post-capillary venules) determine that exposure to hypotonic solutions increases significantly the flow in large-diameter vessels due to better permeability and

hemodilution. The innovative tool of the Linescan, that exploits the high temporal and spatial resolution of the acquisitions with MPM, could represent a useful support for discovering the mechanisms underlying peritoneal permeability and the haemodynamic and rheological processes that occur during PD treatment. Furthermore, as little is known in the literature in terms of *in vivo* studies our method could provide important informations on the physiology of the peritoneum and on the exchange mechanisms, described by a few models, including that of the three pores, which has proved to be one of the most similar to the physiological condition of the peritoneum.

In order to evaluate the possibility to detect morphological and functional changes in pathogenic model we have used the well established model of peritoneal fibrosis derived by 15 days long exposure of the peritoneal membrane to 3.86% glucose dialysate. With this approach we could detect the significant increase in the parameters of cellularity, vascularization, fibrosis and thickening of collagen fibers.

In order to test the sensibility of our approach to the evaluation of the peritoneal membrane senescence parameters, we tested the effect of Oleuropein (Ole) in preventing the damage induced by high glucose containing dialysate. Ole reduced both the thickness and the organization of the collagen fibers and the vascular network, including the number of branch points.

Although the use of Oleuropein has not yet involved patients, the results of the study seem promising for an adequate slowdown and treatment of peritoneal fibrosis, associated with chronic dialysis treatment. For this reason, it is necessary to enhance the antioxidant effects of Oleuropein and, therefore, of its metabolite Hydroxytyrosol evaluated thanks to the use of Multiphoton Microscopy. Effects that occur on preventing the increase of:

1) Thickness of the Parietal Peritoneum, significantly reduced, and irregular structure of the collagen molecules of the sub-mesothelium;

2) angiogenesis and density of vascular branching points, which compromise the function of the peritoneal membrane and are significantly reduced;

3) Cellularity, closely linked to the Epithelial-Mesenchymal Transition process with a reduction of epithelial cells and an increase in fibroblasts.

By ensuring this, peritoneal dialysis could be made more efficient and above all more lasting. In fact, in association with the reduced alteration of the histological aspect of the peritoneal membrane, it is possible not only to maintain, but also to improve its function in terms of solute exchange processes and, therefore, of diffusion, convection and ultrafiltration. The "Ultrafiltration Failure", the main cause of reduced peritoneal permeability, can be prevented. Finally, Oleuropein can be considered as a molecule with multiple functions and, consequently, it is considered suitable for the treatment, slowdown and prevention of numerous pathologies and / or complications of them. In fact, it has numerous other properties and among them we certainly include the anti-inflammatory and anti-atherogenic ones: inhibits the secretion of Leukotriene B4 and pro-inflammatory cytokines (especially TNF-α) [185]. TNF-α is essential for vasodilation, chemotaxis and for the activation of iNOS and COX-2 (sources of free radicals). It also reduces the production of IL-1β from monocyte-macrophage class cells upon stimulation of Lipopolysaccharide (LPS) [186] and IL-6. In the context of ischemic heart disease, Oleuropein performs various functions that can reduce oxidative stress, derived from ischemia, thanks to its vasodilatory properties. antiplatelet agents and by reducing oxidized LDL, the production of superoxide anion and thromboxanes and by activating the Nrf2-mediated pathway [187]. Hepato-protectivity is also contemplated in the function of Oleuropein: studies have shown the slowing of the progression of steatosis to non-alcoholic steatohepatitis, inhibiting the accumulation of lipids within the cytoplasm of hepatocytes and of collagen molecules in the interstitium [188]. Furthermore, the antimicrobial effect of the molecule is of considerable importance, especially against Gram + and Gram- germs, but above all: *Bacillus Cereus, Salmonella Enteriditis and Mycoplasma*. The mechanism behind this process is not yet clear. In addition to the antimicrobial function, the antiviral function on HBV and HIV must be included. With regard to the first, Oleuropein inhibits the secretion of HbsAg and reduces viraemia [189], while with regard to the second function, it interacts and negatively regulates retroviral intravascularity. Neuroprotectivity is counted among the functions of the molecule and, above all, its use in various degenerative pathologies has been tested. In fact, the administration of Oleuropein, inside the peritoneal cavity of rats once a day for six months, revealed a

neuroprotective effect. The latter occurs at the level of the brain stem and, more precisely, on the cells of the substantia nigra: it has therefore been hypothesized that its use in the prevention or in any case on the slowing of degenerative process in dopaminergic neurons [190]. However, the most surprising data concerns Alzheimer's disease: it was noted that Oleuropein interacts with the amino acids essential for the polymerization of β-amyloid, thus inhibiting the formation of plaques (elements at the basis of the pathogenesis of neurodegenerative disease) and that it also has an effect on intraneuronal Tau proteins [191]. Cardioprotectivity is also an important element to be taken into account: long-term administration of Ketamine causes an increase in sympathetic tone and the release of norepinephrine and adrenaline and can determine an important alteration of myocardial histology through tissue necrosis and deposition of fibrous material, a source of fatal arrhythmias. All this comes from the lipid peroxidation process which is inhibited by Oleuropein [192] thanks to its anti-inflammatory and regenerative properties. It also has a nephroprotective activity, reducing oxidative stress secondary to renal reperfusion in rats, also improving its functionality in a short time. The increase in the function of catalase and superoxide dismutase, together with the scavenging of the superoxide anion, the cleavage of Caspase-3, the phosphorylation of GSK3β (anti-apoptotic properties) and the phosphorylation of IkBα (anti-inflammatory effect), is the best representation of Nephroprotectivity [193]. However, it is also necessary to evaluate how Oleuropein can reduce the toxic effects of rhabdomyolysis on the kidney. Glycerol was used to induce the destruction of striated skeletal muscle fibers (resulting in myoglobinemia and myoglobinuria; the latter causes Renal AKI from Acute Tubular Necrosis) [194] and oxidative damage to the renal tissue from increased activity of Catalase and Superoxide dismutase, from consumption of Glutathione and from an increase in the concentration of Nitric Oxide and Malondialdehyde. Oleuropein can mitigate the effects of glycerol countering them [194]. Since oxidative stress is at the basis of the onset of neoplastic transformation, it can also be considered as an antitumor molecule. It was concluded that Oleuropein has a pro-apoptotic effect on malignant epithelial cells derived from the mucous membrane of colon, arresting them in the S phase of the cell cycle and in the G2-M transition phase [195]; the same effect was noted on

leukemia cells, prostate adenocarcinoma cells, thyroid carcinoma, neuroblastoma, mesothelioma and glioblastoma cells. In "Non-small Cells Lung Cancer", it is the signal transduction pathway activated by Akt that is the protagonist of neoplastic onset and progression. Oleuropein not only blocks its synthesis, but at the same time increases the activity of the pro-apoptotic mitochondrial enzyme glyoxalase-2 (mGlo2, which interacts with Bax, activating it) thanks to the up-regulation of superoxide dismutase-2 and to the consequent inhibition of Akt [196]. It induces apoptosis, increasing the effect of Capase-3 and -8 and inhibiting Bcl-2 [197], in hepatocarcinoma tissue, while on pancreatic adenocarcinoma cells it is more toxic than the antineoplastics themselves [198]. Further effects of Oleuropein are certainly: the antihypertensive one (at a dosage of 500mg / day it is able to reduce both systolic and diastolic blood pressure, even in patients suffering from renal insufficiency and type 2 diabetes mellitus) and the hypocholesterolemic process (process which most likely involves Phospholipase C and metabolites of arachidonic acid [199], reducing total cholesterol, oxidized LDL and triglycerides). The inhibition of the release of IL-6, a cytokine factor important for the colonic inflammatory process and the attenuation of the oxidative cytotoxic effects following a trauma to the spinal cord are guaranteed by Oleuropein, reducing the symptoms in the first case [200] and inflammatory factors in the second case [201]. Finally, it is necessary also to add the inhibitory effect against mTOR, the "Mammalian target of Rapamicin", implicated in various degenerative, cancerous, metabolic and cellular aging pathologies [202]. The discovery of new substances, such as Ole, used during dialysis treatment, could allow the replacement of the standard solution with a high concentration of glucose, which in the long term can cause problems such as fibrosis of the peritoneum.

Thanks to the implementation of this innovative approach to the study of the peritoneal membrane, a partnership has been established with an Italian company that produces new dialysate solutions that are technologically innovative in composition: Iperboreal Pharma. This partnership is based on innovation research projects that will allow to continue the study in this area.

Limited progress has been made in the last 50 years of peritoneal dialysis, regarding glucose replacement with a novel osmotic agent. Glucose-based solutions are still the most used and PD treatment still confers serious local and systemic toxicity.

To improve this field or research, a treatment carried out using the Xylitol and Carnitine as osmo-metabolic agents in the PD solutions has shown beneficial effects against the triggering of fibrotic and angiogenetic phenomena induced by conventional solutions with high concentration of glucose.

This study confirmed the data present in the literature from an *in vitro* study on the effects of the formulation on human mesothelial cells [114]. Here, this novel formulation shows better performance in terms of higher cell viability, better preservation of the integrity of the mesothelial layer and reduced release of pro-inflammatory cytokines. This new formulation could represent a step forward towards obtaining PD solutions with high biocompatibility. *In vivo* studies such as the one proposed in this phD project will examine the safety, tolerability, and efficacy of the new PD solutions not only on preservation of peritoneal membrane and residual kidney function, but also on underlying comorbidities able to increase cardiovascular risk.

Furthermore, this experimental model will allow to study the characteristics of the peritoneal membrane *in vivo* upon exposure to other different types of dialysate, not only based on glucose, but also other osmotic components as well as the different electrolyte composition. This method will offer great potential for also testing new pharmacological approaches aimed at preserving the structural and functional integrity of the peritoneal membrane and it will able to provide an innovative tool for clinical applications.

11. References

1. Ansari, N., *Peritoneal dialysis in renal replacement therapy for patients with acute kidney injury.* Int J Nephrol, 2011. **2011**: p. 739794.
2. La Milia, V., *Peritoneal transport testing.* J Nephrol, 2010. **23**(6): p. 633-47.
3. Li, P.K. and K.M. Chow, *Maximizing the success of peritoneal dialysis in high transporters.* Perit Dial Int, 2007. **27 Suppl 2**: p. S148-52.
4. Mujais, S., et al., *Evaluation and management of ultrafiltration problems in peritoneal dialysis. International Society for Peritoneal Dialysis Ad Hoc Committee on Ultrafiltration Management in Peritoneal Dialysis.* Perit Dial Int, 2000. **20 Suppl 4**: p. S5-21.
5. Bammens, B., *Urea and uremic solutes: how does peritoneal dialysis work?* Semin Nephrol, 2011. **31**(2): p. 127-37.
6. Gokal, R., *Peritoneal dialysis in the 21st century: an analysis of current problems and future developments.* J Am Soc Nephrol, 2002. **13 Suppl 1**: p. S104-16.
7. Dombros, N., et al., *European best practice guidelines for peritoneal dialysis. 2 The initiation of dialysis.* Nephrol Dial Transplant, 2005. **20 Suppl 9**: p. ix3-ix7.
8. Goffin, E., *Peritoneal membrane structural and functional changes during peritoneal dialysis.* Semin Dial, 2008. **21**(3): p. 258-65.
9. Aune, S., *Transperitoneal exchange. II. Peritoneal blood flow estimated by hydrogen gas clearance.* Scand J Gastroenterol, 1970. **5**(2): p. 99-104.
10. Sachdeva, B. and K. Abreo, *The history of interventional nephrology.* Adv Chronic Kidney Dis, 2009. **16**(5): p. 302-8.
11. Dakwar, G.R., et al., *Nanomedicine-based intraperitoneal therapy for the treatment of peritoneal carcinomatosis - Mission possible?* Adv Drug Deliv Rev, 2017. **108**: p. 13-24.
12. Jain, A.K., et al., *Global trends in rates of peritoneal dialysis.* J Am Soc Nephrol, 2012. **23**(3): p. 533-44.
13. Sam, R., et al., *Addition of monosodium dihydrogen phosphate to an acid concentrate to prepare a phosphate-enriched, bicarbonate-based hemodialysis solution.* Artif Organs, 2014. **38**(9): p. 824-5.
14. Nagai, K., et al., *Assessment of environmental sustainability in renal healthcare.* J Rural Med, 2021. **16**(3): p. 132-138.
15. Verger, C., et al., *Structural and ultrastructural peritoneal membrane changes and permeability alterations during continuous ambulatory peritoneal dialysis.* Proc Eur Dial Transplant Assoc, 1981. **18**: p. 199-205.
16. van Baal, J.O., et al., *The histophysiology and pathophysiology of the peritoneum.* Tissue Cell, 2017. **49**(1): p. 95-105.
17. Kastelein, A.W., et al., *Embryology, anatomy, physiology and pathophysiology of the peritoneum and the peritoneal vasculature.* Semin Cell Dev Biol, 2019. **92**: p. 27-36.
18. Mutsaers, S.E., *The mesothelial cell.* Int J Biochem Cell Biol, 2004. **36**(1): p. 9-16.
19. Mutsaers, S.E., *Mesothelial cells: their structure, function and role in serosal repair.* Respirology, 2002. **7**(3): p. 171-91.
20. Witz, C.A., et al., *Composition of the extracellular matrix of the peritoneum.* J Soc Gynecol Investig, 2001. **8**(5): p. 299-304.
21. Verger, C., *Peritoneal Ultrastrucure.* 1985.

22. Rippe, B., *A three-pore model of peritoneal transport.* Perit Dial Int, 1993. **13 Suppl 2**: p. S35-8.
23. Zhao, Y.L., et al., *[Ultrafiltration versus intravenous diuretics in decompensated heart failure: a meta-analysis of randomized controlled trials].* Zhonghua Yi Xue Za Zhi, 2013. **93**(30): p. 2345-50.
24. Rippe, B., G. Stelin, and B. Haraldsson, *Computer simulations of peritoneal fluid transport in CAPD.* Kidney Int, 1991. **40**(2): p. 315-25.
25. Devuyst, O. and B. Rippe, *Water transport across the peritoneal membrane.* Kidney Int, 2014. **85**(4): p. 750-8.
26. Kuzlan, M., et al., *Peritoneal surface area and its permeability in rats.* Perit Dial Int, 1997. **17**(3): p. 295-300.
27. Rippe, B., B.I. Rosengren, and D. Venturoli, *The peritoneal microcirculation in peritoneal dialysis.* Microcirculation, 2001. **8**(5): p. 303-20.
28. Leypoldt, J.K., et al., *Dialysate to blood transport of macromolecules during peritoneal dialysis.* Am J Physiol, 1989. **257**(6 Pt 2): p. H1851-9.
29. Ni, J., et al., *Aquaporin-1 plays an essential role in water permeability and ultrafiltration during peritoneal dialysis.* Kidney Int, 2006. **69**(9): p. 1518-25.
30. Morelle, J., et al., *Quantification of osmotic water transport in vivo using fluorescent albumin.* Am J Physiol Renal Physiol, 2014. **307**(8): p. F981-9.
31. Zhang, W., et al., *Novel Endothelial Cell-Specific AQP1 Knockout Mice Confirm the Crucial Role of Endothelial AQP1 in Ultrafiltration during Peritoneal Dialysis.* PLoS One, 2016. **11**(1): p. e0145513.
32. Michailova, K.N. and K.G. Usunoff, *Serosal membranes (pleura, pericardium, peritoneum). Normal structure, development and experimental pathology.* Adv Anat Embryol Cell Biol, 2006. **183**: p. i-vii, 1-144, back cover.
33. Hain, H., et al., *Ultrafiltration and absorption characteristics of hydroxyethylstarch and dextran during long dwell peritoneal dialysis exchanges in rats.* Adv Perit Dial, 1989. **5**: p. 28-30.
34. Flessner, M.F., R.L. Dedrick, and J.S. Schultz, *A distributed model of peritoneal-plasma transport: theoretical considerations.* Am J Physiol, 1984. **246**(4 Pt 2): p. R597-607.
35. Morelle, J., et al., *ISPD recommendations for the evaluation of peritoneal membrane dysfunction in adults: Classification, measurement, interpretation and rationale for intervention.* Perit Dial Int, 2021. **41**(4): p. 352-372.
36. Wang, T., et al., *Hyaluronan decreases peritoneal fluid absorption in peritoneal dialysis.* J Am Soc Nephrol, 1997. **8**(12): p. 1915-20.
37. Ho-dac-Pannekeet, M.M., et al., *Analysis of ultrafiltration failure in peritoneal dialysis patients by means of standard peritoneal permeability analysis.* Perit Dial Int, 1997. **17**(2): p. 144-50.
38. Twardowski, Z.J., et al., *Short peritoneal equilibration test: impact of preceding dwell time.* Adv Perit Dial, 2003. **19**: p. 53-8.
39. Twardowski, Z.J., K.D. Nolph, and R. Khanna, *Limitations of the peritoneal equilibration test.* Nephrol Dial Transplant, 1995. **10**(11): p. 2160-1.
40. Romani, R.F., et al., *Comparison of three PET methods to assess peritoneal membrane transport.* Braz J Med Biol Res, 2019. **52**(8): p. e8596.
41. Massou, S., et al., *[Systemic candidiasis in medical intensive care unit: analysis of risk factors and the contribution of colonization index].* Pathol Biol (Paris), 2013. **61**(3): p. 108-12.

42. Cueto-Manzano, A.M., *Rapid solute transport in the peritoneum: physiologic and clinical consequences.* Perit Dial Int, 2009. **29 Suppl 2**: p. S90-5.
43. Agrawal, A. and K.D. Nolph, *Management of high peritoneal transporters.* Perit Dial Int, 2000. **20 Suppl 2**: p. S160-5.
44. Devuyst, O., et al., *Regulation of NO synthase isoforms in the peritoneum: implications for ultrafiltration failure in peritoneal dialysis.* Nephrol Dial Transplant, 2001. **16**(3): p. 675-8.
45. Diaz-Buxo, J.A., *Continuous ambulatory peritoneal dialysis (CAPD) and hemodialysis: pride and prejudice.* Perit Dial Int, 1990. **10**(1): p. 5-7.
46. Devuyst, O., et al., *Aquaporin-1 and endothelial nitric oxide synthase expression in capillary endothelia of human peritoneum.* Am J Physiol, 1998. **275**(1): p. H234-42.
47. Fujiyoshi, Y., et al., *Structure and function of water channels.* Curr Opin Struct Biol, 2002. **12**(4): p. 509-15.
48. Sui, H., et al., *Structural basis of water-specific transport through the AQP1 water channel.* Nature, 2001. **414**(6866): p. 872-8.
49. Yang, B., et al., *Reduced osmotic water permeability of the peritoneal barrier in aquaporin-1 knockout mice.* Am J Physiol, 1999. **276**(1): p. C76-81.
50. Carlsson, O., et al., *In vivo inhibition of transcellular water channels (aquaporin-1) during acute peritoneal dialysis in rats.* Am J Physiol, 1996. **271**(6 Pt 2): p. H2254-62.
51. Corciulo, S., et al., *AQP1-Containing Exosomes in Peritoneal Dialysis Effluent As Biomarker of Dialysis Efficiency.* Cells, 2019. **8**(4).
52. La Milia, V., et al., *Mini-peritoneal equilibration test: A simple and fast method to assess free water and small solute transport across the peritoneal membrane.* Kidney Int, 2005. **68**(2): p. 840-6.
53. Morelle, J., et al., *AQP1 Promoter Variant, Water Transport, and Outcomes in Peritoneal Dialysis.* N Engl J Med, 2021. **385**(17): p. 1570-1580.
54. Krediet, R.T., et al., *Alterations in the peritoneal transport of water and solutes during peritonitis in continuous ambulatory peritoneal dialysis patients.* Eur J Clin Invest, 1987. **17**(1): p. 43-52.
55. Stoenoiu, M.S., et al., *Corticosteroids induce expression of aquaporin-1 and increase transcellular water transport in rat peritoneum.* J Am Soc Nephrol, 2003. **14**(3): p. 555-65.
56. Devuyst, O. and J. Ni, *Aquaporin-1 in the peritoneal membrane: Implications for water transport across capillaries and peritoneal dialysis.* Biochim Biophys Acta, 2006. **1758**(8): p. 1078-84.
57. Yool, A.J. and E.M. Campbell, *Structure, function and translational relevance of aquaporin dual water and ion channels.* Mol Aspects Med, 2012. **33**(5-6): p. 553-61.
58. Fullerton, G.D. and M.R. Amurao, *Evidence that collagen and tendon have monolayer water coverage in the native state.* Cell Biol Int, 2006. **30**(1): p. 56-65.
59. Nolph, K.D., J.E. Hano, and P.E. Teschan, *Peritoneal sodium transport during hypertonic peritoneal dialysis. Physiologic mechanisms and clinical implications.* Ann Intern Med, 1969. **70**(5): p. 931-41.
60. Wang, T., et al., *A quantitative analysis of sodium transport and removal during peritoneal dialysis.* Kidney Int, 1997. **52**(6): p. 1609-16.
61. Uribarri, J., J. Buquing, and M.S. Oh, *Acid-base balance in chronic peritoneal dialysis patients.* Kidney Int, 1995. **47**(1): p. 269-73.

62. Mortier, S., et al., *Long-term exposure to new peritoneal dialysis solutions: Effects on the peritoneal membrane.* Kidney Int, 2004. **66**(3): p. 1257-65.
63. Margetts, P.J., et al., *Gene transfer of transforming growth factor-beta1 to the rat peritoneum: effects on membrane function.* J Am Soc Nephrol, 2001. **12**(10): p. 2029-2039.
64. Lee, S.H., et al., *The monocyte chemoattractant protein-1 (MCP-1)/CCR2 system is involved in peritoneal dialysis-related epithelial-mesenchymal transition of peritoneal mesothelial cells.* Lab Invest, 2012. **92**(12): p. 1698-711.
65. Li, Z., et al., *Astragalus membranaceus inhibits peritoneal fibrosis via monocyte chemoattractant protein (MCP)-1 and the transforming growth factor-beta1 (TGF-beta1) pathway in rats submitted to peritoneal dialysis.* Int J Mol Sci, 2014. **15**(7): p. 12959-71.
66. Nakamoto, H., et al., *Role of the renin-angiotensin system in the pathogenesis of peritoneal fibrosis.* Perit Dial Int, 2008. **28 Suppl 3**: p. S83-7.
67. Nessim, S.J., J. Perl, and J.M. Bargman, *The renin-angiotensin-aldosterone system in peritoneal dialysis: is what is good for the kidney also good for the peritoneum?* Kidney Int, 2010. **78**(1): p. 23-8.
68. Strutz, F., et al., *Basic fibroblast growth factor expression is increased in human renal fibrogenesis and may mediate autocrine fibroblast proliferation.* Kidney Int, 2000. **57**(4): p. 1521-38.
69. Inagi, R., et al., *Glucose degradation product methylglyoxal enhances the production of vascular endothelial growth factor in peritoneal cells: role in the functional and morphological alterations of peritoneal membranes in peritoneal dialysis.* FEBS Lett, 1999. **463**(3): p. 260-4.
70. Welten, A.G., et al., *Single exposure of mesothelial cells to glucose degradation products (GDPs) yields early advanced glycation end-products (AGEs) and a proinflammatory response.* Perit Dial Int, 2003. **23**(3): p. 213-21.
71. Kitamura, M., et al., *Epigallocatechin gallate suppresses peritoneal fibrosis in mice.* Chem Biol Interact, 2012. **195**(1): p. 95-104.
72. Loureiro, J., et al., *BMP-7 blocks mesenchymal conversion of mesothelial cells and prevents peritoneal damage induced by dialysis fluid exposure.* Nephrol Dial Transplant, 2010. **25**(4): p. 1098-108.
73. Yanez-Mo, M., et al., *Peritoneal dialysis and epithelial-to-mesenchymal transition of mesothelial cells.* N Engl J Med, 2003. **348**(5): p. 403-13.
74. Strippoli, R., et al., *Epithelial-to-mesenchymal transition of peritoneal mesothelial cells is regulated by an ERK/NF-kappaB/Snail1 pathway.* Dis Model Mech, 2008. **1**(4-5): p. 264-74.
75. Aguilera, A., *The Mesothelial to Mesenchymal Transition a Pathogenic and Therapeutic Key for Peritoneal Membrane Failure.* 2013.
76. Xiao, J., et al., *IL-6 promotes epithelial-to-mesenchymal transition of human peritoneal mesothelial cells possibly through the JAK2/STAT3 signaling pathway.* Am J Physiol Renal Physiol, 2017. **313**(2): p. F310-F318.
77. Mujais, S. and K. Story, *Peritoneal dialysis in the US: evaluation of outcomes in contemporary cohorts.* Kidney Int Suppl, 2006(103): p. S21-6.
78. Teitelbaum, I., *Ultrafiltration failure in peritoneal dialysis: a pathophysiologic approach.* Blood Purif, 2015. **39**(1-3): p. 70-3.
79. Fusshoeller, A., *Histomorphological and functional changes of the peritoneal membrane during long-term peritoneal dialysis.* Pediatr Nephrol, 2008. **23**(1): p. 19-25.

80. de Alvaro, F., et al., *Peritoneal resting is beneficial in peritoneal hyperpermeability and ultrafiltration failure.* Adv Perit Dial, 1993. **9**: p. 56-61.
81. Kolesnyk, I., et al., *A positive effect of AII inhibitors on peritoneal membrane function in long-term PD patients.* Nephrol Dial Transplant, 2009. **24**(1): p. 272-7.
82. Goffin, E., et al., *Expression of aquaporin-1 in a long-term peritoneal dialysis patient with impaired transcellular water transport.* Am J Kidney Dis, 1999. **33**(2): p. 383-8.
83. Aroeira, L.S., et al., *Epithelial to mesenchymal transition and peritoneal membrane failure in peritoneal dialysis patients: pathologic significance and potential therapeutic interventions.* J Am Soc Nephrol, 2007. **18**(7): p. 2004-13.
84. Kinashi, H., et al., *TGF-beta1 promotes lymphangiogenesis during peritoneal fibrosis.* J Am Soc Nephrol, 2013. **24**(10): p. 1627-42.
85. Baranowska-Daca, E., et al., *Use of bethanechol chloride to increase available ultrafiltration in CAPD.* Adv Perit Dial, 1995. **11**: p. 69-72.
86. Plum, J., G. Schoenicke, and B. Grabensee, *Osmotic agents and buffers in peritoneal dialysis solution: monocyte cytokine release and in vitro cytotoxicity.* Am J Kidney Dis, 1997. **30**(3): p. 413-22.
87. Ando, M., T. Sanaka, and H. Nihei, *Eicosapentanoic acid reduces plasma levels of remnant lipoproteins and prevents in vivo peroxidation of LDL in dialysis patients.* J Am Soc Nephrol, 1999. **10**(10): p. 2177-84.
88. Islam, K.N., et al., *Alpha-tocopherol supplementation decreases the oxidative susceptibility of LDL in renal failure patients on dialysis therapy.* Atherosclerosis, 2000. **150**(1): p. 217-24.
89. Aruoma, O.I., et al., *The antioxidant action of N-acetylcysteine: its reaction with hydrogen peroxide, hydroxyl radical, superoxide, and hypochlorous acid.* Free Radic Biol Med, 1989. **6**(6): p. 593-7.
90. Seo, E.Y., et al., *Stability of N-acetylcysteine in peritoneal dialysis solution.* Perit Dial Int, 2010. **30**(1): p. 105-8.
91. Nevado, J., et al., *Amadori adducts activate nuclear factor-kappaB-related proinflammatory genes in cultured human peritoneal mesothelial cells.* Br J Pharmacol, 2005. **146**(2): p. 268-79.
92. Shrikanta, A., A. Kumar, and V. Govindaswamy, *Resveratrol content and antioxidant properties of underutilized fruits.* J Food Sci Technol, 2015. **52**(1): p. 383-90.
93. Nomura, M., et al., *Inhibition of 12-O-tetradecanoylphorbol-13-acetate-induced NF-kappaB activation by tea polyphenols, (-)-epigallocatechin gallate and theaflavins.* Carcinogenesis, 2000. **21**(10): p. 1885-90.
94. Wirtz, H.R., *[Effect of ambroxol on surfactant secretion and synthesis in isolated type II alveolar cells].* Pneumologie, 2000. **54**(7): p. 278-83.
95. Dobbie, J.W., J.D. Anderson, and C. Hind, *Long-term effects of peritoneal dialysis on peritoneal morphology.* Perit Dial Int, 1994. **14 Suppl 3**: p. S16-20.
96. Dobbie, J.W. and J.D. Anderson, *Ultrastructure, distribution, and density of lamellar bodies in human peritoneum.* Perit Dial Int, 1996. **16**(5): p. 488-96.
97. Kanlaya, R., et al., *Protective effect of epigallocatechin-3-gallate (EGCG) via Nrf2 pathway against oxalate-induced epithelial mesenchymal transition (EMT) of renal tubular cells.* Sci Rep, 2016. **6**: p. 30233.
98. Higuera-Ciapara, I., L. Felix-Valenzuela, and F.M. Goycoolea, *Astaxanthin: a review of its chemistry and applications.* Crit Rev Food Sci Nutr, 2006. **46**(2): p. 185-96.
99. Sztretye, M., et al., *Astaxanthin: A Potential Mitochondrial-Targeted Antioxidant Treatment in Diseases and with Aging.* Oxid Med Cell Longev, 2019. **2019**: p. 3849692.

100. Lindsley, R.C., et al., *Mesp1 coordinately regulates cardiovascular fate restriction and epithelial-mesenchymal transition in differentiating ESCs.* Cell Stem Cell, 2008. **3**(1): p. 55-68.
101. Aguilera, A., et al., *Epithelial to mesenchymal transition as a triggering factor of peritoneal membrane fibrosis and angiogenesis in peritoneal dialysis patients.* Curr Opin Investig Drugs, 2005. **6**(3): p. 262-8.
102. Liu, T., et al., *NF-kappaB signaling in inflammation.* Signal Transduct Target Ther, 2017. **2**.
103. Nakayama, M., et al., *Dissolved molecular hydrogen (H2) in Peritoneal Dialysis (PD) solutions preserves mesothelial cells and peritoneal membrane integrity.* BMC Nephrol, 2017. **18**(1): p. 327.
104. Ditsawanon, P. and P. Aramwit, *Preserving the peritoneal membrane in long-term peritoneal dialysis patients.* J Clin Pharm Ther, 2015. **40**(5): p. 508-516.
105. Schaefer, B., et al., *Neutral pH and low-glucose degradation product dialysis fluids induce major early alterations of the peritoneal membrane in children on peritoneal dialysis.* Kidney Int, 2018. **94**(2): p. 419-429.
106. Arfeen, S., et al., *The nutritional/metabolic and hormonal effects of 8 weeks of continuous ambulatory peritoneal dialysis with a 1% amino acid solution.* Clin Nephrol, 1990. **33**(4): p. 192-99.
107. Bonomini, M., et al., *The osmo-metabolic approach: a novel and tantalizing glucose-sparing strategy in peritoneal dialysis.* J Nephrol, 2021. **34**(2): p. 503-519.
108. Bonomini, M., et al., *Current Opinion on Usage of L-Carnitine in End-Stage Renal Disease Patients on Peritoneal Dialysis.* Molecules, 2019. **24**(19).
109. Gaggiotti, E., et al., *Prevention of peritoneal sclerosis: a new proposal to substitute glucose with carnitine dialysis solution (biocompatibility testing in vitro and in rabbits).* Int J Artif Organs, 2005. **28**(2): p. 177-87.
110. Bonomini, M., et al., *L-carnitine is an osmotic agent suitable for peritoneal dialysis.* Kidney Int, 2011. **80**(6): p. 645-54.
111. Bonomini, M., et al., *Effect of an L-carnitine-containing peritoneal dialysate on insulin sensitivity in patients treated with CAPD: a 4-month, prospective, multicenter randomized trial.* Am J Kidney Dis, 2013. **62**(5): p. 929-38.
112. Bazzato, G., et al., *Xylitol as osmotic agent in CAPD: an alternative to glucose for uremic diabetic patients?* Trans Am Soc Artif Intern Organs, 1982. **28**: p. 280-6.
113. Chukwuma, C.I. and S. Islam, *Xylitol Improves Anti-Oxidative Defense System in Serum, Liver, Heart, Kidney and Pancreas of Normal and Type 2 Diabetes Model of Rats.* Acta Pol Pharm, 2017. **74**(3): p. 817-826.
114. Piccapane, F., et al., *A Novel Formulation of Glucose-Sparing Peritoneal Dialysis Solutions with l-Carnitine Improves Biocompatibility on Human Mesothelial Cells.* Int J Mol Sci, 2020. **22**(1).
115. Abaza, L., et al., *Olive Tree (Olea europeae L.) Leaves: Importance and Advances in the Analysis of Phenolic Compounds.* Antioxidants (Basel), 2015. **4**(4): p. 682-98.
116. Mahmoudi, A., et al., *Oleuropein and hydroxytyrosol rich extracts from olive leaves attenuate liver injury and lipid metabolism disturbance in bisphenol A-treated rats.* Food Funct, 2018. **9**(6): p. 3220-3234.
117. Huang, P.L., *Oleuropein and Related Compounds Reduce Atherosclerosis.* 2010
118. Sivakumar, G., N.A. Uccella, and L. Gentile, *Probing Downstream Olive Biophenol Secoiridoids.* Int J Mol Sci, 2018. **19**(10).

119. Lupinacci, S., et al., *Olive leaf extract counteracts epithelial to mesenchymal transition process induced by peritoneal dialysis, through the inhibition of TGFbeta1 signaling.* Cell Biol Toxicol, 2019. **35**(2): p. 95-109.
120. Derynck, R. and Y.E. Zhang, *Smad-dependent and Smad-independent pathways in TGF-beta family signalling.* Nature, 2003. **425**(6958): p. 577-84.
121. Omar, S.H., *Oleuropein in olive and its pharmacological effects.* Sci Pharm, 2010. **78**(2): p. 133-54.
122. Cicerale, S., L. Lucas, and R. Keast, *Biological activities of phenolic compounds present in virgin olive oil.* Int J Mol Sci, 2010. **11**(2): p. 458-79.
123. Boss, A., et al., *Evidence to Support the Anti-Cancer Effect of Olive Leaf Extract and Future Directions.* Nutrients, 2016. **8**(8).
124. Bisignano, G., et al., *On the in-vitro antimicrobial activity of oleuropein and hydroxytyrosol.* J Pharm Pharmacol, 1999. **51**(8): p. 971-4.
125. Ogun, M., et al., *Oleuropein ameliorates arsenic induced oxidative stress in mice.* J Trace Elem Med Biol, 2016. **36**: p. 1-6.
126. Janahmadi, Z., et al., *Oleuropein attenuates the progression of heart failure in rats by antioxidant and antiinflammatory effects.* Naunyn Schmiedebergs Arch Pharmacol, 2017. **390**(3): p. 245-252.
127. Romero, M., et al., *Antihypertensive effects of oleuropein-enriched olive leaf extract in spontaneously hypertensive rats.* Food Funct, 2016. **7**(1): p. 584-93.
128. Zarzuelo, A., et al., *Vasodilator effect of olive leaf.* Planta Med, 1991. **57**(5): p. 417-9.
129. Puel, C., et al., *Dose-response study of effect of oleuropein, an olive oil polyphenol, in an ovariectomy/inflammation experimental model of bone loss in the rat.* Clin Nutr, 2006. **25**(5): p. 859-68.
130. Ahmadvand, H., et al., *Protective effects of oleuropein against renal injury oxidative damage in alloxan-induced diabetic rats; a histological and biochemical study.* J Nephropathol, 2017. **6**(3): p. 204-209.
131. Liu, Y., W. Dai, and S. Ye, *The olive constituent oleuropein exerts nephritic protective effects on diabetic nephropathy in db/db mice.* Arch Physiol Biochem, 2022. **128**(2): p. 455-462.
132. M., G.-M., *Elementary processes with two quantum transitions*. 1931.
133. Schiessl, I.M. and H. Castrop, *Deep insights: intravital imaging with two-photon microscopy.* Pflugers Arch, 2016. **468**(9): p. 1505-16.
134. Helmchen, F. and W. Denk, *Deep tissue two-photon microscopy.* Nat Methods, 2005. **2**(12): p. 932-40.
135. Hall, A.M. and B.A. Molitoris, *Dynamic multiphoton microscopy: focusing light on acute kidney injury.* Physiology (Bethesda), 2014. **29**(5): p. 334-42.
136. Molitoris, B.A. and R.M. Sandoval, *Intravital multiphoton microscopy of dynamic renal processes.* Am J Physiol Renal Physiol, 2005. **288**(6): p. F1084-9.
137. Levene, M.J., et al., *In vivo multiphoton microscopy of deep brain tissue.* J Neurophysiol, 2004. **91**(4): p. 1908-12.
138. Kobat, D., N.G. Horton, and C. Xu, *In vivo two-photon microscopy to 1.6-mm depth in mouse cortex.* J Biomed Opt, 2011. **16**(10): p. 106014.
139. Rocheleau, J.V. and D.W. Piston, *Two-photon excitation microscopy for the study of living cells and tissues.* Curr Protoc Cell Biol, 2003. **Chapter 4**: p. Unit 4 11.
140. Svoboda, K. and R. Yasuda, *Principles of two-photon excitation microscopy and its applications to neuroscience.* Neuron, 2006. **50**(6): p. 823-39.

141. Zipfel, W.R., R.M. Williams, and W.W. Webb, *Nonlinear magic: multiphoton microscopy in the biosciences.* Nat Biotechnol, 2003. **21**(11): p. 1369-77.
142. Rubart, M., *Two-photon microscopy of cells and tissue.* Circ Res, 2004. **95**(12): p. 1154-66.
143. Helmchen, F. and W. Denk, *New developments in multiphoton microscopy.* Curr Opin Neurobiol, 2002. **12**(5): p. 593-601.
144. Laiho, L.H., et al., *Two-photon 3-D mapping of ex vivo human skin endogenous fluorescence species based on fluorescence emission spectra.* J Biomed Opt, 2005. **10**(2): p. 024016.
145. Thorling, C.A., et al., *Multiphoton microscopy in defining liver function.* J Biomed Opt, 2014. **19**(9): p. 90901.
146. Dunn, K.W., et al., *Functional studies of the kidney of living animals using multicolor two-photon microscopy.* Am J Physiol Cell Physiol, 2002. **283**(3): p. C905-16.
147. Cahalan, M.D., et al., *Two-photon tissue imaging: seeing the immune system in a fresh light.* Nat Rev Immunol, 2002. **2**(11): p. 872-80.
148. Perrin, L., B. Bayarmagnai, and B. Gligorijevic, *Frontiers in Intravital Multiphoton Microscopy of Cancer.* Cancer Rep (Hoboken), 2020. **3**(1): p. e1192.
149. Kang, J.J., et al., *Quantitative imaging of basic functions in renal (patho)physiology.* Am J Physiol Renal Physiol, 2006. **291**(2): p. F495-502.
150. Kowalewska, P.M., A.L. Patrick, and A.E. Fox-Robichaud, *Syndecan-1 in the mouse parietal peritoneum microcirculation in inflammation.* PLoS One, 2014. **9**(9): p. e104537.
151. Honkura, N., et al., *Intravital imaging-based analysis tools for vessel identification and assessment of concurrent dynamic vascular events.* Nat Commun, 2018. **9**(1): p. 2746.
152. Schiessl, I.M., et al., *Just Look! Intravital Microscopy as the Best Means to Study Kidney Cell Death Dynamics.* Semin Nephrol, 2016. **36**(3): p. 220-36.
153. Pawlaczyk, K., et al., *Animal Models of Peritoneal Dialysis: Thirty Years of Our Own Experience.* Biomed Res Int, 2015. **2015**: p. 261813.
154. Ni, J., et al., *Functional and molecular characterization of a peritoneal dialysis model in the C57BL/6J mouse.* Kidney Int, 2005. **67**(5): p. 2021-31.
155. Ferrantelli, E., et al., *A Novel Mouse Model of Peritoneal Dialysis: Combination of Uraemia and Long-Term Exposure to PD Fluid.* Biomed Res Int, 2015. **2015**: p. 106902.
156. Lameire, N., et al., *Experimental models in peritoneal dialysis: a European experience.* Kidney Int, 1998. **54**(6): p. 2194-206.
157. Rosengren, B.I. and B. Rippe, *Blood flow limitation in vivo of small solute transfer during peritoneal dialysis in rats.* J Am Soc Nephrol, 2003. **14**(6): p. 1599-604.
158. Kowalewska, P.M., P.J. Margetts, and A.E. Fox-Robichaud, *Peritoneal Dialysis Catheter Increases Leukocyte Recruitment in the Mouse Parietal Peritoneum Microcirculation and Causes Fibrosis.* Perit Dial Int, 2016. **36**(1): p. 7-15.
159. Ahmadvand, H., et al., *Biochemical effects of oleuropein in gentamicin-induced nephrotoxicity in rats.* ARYA Atheroscler, 2016. **12**(2): p. 87-93.
160. Alirezaei, M., et al., *Oleuropein prevents ethanol-induced gastric ulcers via elevation of antioxidant enzyme activities in rats.* J Physiol Biochem, 2012. **68**(4): p. 583-92.
161. Potocnjak, I., et al., *Oral administration of oleuropein attenuates cisplatin-induced acute renal injury in mice through inhibition of ERK signaling.* Mol Nutr Food Res, 2016. **60**(3): p. 530-41.

162. Sumiyoshi, M. and Y. Kimura, *Effects of olive leaf extract and its main component oleuroepin on acute ultraviolet B irradiation-induced skin changes in C57BL/6J mice.* Phytother Res, 2010. **24**(7): p. 995-1003.
163. Cavallini, N. and M. Braide, *Catheter patency and peritoneal morphology and function in a rat model of citrate-buffered peritoneal dialysis.* Perit Dial Int, 2010. **30**(6): p. 602-10.
164. Kreshuk, A. and C. Zhang, *Machine Learning: Advanced Image Segmentation Using ilastik.* Methods Mol Biol, 2019. **2040**: p. 449-463.
165. Zudaire, E., et al., *A computational tool for quantitative analysis of vascular networks.* PLoS One, 2011. **6**(11): p. e27385.
166. Corliss, B.A., et al., *Methods to label, image, and analyze the complex structural architectures of microvascular networks.* Microcirculation, 2019. **26**(5): p. e12520.
167. Goulam Houssen, Y., et al., *Monitoring micrometer-scale collagen organization in rat-tail tendon upon mechanical strain using second harmonic microscopy.* J Biomech, 2011. **44**(11): p. 2047-52.
168. Strupler, M., et al., *Second harmonic microscopy to quantify renal interstitial fibrosis and arterial remodeling.* J Biomed Opt, 2008. **13**(5): p. 054041.
169. Ranjit, S., et al., *Label-free fluorescence lifetime and second harmonic generation imaging microscopy improves quantification of experimental renal fibrosis.* Kidney Int, 2016. **90**(5): p. 1123-1128.
170. Strupler, M., et al., *Second harmonic imaging and scoring of collagen in fibrotic tissues.* Opt Express, 2007. **15**(7): p. 4054-65.
171. Dobbie, J.W., *Morphology of the peritoneum in CAPD.* Blood Purif, 1989. **7**(2-3): p. 74-85.
172. Dobbie, J.W., *New concepts in molecular biology and ultrastructural pathology of the peritoneum: their significance for peritoneal dialysis.* Am J Kidney Dis, 1990. **15**(2): p. 97-109.
173. Balzer, M.S., et al., *SGLT2 Inhibition by Intraperitoneal Dapagliflozin Mitigates Peritoneal Fibrosis and Ultrafiltration Failure in a Mouse Model of Chronic Peritoneal Exposure to High-Glucose Dialysate.* Biomolecules, 2020. **10**(11).
174. Shi, Y., et al., *Protective effect of COMP-angiopoietin-1 on peritoneal vascular permeability and peritoneal transport function in uremic peritoneal dialysis rats.* Am J Transl Res, 2019. **11**(9): p. 5932-5943.
175. Gonzalez-Mateo, G.T., et al., *Paricalcitol reduces peritoneal fibrosis in mice through the activation of regulatory T cells and reduction in IL-17 production.* PLoS One, 2014. **9**(10): p. e108477.
176. Perl, J., et al., *Modification of the glucose correction factor by peritoneal dialysis solution type in the peritoneal equilibration test.* Perit Dial Int, 2010. **30**(6): p. 647-50.
177. Milanizadeh, S. and M. Reza Bigdeli, *Pro-Apoptotic and Anti-Angiogenesis Effects of Olive Leaf Extract on Spontaneous Mouse Mammary Tumor Model by Balancing Vascular Endothelial Growth Factor and Endostatin Levels.* Nutr Cancer, 2019. **71**(8): p. 1374-1381.
178. Song, H., et al., *Dietary oleuropein inhibits tumor angiogenesis and lymphangiogenesis in the B16F10 melanoma allograft model: a mechanism for the suppression of high-fat diet-induced solid tumor growth and lymph node metastasis.* Oncotarget, 2017. **8**(19): p. 32027-32042.

179. Kleinfeld, D., et al., *Fluctuations and stimulus-induced changes in blood flow observed in individual capillaries in layers 2 through 4 of rat neocortex.* Proc Natl Acad Sci U S A, 1998. **95**(26): p. 15741-6.
180. Chaigneau, E., M. Roche, and S. Charpak, *Unbiased Analysis Method for Measurement of Red Blood Cell Size and Velocity With Laser Scanning Microscopy.* Front Neurosci, 2019. **13**: p. 644.
181. Chaigneau, E., et al., *Two-photon imaging of capillary blood flow in olfactory bulb glomeruli.* Proc Natl Acad Sci U S A, 2003. **100**(22): p. 13081-6.
182. Chhatbar, P.Y. and P. Kara, *Improved blood velocity measurements with a hybrid image filtering and iterative Radon transform algorithm.* Front Neurosci, 2013. **7**: p. 106.
183. Dunn, K.W., T.A. Sutton, and R.M. Sandoval, *Live-animal imaging of renal function by multiphoton microscopy.* Curr Protoc Cytom, 2007. **Chapter 12**: p. Unit12 9.
184. Bordoni, L., et al., *A new experimental mouse model of water intoxication with sustained increased intracranial pressure and mild hyponatremia without side effects of antidiuretics.* Exp Anim, 2020. **69**(1): p. 92-103.
185. de la Puerta, R., V. Ruiz Gutierrez, and J.R. Hoult, *Inhibition of leukocyte 5-lipoxygenase by phenolics from virgin olive oil.* Biochem Pharmacol, 1999. **57**(4): p. 445-9.
186. Miles, E.A., P. Zoubouli, and P.C. Calder, *Differential anti-inflammatory effects of phenolic compounds from extra virgin olive oil identified in human whole blood cultures.* Nutrition, 2005. **21**(3): p. 389-94.
187. Omar, S.H., *Cardioprotective and neuroprotective roles of oleuropein in olive.* Saudi Pharm J, 2010. **18**(3): p. 111-21.
188. Poudyal, H., F. Campbell, and L. Brown, *Olive leaf extract attenuates cardiac, hepatic, and metabolic changes in high carbohydrate-, high fat-fed rats.* J Nutr, 2010. **140**(5): p. 946-53.
189. Zhao, G., Z. Yin, and J. Dong, *Antiviral efficacy against hepatitis B virus replication of oleuropein isolated from Jasminum officinale L. var. grandiflorum.* J Ethnopharmacol, 2009. **125**(2): p. 265-8.
190. Sarbishegi, M., F. Mehraein, and M. Soleimani, *Antioxidant role of oleuropein on midbrain and dopaminergic neurons of substantia nigra in aged rats.* Iran Biomed J, 2014. **18**(1): p. 16-22.
191. Bazoti, F.N., et al., *Localization of the noncovalent binding site between amyloid-beta-peptide and oleuropein using electrospray ionization FT-ICR mass spectrometry.* J Am Soc Mass Spectrom, 2008. **19**(8): p. 1078-85.
192. Janahmadi, Z., et al., *Oleuropein offers cardioprotection in rats with acute myocardial infarction.* Cardiovasc Toxicol, 2015. **15**(1): p. 61-8.
193. Potz, B.A., et al., *Calpain inhibition decreases inflammatory protein expression in vessel walls in a model of chronic myocardial ischemia.* Surgery, 2017. **161**(5): p. 1394-1404.
194. Yin, M., et al., *Oleuropein suppresses oxidative, inflammatory, and apoptotic responses following glycerol-induced acute kidney injury in rats.* Life Sci, 2019. **232**: p. 116634.
195. Notarnicola, M., et al., *Effects of olive oil polyphenols on fatty acid synthase gene expression and activity in human colorectal cancer cells.* Genes Nutr, 2011. **6**(1): p. 63-9.

196. Baumgartner, U., et al., *miR-19b enhances proliferation and apoptosis resistance via the EGFR signaling pathway by targeting PP2A and BIM in non-small cell lung cancer.* Mol Cancer, 2018. **17**(1): p. 44.
197. Yan, C.M., et al., *Oleuropein induces apoptosis via activation of caspases and suppression of phosphatidylinositol 3-kinase/protein kinase B pathway in HepG2 human hepatoma cell line.* Mol Med Rep, 2015. **11**(6): p. 4617-24.
198. Goldsmith, C.D., et al., *Phytochemical properties and anti-proliferative activity of Olea europaea L. leaf extracts against pancreatic cancer cells.* Molecules, 2015. **20**(7): p. 12992-3004.
199. Singh, I., et al., *The effects of polyphenols in olive leaves on platelet function.* Nutr Metab Cardiovasc Dis, 2008. **18**(2): p. 127-32.
200. Giner, E., et al., *Oleuropein protects against dextran sodium sulfate-induced chronic colitis in mice.* J Nat Prod, 2013. **76**(6): p. 1113-20.
201. Khalatbary, A.R. and G.R. Zarrinjoei, *Anti-inflammatory effect of oleuropein in experimental rat spinal cord trauma.* Iran Red Crescent Med J, 2012. **14**(4): p. 229-34.
202. Nediani, C., et al., *Oleuropein, a Bioactive Compound from Olea europaea L., as a Potential Preventive and Therapeutic Agent in Non-Communicable Diseases.* Antioxidants (Basel), 2019. **8**(12).

La borsa di dottorato è stata cofinanziata con risorse del
Programma Operativo Nazionale Ricerca e Innovazione 2014-2020 (CCI 2014IT16M2OP005),
Fondo Sociale Europeo, Azione I.1 "Dottorati Innovativi con caratterizzazione Industriale"